

國立臺灣大學理學院地質科學研究所



碩士論文

Department of Geosciences

College of Science

National Taiwan University

Master Thesis

以 *SmKS* 波到時探討地球外核頂部的速度結構

Using *SmKS* Traveltimes to Investigate the Velocity Structure
near the Top of the Earth's Outer Core

唐楚欣

Vivian Tang

指導教授：趙里 博士 洪淑蕙 博士

Advisors: Li Zhao, Ph.D. Shu-Huei Hung, Ph.D.

中華民國 103 年 7 月

July 2014

誌謝



能完成這篇論文，我要特別感謝我的指導教授趙里老師與洪淑蕙老師。從在中研院當暑期生就開始跟著趙里老師學習，趙老師非常的用心指導我，不管是在研究還是課業方面，對於我的問題總是耐心、細心的回答，並且培養我對研究的熱情與信心，對於老師給予我的幫助實在難以用言語表達我內心中的感謝，真的非常謝謝老師！到台大後有了洪淑蕙老師一同指導我，讓我能從不同的方向去思考研究問題，感謝洪老師與我討論並且提供建議，幫助我更透徹的了解問題，也使我的論文更完整。謝謝喬凌雲老師、郁文哲老師和龔源成老師共同擔任我的碩士口試委員，替我批改論文，提出不同觀點的意見，也給予我鼓勵。此外，也非常感謝欣穎、侑頻、柯彥廷和珮如等實驗室的強者學長姐們對我的幫忙與鼓勵，在我遇到問題時總能向他們尋求到答案。羅翊菁、林姿綺和其他的學弟妹，謝謝在我忙碌之時，願意幫我買飯或是拿食物餵食我，也陪我聊天舒壓，讓研究之路多了些趣味性。幸運的是在這裡我還有一群從大學時期一起奮鬥努力的好朋友相伴，李詩婷、吳欣玫、陳力維、秦念祺、葉德揚和蔣盼忻，以及其他在中央大學的好友們，雖然無法一一列舉，但心中時常覺得有這些朋友一起上課、討論問題、吃飯聊天和互相鼓勵，真的是難得可貴的情誼。尤其是李詩婷和我從大學時期不僅是摯友也是室友，在台大過的幾乎是24小時形影不離的生活，特別謝謝她在身邊，不論何時總是帶給我歡笑，我想我畢業之後會很懷念她在房間唱的那些台語歌！還有謝謝其他在我周邊給我支持鼓勵的好朋友們，為了配合我的時間，約吃飯地點永遠是公館跟師大。

最後，我要感謝我的父母與妹妹，從小到大在爸媽細心關懷與照料下樂觀開朗的成長，會有今天的我，都要感謝他們的支持與栽培。謝謝爸媽的信任給我很大的發揮空間，也在我趕進度忙碌不能回家時總能體諒。當我心情低落遇到困難時開導我，還有時常北上給我鼓勵，回家也總是有滿滿的一桌好菜替我補身體！爸媽對於我的付出，是我繼續努力的動力。謝謝所有曾經給過我幫助和鼓勵的家人、老師以及朋友們，沒有大家就不會這般順利且愉快的研究生活！

中文摘要



地球的固態內核之主要成份為鐵和鎳，另外還有少部分的氧、硫和矽等之比重相對較輕的物質。動力學研究認為這些較輕的物質會因浮力作用上浮而聚集在地球液態外核的頂部，但目前零星的地震學觀測結果尚未能夠對此說法給出明確的證據。從地震波觀測的角度來看，地球外核頂部若聚集有此較輕的物質，將會使核幔邊界(CMB)以下一部分深度區域內的密度和 P 波（即外核內 K 波）速度低於它們在該深度上的全球平均模型 PREM 的速度值。因此，通過在全球不同地區對在外核頂部傳播的 K 波之系統性觀測，並且與不同外核頂部速度模型所得到的理論模擬結果進行比較，就可以判斷外核頂部是否有低速區域存在。

本研究中，我們首先收集震央距為 120° - 140° 範圍內的測站之寬頻地震波形記錄，並測量 SKKS 波與 SmKS 組合波（包括 S3KS、S4KS 和 S5KS，但主要是 S3KS）的到時，將 SKKS 波與希爾伯特轉換之 S3KS 波透過交互相關函數得到兩者之間觀測的相對到時差。然後我們使用 Direct Solution Method (DSM) 來模擬全球平均模型 PREM 中在相同測站的理論波形，並從理論地震圖上得到模型預測的相對到時差。我們還可以進一步降低 CMB 以下一部分深度範圍內的 P 波速度，再計算其 DSM 理論地震圖，得到外核頂部有低速層存在的模型預測之相對到時差。由於 S3KS 波在外核頂部的 K 波部分射線長度大於 SKKS 波，外核頂部速度對 S3KS 波的影響會比對 SKKS 影響大。因此外核頂部低速層的存在會使 S3KS-SKKS 相對到時差增大。我們從全球地震數據中心 IRIS 搜集全球分布規模大於 6.0 且深度大於 400 公里之地震，並系統性地處理時間從 1990 年至今之 78 個地震，測量得到 606 筆精確的 S3KS-SKKS 相對到時差。由我們測量之結果顯示 CMB 底下 400 公里的部分有相對於 PREM 模型的低速層存在。最後透過 Bayesian 逆推方法來尋找統計上的期望值模型。逆推結果也顯示，在 CMB 底下 550 公里深度範圍內地球外核的實際速度低於 PREM 模型將近 0.11%，所以我們的研究結果為外核頂部有輕物質的存在提供了強有力的證據。

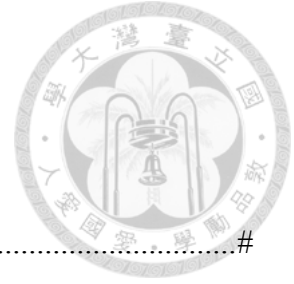
關鍵字：外核、Direct-Solution Method (DSM)、SmKS 波、Bayesian 逆推。

ABSTRACT



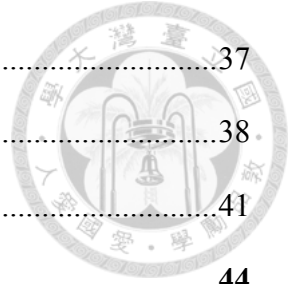
The solid inner core of the Earth consists of heavy minerals Fe and Ni with a fraction of light elements such as O, S and Si. These lighter elements are expelled from the inner core during its formation, rise up through the outer core as the result of buoyancy, and are trapped below the core-mantle boundary (CMB). Seismological evidence has been presented both for and against the existence of light materials at the top of the outer core. In this study, we use waveforms of recorded and modeled S_{mKS} waves to investigate the effect of velocity perturbation under the CMB on the differential traveltimes between SKKS and S3KS waves. Due to the long propagation distance and interference with neighboring phases, the arrival times of SKKS and S3KS waves are difficult to define accurately in the records. Therefore, in our analysis we measure both the observed and model-predicted traveltimes by cross-correlating the waveform of the Hilbert-transformed S3KS with that of SKKS. We obtained 606 high-quality S3KS-SKKS differential traveltimes from 78 deep earthquakes (depth \geq 400 km). We use synthetic seismograms calculated by the direct-solution method (DSM) in a suite of one-dimensional models with different structural profiles under the CMB to examine the existence of a zone of lowered velocity at the top of the outer core. Then we conduct a Bayesian inversion of the observed differential traveltimes for the velocity structure at the top of the outer core. The Metropolis-Hastings Monte Carlo algorithm is adopted for an efficient sampling of the model space. Inversion result indicates that the seismic velocity in the 550-km layer under the CMB is on average 0.11% lower than that in PREM. The clear depth-dependent velocity profile strongly favors the existence of light elements and chemical stratification at the top of the Earth's outer core.

CONTENTS



口試委員會審定書	#
誌謝	i
中文摘要	ii
ABSTRACT	iii
CONTENTS	iv
LIST OF FIGURES	vi
LIST OF TABLES	ix
Chapter 1 Introduction.....	1
Chapter 2 Data and Methodology	5
2.1 Seismic Phases for Studying the Top of the Outer Core.....	5
2.2 Deep Earthquakes and Records Used in This Study.....	6
2.3 Waveform Simulation: the Direct-solution Method	10
2.4 Differential Traveltime Measurements from Records	15
2.5 Differential Traveltime Measurements from Synthetics.....	17
2.6 Quality Control of Differential Traveltime Measurements	18
Chapter 3 Modeling <i>SmKS</i> Differential Traveltimes.....	23
3.1 Ray Theory Features of SKKS and S3KS Waves.....	23
3.2 Observed and Model-predicted Differential Traveltimes	25
3.3 Double-differential Travel times.....	28
3.4 Quantitative Assessment of Tested Models	32
Chapter 4 Inversion of <i>SmKS</i> Differential Traveltimes.....	35
4.1 Bayesian Inversion	35

4.2	Metropolis-Hastings Monte Carlo Algorithm.....	37
4.3	Bayesian Inversion of S_mKS Differential Traveltimes	38
4.4	A Slower Outer Core Model from Bayesian Inversion	41
Chapter 5	Discussions and Conclusions.....	44
	REFERENCES	46
Appendix A	Earthquake Information.....	49
Appendix B	Station Information	52
Appendix C	S3KS-SKKS Differential Travelttime Measurements.....	61

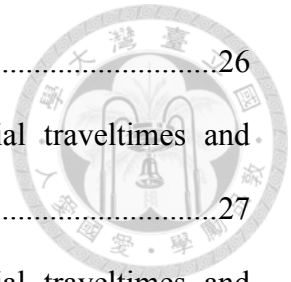


LIST OF FIGURES



Fig. 1.1	Cartoon showing outer core with light materials on its top.....	2
Fig. 2.1	SKKS and S3KS ray paths in model PREM	6
Fig. 2.2	Distributions of earthquakes and stations.....	7
Fig. 2.3	Great-circle paths and waveforms from Sumatra earthquake to stations in North America	9
Fig. 2.4	Model PREM and four PREM-like models.....	12
Fig. 2.5	DSM synthetics for PREM and PREM-OC1	13
Fig. 2.6	Zoom-in of DSM synthetics for PREM and PREM-OC1	14
Fig. 2.7	Measuring S3KS-SKKS differential traveltimes from a record.....	16
Fig. 2.8	Measuring S3KS-SKKS differential traveltimes from a synthetic	18
Fig. 2.9	Recorded and synthetic SKKS/S3KS waveforms with quality score 19.....	19
Fig. 2.10	Recorded and synthetic SKKS/S3KS waveforms with quality score 18.....	20
Fig. 2.11	Recorded and synthetic SKKS/S3KS waveforms with quality score 17.....	21
Fig. 2.12	Recorded and synthetic SKKS/S3KS waveforms with quality score 16.....	21
Fig. 2.13	Recorded and synthetic SKKS/S3KS waveforms with quality score 15.....	22
Fig. 3.1	Ray parameters and turning depths of SKKS and S3KS in PREM and PREM-OC1.....	24
Fig. 3.2	S3KS-SKKS TauP differential times in PREM and PREM-OC1	24
Fig. 3.3	Observed S3KS-SKKS differential traveltimes.....	25
Fig. 3.4	Comparison between observed S3KS-SKKS differential traveltimes and predictions by PREM.....	26
Fig. 3.5	Comparison between observed S3KS-SKKS differential traveltimes and	

	predictions by PREM-OC1.....	26
Fig. 3.6	Comparison between observed S3KS-SKKS differential traveltimes and predictions by PREM-OC2.....	27
Fig. 3.7	Comparison between observed S3KS-SKKS differential traveltimes and predictions by PREM-OC3.....	27
Fig. 3.8	Comparison between observed S3KS-SKKS differential traveltimes and predictions by PREM-OC4.....	28
Fig. 3.9	Double-differential traveltimes for PREM.....	29
Fig. 3.10	Double-differential traveltimes for PREM-OC2.....	30
Fig. 3.11	Double-differential traveltimes for PREM-OC3.....	31
Fig. 3.12	Double-differential traveltimes for PREM-OC4.....	32
Fig. 3.13	Histograms of the double-differential traveltimes.....	33
Fig. 4.1	Difference in TauP- and DSM-predicted S3KS-SKKS differential times for PREM.....	39
Fig. 4.2	Observed S3KS-SKKS differential traveltimes used in inversion.....	40
Fig. 4.3	Models involved in Bayesian inversion.....	41
Fig. 4.4	Histogram of double-differential traveltimes for PREM-SOC.....	42
Fig. 4.5	Comparison with previous study.....	43



LIST OF TABLES



Table A.1	List of Deep Earthquakes Used in This Study	49
Table B.1	List of Stations Yielding Data.....	52
Table C.1	List of 606 S3KS-SKKS Differential Traveltime Measurements.....	61

Chapter 1 Introduction



To the lowest order, the seismic structure of the Earth's interior can be simply divided into several layered spherical shells, including an outer solid crust, a highly viscous upper mantle, a solid mid and lower mantle, a liquid outer core that is much less viscous than the upper mantle, and a solid inner core.

It has been widely accepted that the Earth's solid inner core consists mainly of heavy minerals Fe (~85%) and Ni (~6%) with a significant fraction of light elements such as O, S and Si (*e.g.* Jephcoat & Olson, 1987; Stixrude *et al.*, 1997). As the temperature cools with time, Fe and Ni solidify and the inner core grows in radius. In the process, the light elements O, S and Si are expelled from the inner core into the outer core.

The outer core is composed of the same heavy materials Fe and Ni as the inner core but in a liquid state. There has been much less interest in studying the seismic structure of the outer core in comparison to the other regions. One reason is that the liquid outer core has only compressional wave which puts a stronger limitation on our ability to resolve its structural details. The other reason is that the outer core has always been considered to be more or less chemically homogenized by vigorous internal convection (Masters, 1979). Any variation in the structure of the outer core is thought of purely due to the depth gradient of pressure and temperature. This consideration is also the basis in establishing the outer core structure in the global average one-dimensional (1D) models such as PREM (Dziewonski & Anderson, 1981).

However, the light elements O, S and Si expelled from the inner core may alter this situation. Because of gravitational buoyancy, these lighter materials rise up through the Fe/Ni filled outer core and become trapped beneath the core-mantle boundary (CMB), a

solid thermal-chemical barrier, as illustrated in **Fig.1.1**. Such a scenario implies that there are light materials (in comparison to the expected heavy elements Fe and Ni), and therefore a chemical stratification may exist at the top of the outer core (e.g. Lister & Buffett, 1998; Buffett & Seagle, 2010; Frost *et al*, 2010), but the validity of this scenario needs to be confirmed by evidence gathered from geophysical (especially seismology) observations, laboratory experiments, and numerical modelings.

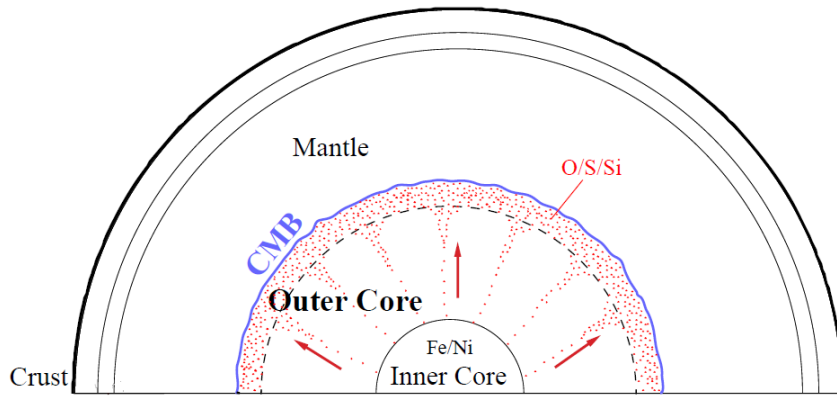
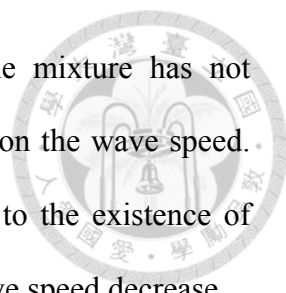


Fig. 1.1 Cartoon illustrating the schematic model of an outer core with light materials on its top. The light blue curvy arc indicates the CMB with possible topography. The inner core consists mainly heavy elements Fe and Ni, and a fraction of light materials O, S and Si (red dots), which are expelled from the inner core during its formation, rise up through the outer core, and are eventually trapped beneath the CMB.

The seismic waves propagating through the outer core, such as SKS and its core multiples $SmKS$, provide us the direct means to estimate the wave speed in the outer core and to infer the structure there. The effect of lighter materials on wave speed seems to be straightforward. In the liquid outer core, the speed of the compressional K wave is

$$\alpha = \sqrt{\frac{\kappa}{\rho}}, \quad (1.1)$$

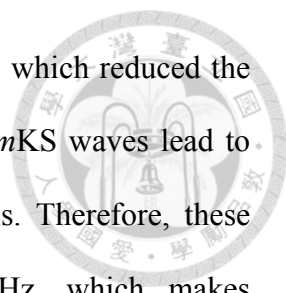
where κ and ρ are the bulk modulus and density, respectively. Therefore, intuitively a density decrease associated with the existence of lighter elements would result in an increase in wave speed. However, Helffrich (2012) demonstrated that the elastic



property of a multi-component liquid behaves non-linearly if the mixture has not reached an ideal state, and may offset the effect of density change on the wave speed. Therefore, chemical stratification at the top of the outer core due to the existence of lighter materials there could lead to the non-intuitive outcome of wave speed decrease.

The rapid increase in global deployments of permanent and temporary networks has provided more and more opportunities of obtaining high-quality records of *SmKS* waveforms which make the detailed investigation of the outer core feasible. Various seismic observations have been reported. Based on a limited dataset using earthquakes in Indonesia and stations in Africa, Tanaka (2004) reported possible low P-wave speed in a 50-km layer below the CMB. Eaton & Kendall (2006) found that a 12-km thick high-speed/low-density layer below the CMB best explained their *SmKS* traveltimes obtained from broadband seismograms at stations in Canada from a few earthquakes in Indonesia and Fiji. Tanaka (2007) analyzed a series of global records of *SmKS*, and proposed a model with a 1.4% lower speed than PREM in the top of 90 km of the outer core. More recently, a pair of studies by two independent groups reported very different findings. Alexandrakis & Eaton (2010) carefully analyzed *SmKS* traveltimes from 44 teleseismic earthquakes with a variety of source depths and in epicentral distance range 124° - 140° , and concluded that there is no evidence for outer core stratification. In contrast, Helffrich & Kaneshima (2010) modeled the *SmKS* traveltimes along the two paths from South America to Japan and from Fiji to Europe, and suggested that the wave speed in the 300-km layer below the CMB can be up to 0.3% lower than PREM.

The validity of the previous studies on the outer core structure using the *SmKS* traveltimes may be limited by three aspects. First, all these authors have used relatively few earthquakes and stations, and their data are limited in both quantity and geographical coverage. Secondly, most of them have used the traveltimes of *SmKS* up

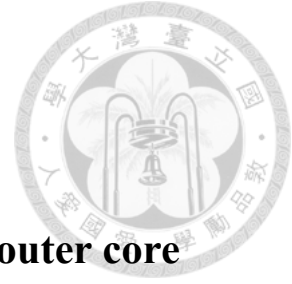


to S5KS, which are often weak and have low signal-to-noise ratios, which reduced the measurement quality. Finally, the long traveling distances of the *SmKS* waves lead to attenuation of high-frequency contents and in the recorded signals. Therefore, these waves are usually best observed at frequencies below 0.2 Hz, which makes measurement of the onset times of arrivals very difficult. However, all the previous studies have been using ray theory to model the *SmKS* traveltimes, but the bias introduced by finite-frequency effect are not addressed.

The purpose of this study is to conduct a careful and thorough investigation of the seismic structure at the top of the outer core by establishing a larger and higher-quality dataset of *SmKS* traveltimes from globally distributed earthquakes and stations, and a more accurate modeling of these traveltimes. We focus on the differential traveltimes between SKKS and S3KS waves to both ensure the quality of the measurements and eliminate the possible contributions from factors such as source location errors and lateral structural variations along the paths in the mantle. We measure the differential traveltimes by the cross correlation of SKKS and (Hilbert-transformed) S3KS waveforms, and we model the finite-frequency differential traveltimes by the cross correlation of waveforms calculated by the direct-solution method (DSM).

The outline of this thesis is as follows. In Chapter 2, we describe the process for measuring the S3KS-SKKS differential traveltimes, and the DSM method used in modeling these data. Then we present the observed S3KS-SKKS differential traveltimes as well as predictions by PREM and several PREM-like models in Chapter 3. In Chapter 4, we carry out inversion method to search more models to understand the velocity structure below CMB 550 km. Finally we discuss and summarize our results in Chapter 5.

Chapter 2 Data and Methodology



2.1 Seismic phases for studying the top of the outer core

Similar to the investigation of the other parts of the Earth's interior, the best means to probe the properties of the outer core is by analyzing the seismic waves that passing through it, namely the phases with a K-wave (compressional wave in the liquid outer core) segment, such as the SKS wave. The seismic properties of the outer core revealed by these waves can be combined with thermal-dynamical laws derived from laboratory experiments and/or theoretical studies to infer the chemical compositions and physical conditions of the outer core.

The most direct and robust observation on the seismic property at the top of the outer core can be obtained from the difference between the travel times of SKKS wave and the group arrival of S_mKS waves, with m being 3, 4 and 5 (i.e. S3KS, S4KS and S5KS, respectively). The best source-receiver geometry to clearly observe the difference between SKKS and S_mKS phases is in the distance range 120° - 140° and from a deep earthquake (400 km and deeper) to avoid the interference of near-source surface reflections. The S3KS phase dominates S4KS and S5KS in this distance range, S3KS is weaker but beyond 135° , and the waveform of the S_mKS group becomes more complicated and difficult to analyze.

At the distances of 120° , 130° and 140° , SKKS wave turns near the depths of 300 km, 400 km, and 500 km, respectively, below the CMB. The first Fresnel zone width of the SKS wave at this distance range is larger than 500 km at the CMB (Zhao & Chevrot, 2011), where the first Fresnel zones of SKKS and S3KS waves are similar in size. On the other hand, the distance between the CMB-piercing points of SKKS and S3KS is

about 250 km. Therefore, as shown in **Fig.2.1**, the ray paths of SKKS and S3KS in the distance range 120°-140° are also almost completely overlap outside the core, and any anomaly in their differential travel time $T_{S3KS}-T_{SKKS}$ is almost entirely due to the perturbations of the K-wave speed in the top ~400 km of the outer core (between dashed and blue semi-circles in **Fig.2.1**). This makes the differential time $T_{S3KS}-T_{SKKS}$ a very useful observable in studying the top of the outer core.

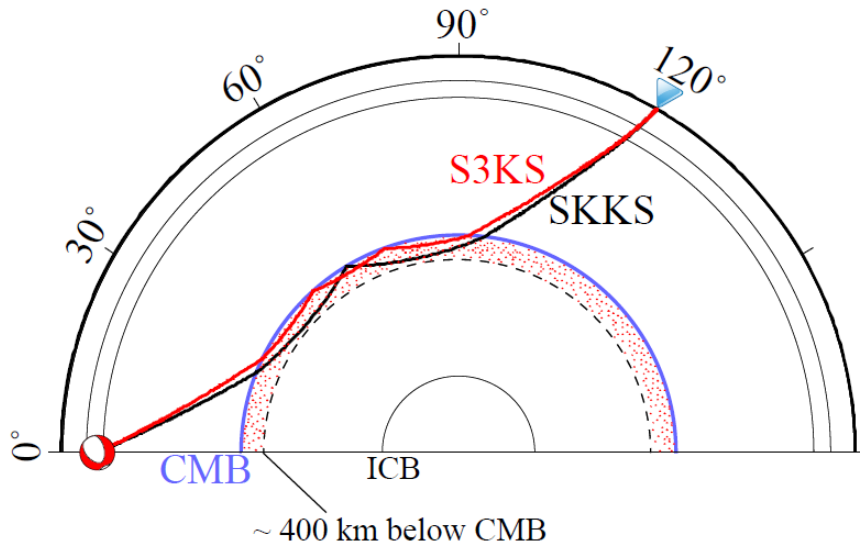


Fig. 2.1 SKKS and S3KS ray paths in model PREM at an epicentral distance of 120° from a deep earthquake with a source depth of ~600 km. The dashed semi-circle is ~400 km below the CMB (light blue semi-circle). In the epicentral distance range 120°-140°, ray paths of SKKS and S3KS almost coincide outside the CMB. As a result, anomalies in the differential traveltime $T_{S3KS}-T_{SKKS}$ are mostly due to velocity perturbations in the ~400-km zone below the CMB.

2.2 Deep earthquakes and records used in this study

In this study, we measure the differential travel times of SKKS and S3KS using records from globally distributed deep earthquakes and seismic stations. Our goal is to have as many measurements as possible, in order to increase the redundancy to reduce data uncertainty and expand the geographical coverage. For this purpose, we

downloaded from IRIS (<http://www.iris.edu/wilber3/>) the two horizontal-component broadband records at stations in the distance range 120° - 140° from earthquakes between 1998 and 2013. The earthquakes have depths greater than 400 km and moment magnitudes $5.7 \leq M_w \leq 8.3$. **Fig.2.2** displays the distributions of earthquakes and stations used in this study. Detailed information on the sources and stations are provided in **Tables A.1** and **B.1** in the Appendix A and B, respectively.

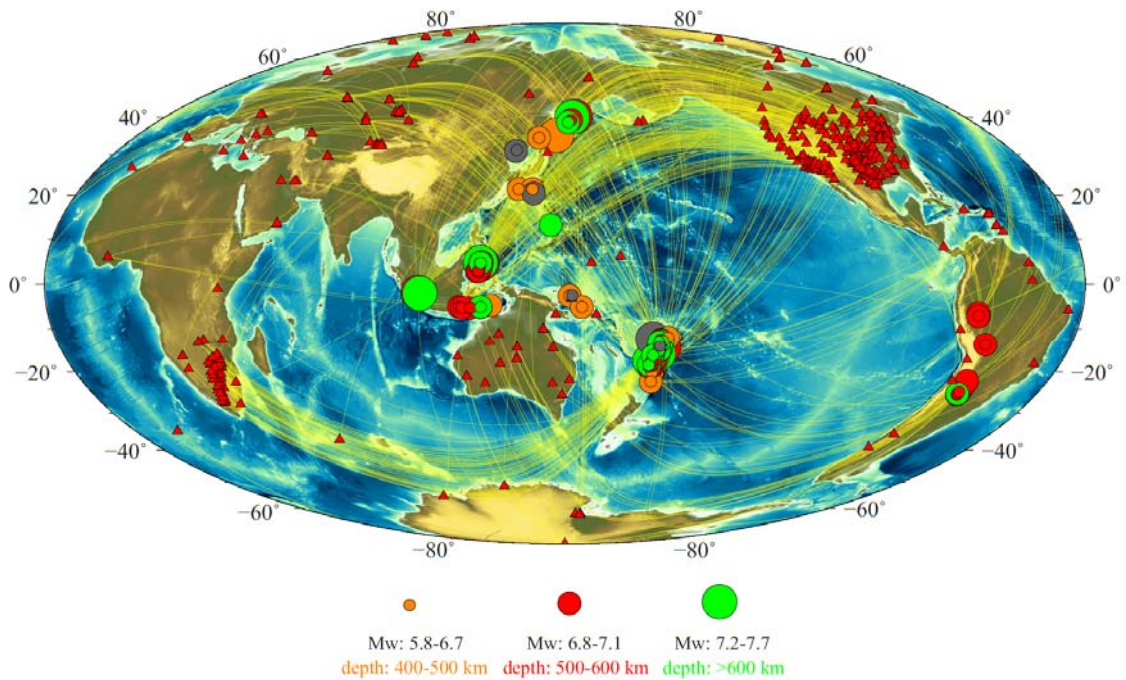
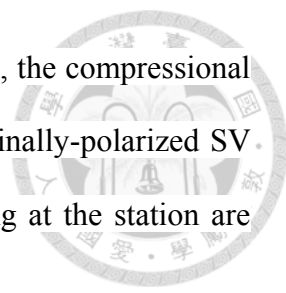


Fig. 2.2 Distributions of the 78 earthquakes (1998-2013) and the stations used in this study. Circles represent earthquakes, with their sizes and colors indicating magnitudes and focal depths, respectively. Red triangles are 744 stations providing waveforms. Gray circles show 6 events analyzed with no usable data. Thin yellow lines are source-receiver great-circle paths with usable data.

We only use the radial component here because all the relevant waves (SKKS and S3KS) arrive at the station as an S wave, with motion perpendicular to the ray path. At 120° - 140° degrees distance, the SKKS and S3KS waves arrive at the station nearly vertically (see **Fig.2.1**), therefore the amplitudes of SKKS and S3KS will be



mostly horizontal. Furthermore, during the transmission at the CMB, the compressional K wave in the outer core only converts to P wave and the longitudinally-polarized SV wave in the mantle. Therefore, the SKKS and S3KS waves arriving at the station are both polarized in the radial component.

An example of the radial-component seismograms is presented in **Fig.2.3** for the 25 July 2004 deep earthquake in Sumatra recorded at 54 stations in North America. Due to the rather long traveling distance, higher frequency content of the SKKS wave and the *SmKS* group is strongly attenuated. As a result, at these long distances these phases have relatively low signal-to-noise ratio (SNR), and it is necessary to remove the high-frequency content of the seismograms to ensure sufficient SNR. Through trial-and-error, we found that the best frequency band to have clear waveforms of both SKKS wave and the *SmKS* group is 0.005-0.2 Hz. The waveforms in **Fig.2.3** have all been deconvolved with the instrument responses to velocity, and bandpass filtered.

There are many publicly available programs, such as the TauP Toolkit (Crotwell *et al.*, 1999), which can be used to calculate the travel times of SKKS and *SmKS* waves based on 1D models (e.g. PREM) easily and quickly. However, these ray-theory travel times are model predictions of the onset times of the corresponding waves at high frequency, which cannot be easily located in the observed seismograms in the distance range 120°-140° used in this study. There are two main reasons for this. One is the fact that we need to filter the recorded seismograms to below 0.2 Hz to achieve sufficient SNR. Another reason is that the interference of nearby phases immediately before the arrivals of SKKS and *SmKS* waves often distorts the beginning parts of these waves and makes it impossible to identify their onset times. As a result, the most accurate and reliable approach to measuring the differential travel time $T_{S3KS}-T_{SKKS}$ is through the cross correlation of the recorded SKKS and *SmKS* waveforms.

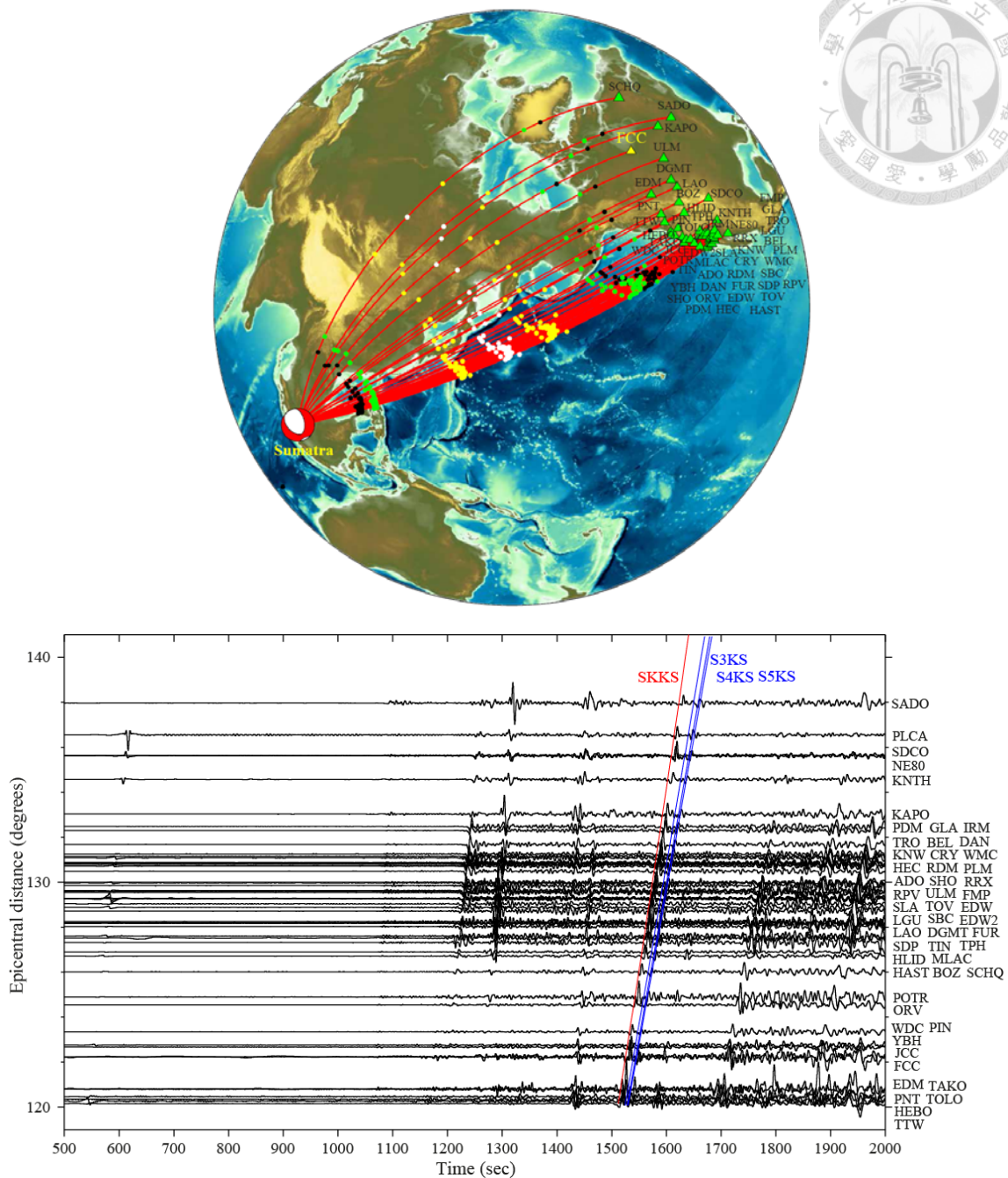
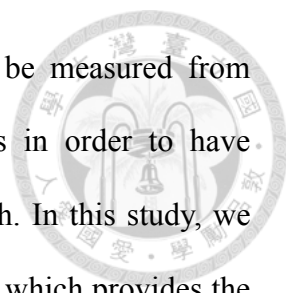


Fig. 2.3 (Top) Focal mechanism (beachball) of the 25 July 2004 Sumatra earthquake ($M_w=7.3$, depth=600.5 km) and the great-circle paths (red lines) to 54 stations (green triangles) in North America in the distance range 120° - 140° . Color dots on the paths are locations where SKKS and S3KS interact with the CMB. (Bottom) Radial-component velocity records from Sumatra earthquake to the 54 stations. Red line is the predicted SKKS traveltimes based on PREM predicted by the TauP Toolkit (Crotwell *et al.*, 1999), whereas the blue lines are predicted traveltimes of S_m KS based on PREM. All waveforms have been bandpass filtered between 0.005 Hz and 0.2 Hz.



Since the SKKS and $SmKS$ differential travel times have to be measured from waveforms, we also need synthetic seismograms of these phases in order to have equivalent model-predicted differential travel times to compare with. In this study, we adopt the numerical algorithm of the direct-solution method (DSM), which provides the exact synthetic seismograms based on 1D models.

2.3 Waveform simulation: the direct-solution method

As mentioned before, the SKKS and S3KS waveforms are best observed at frequencies below 0.2 Hz in records. As a result, their onset times are difficult to pick and have relatively large uncertainties. In order to ensure data quality, we measure the SKKS and S3KS differential traveltimes by cross correlations of their waveforms in records. This requires us to be able to calculate their synthetic seismograms so that we can obtain equivalent measurements to compare. In this study, we use the direct-solution method to compute exact synthetic seismograms based on 1D models (Cummins *et al.*, 1994; Geller & Ohminato, 1994; Kawai *et al.*, 2006).

The direct solution method (DSM) is closely related to the normal-mode summation method. Both methods solve the seismic wave equation by decomposing the solutions into spherical harmonics horizontally and radial eigenfunctions vertically. However, in normal-mode summation, the synthetics are calculated in two steps: (1) compute the radial eigenfunctions (solving the homogeneous equation with no source); and (2) sum the eigenfunctions with weights determined by the earthquake source to get the synthetics. Eigenfunctions calculated in Step (1) can be archived and used for any earthquakes. This makes the normal-mode summation method more efficient in computing synthetics for many earthquakes.

The DSM does not solve for source-free radial eigenfunctions, but finds the radial solutions directly for the inhomogeneous wave equation with an earthquake source. It uses triangular splines as radial basis functions, and the solution is specified by the expansion coefficients. The solution is expressed in the frequency domain:

$$\mathbf{u}(r, \theta, \phi, \omega) = \sum_k \sum_l \sum_m [A_{klm}(\omega) X_k(r) Y_{lm}(\theta, \phi) \hat{\mathbf{r}} + B_{klm}(\omega) X_k(r) \nabla^\Sigma Y_{lm}(\theta, \phi) + C_{klm}(\omega) X_k(r) (\hat{\mathbf{r}} \times \nabla^\Sigma) Y_{lm}(\theta, \phi)], \quad (2.1)$$

where $Y_{lm}(\theta, \phi)$ is the surface spherical harmonic of degree l and order m , and $X_k(r)$ is the k -th radial basis functions of order. The expansion coefficients A_{klm} , B_{klm} and C_{klm} are constrained by the earthquake source and solved by systems of linear equations. Once the frequency-domain solution is obtained, time domain response (waveform) is obtained by an inverse Fourier transform. The steps for calculating DSM synthetics are as follows:

DSM modeling procedure

1. Edit the input file including the Earth model, the earthquake source location and moment tensor; and the station locations (there can be more than one stations at a time). The file also contains parameters for the maximum frequency of the seismograms as well as their length in time.
2. Run the DSM code to compute the frequency-domain responses of the P-SV and SH systems. Since the frequency-domain samples can be divided and calculated independently, the computation can be done in parallel on any number of processors to reduce the CPU time. The P-SV and SH systems calculated on different processors are merged after the parallel computations are completed.
3. Apply an inverse Fourier transform to the merged frequency-domain response to obtain the time-domain seismograms. The DSM results are velocity response.

4. The results are then convolved with a Gaussian-shaped source-time function given by the time shift and half duration in the earthquake's GCMT solution.

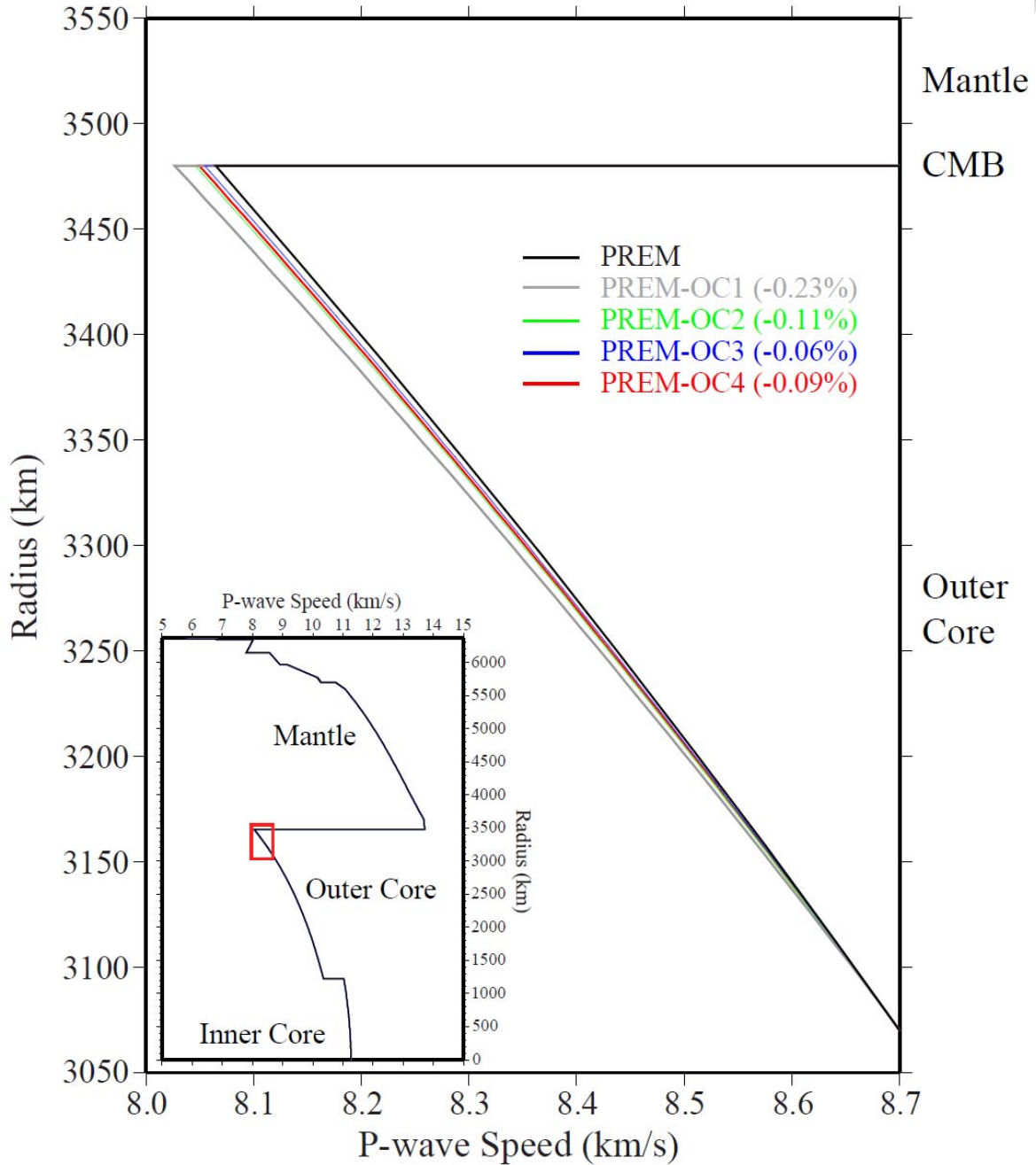


Fig. 2.4 Five models used to study the effect of the structure atop the outer core on differential traveltime $T_{S3KS}-T_{SKKS}$. PREM is shown in black. Gray, green, blue and red lines show models PREM-OC1, PREM-OC2, PREM-OC3 and PREM-OC4 which are the same as PREM except in the 400-km layer immediately below CMB, where the wave speed is reduced by about 0.23%, 0.11%, 0.06% and 0.09% on average.

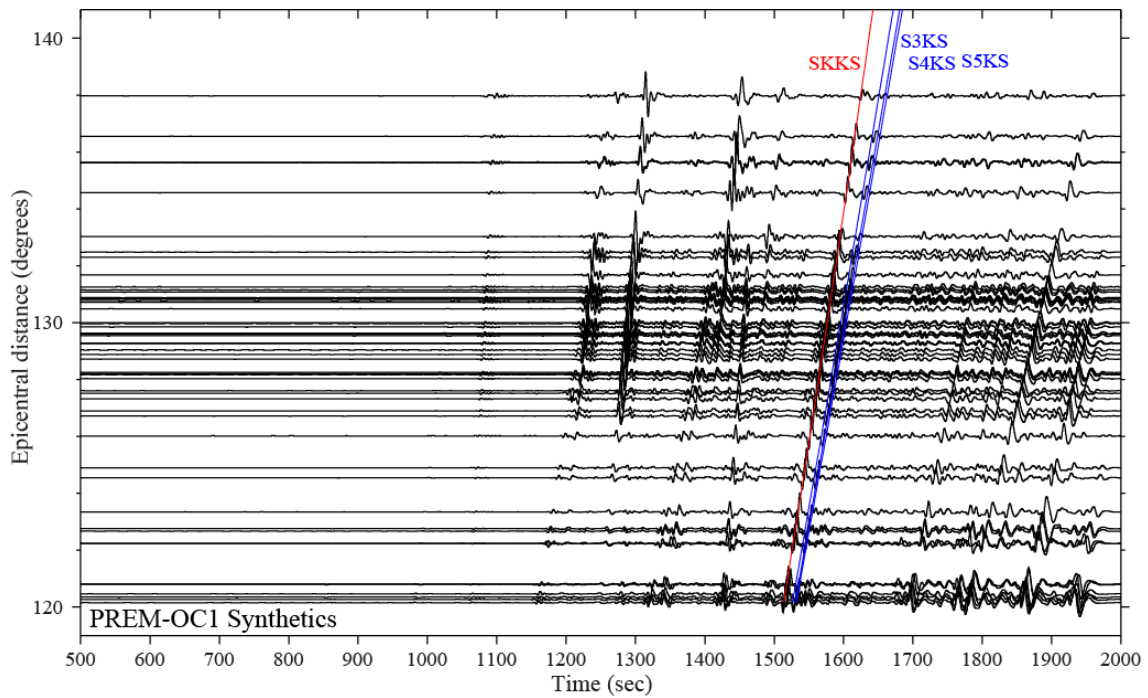
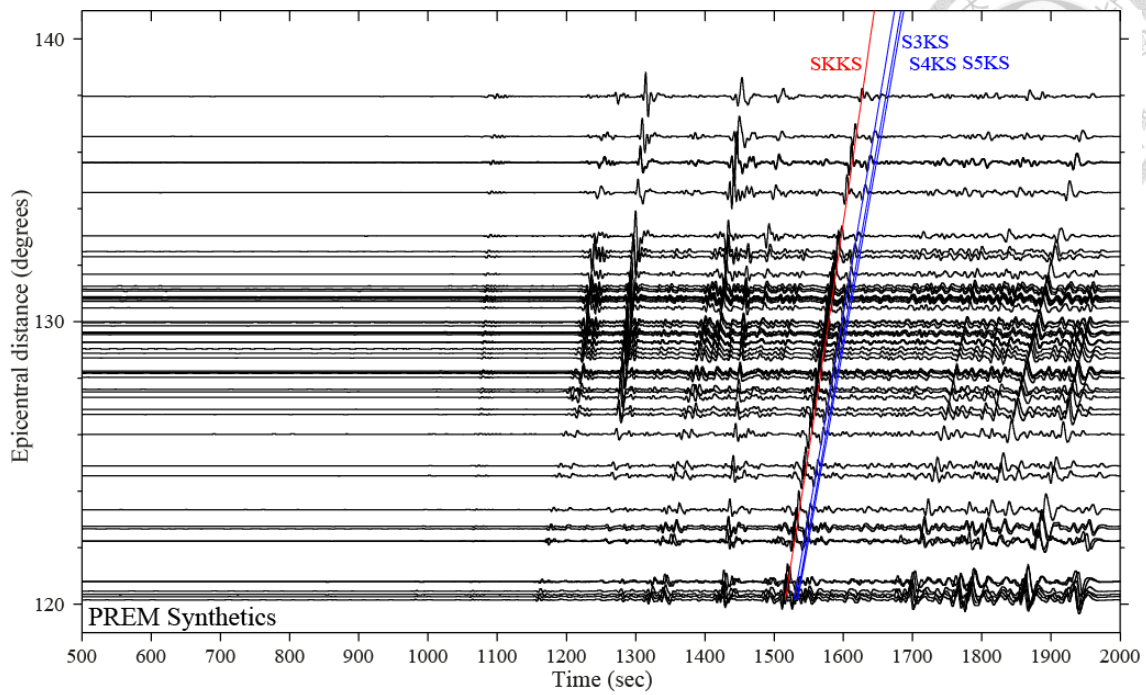


Fig. 2.5 (Top) DSM radial-component synthetics based on PREM for the 2004 Sumatra earthquake at 54 stations in North America (source and station locations are shown in **Fig.2.3**). Red and blue lines are traveltime curves of SKKS and SmKS waves calculated by the TauP Toolkit. (Bottom) Same as the top plot but for Model PREM-OC1. The traveltime curves are for model PREM. All waveforms have been bandpass filtered between 0.005 Hz and 0.2 Hz.

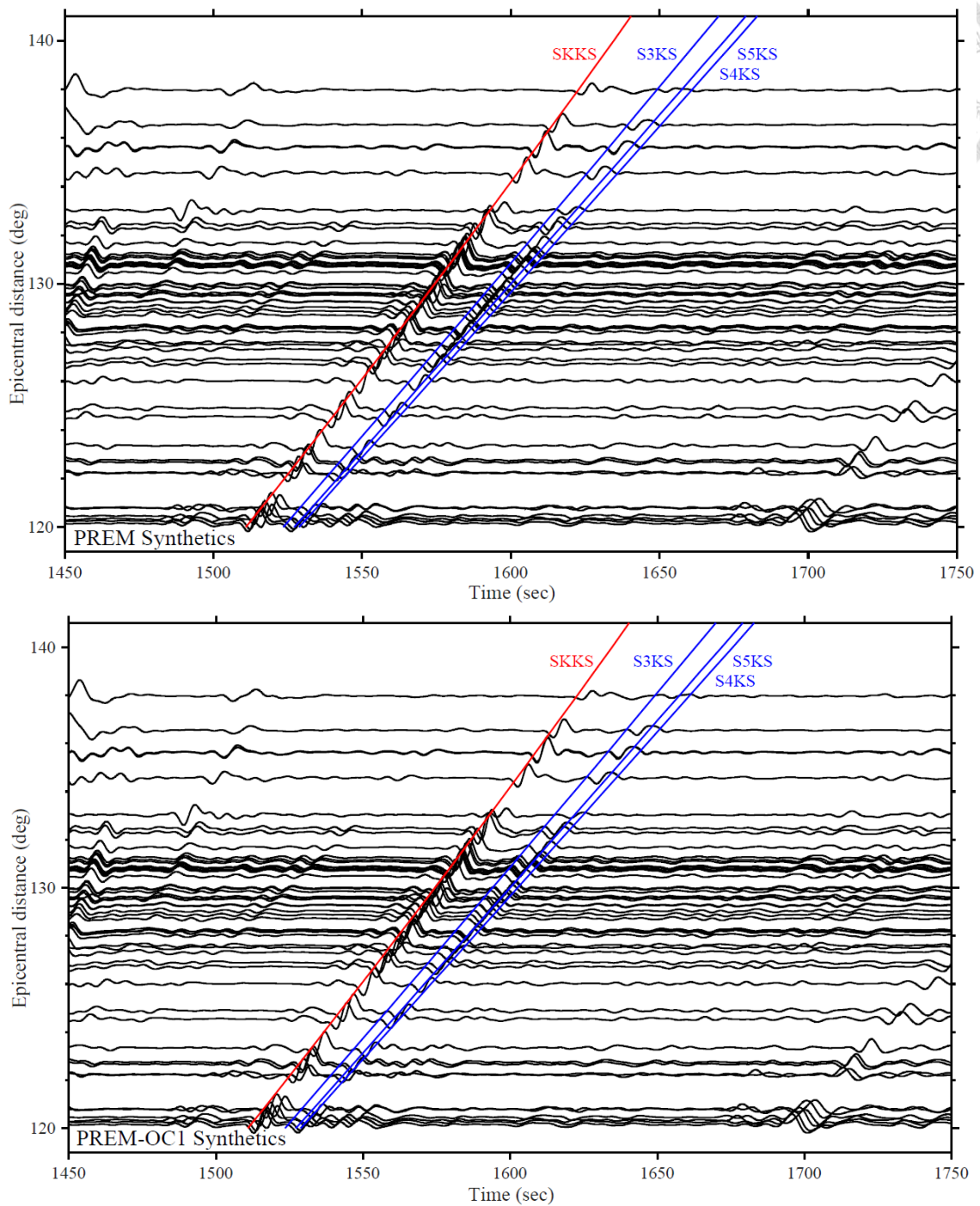


Fig. 2.6 Zoom-in of the waveforms in **Fig. 2.5** around the SKKS and S3KS arrivals. In the bottom plot, delays can be seen in the SKKS and S3KS waveforms relative to the PREM traveltime curves for corresponding waves.

Follow this procedure, it usually takes about 5 hours to compute the DSM synthetics up to 1 Hz using 8 computing nodes (12 cores on each node). The radial-component

synthetics are then filtered in the same way as the records to make S3KS-SKKS differential traveltime measurements. Using DSM it is very easy to replace the Earth model or the earthquake source and calculate their DSM synthetics. **Fig.2.4** shows the model PREM as well as several PREM-like models we use in this study. **Fig.2.5** displays the DSM synthetic seismograms for the same earthquake and stations as those in **Fig.2.3** but for two different Earth models: PREM and PREM-OC1. PREM-OC1 is the same as PREM everywhere except for the top 400 km of the outer core, where the P-wave speed is reduced by $\sim 0.23\%$ on average. The synthetics clearly show that the S3KS-SKKS differential traveltimes are larger based on PREM-OC1, a model with a lower speed at the top of the outer core.

2.4 Differential traveltime measurements from records

Here we describe the process for measuring the differential travel times between the SKKS and the S3KS waves. **Fig.2.3** shows the recorded radial-component seismograms from the 2004 Sumatra earthquake at 54 stations in North America in the distance range 120° - 140° . We take the station FCC as an example to illustrate the measurement process, as shown in **Fig.2.6**.

First we choose an appropriate time window for the SKKS wave based on its TauP-predicted travel time in PREM. Usually the waveform of SKKS can be clearly identified, and we choose its window with a width of only half of its period in order to minimize the contamination of neighboring phases (**Fig.2.6a**). Then we apply a Hilbert transform to the recorded waveform with a focus on the S3KS wave:

$$Hu_{S3KS}(t) = h(t) * u_{S3KS}(t) = \int_{-\infty}^{\infty} u_{S3KS}(\tau) h(t-\tau) d\tau = \frac{1}{\pi} \int_{-\infty}^{\infty} \frac{u_{S3KS}(\tau)}{t-\tau} d\tau, \quad (2.2)$$

where $h(t)$ stands for the Heaviside-step function. The definition in eq.(2.2) shows that

the Hilbert transform adds a $\pi/2$ phase shift to the S3KS waveform. This is to account for the extra caustic along the S3KS ray path in comparison to SKKS. A time window is also determined in the Hilbert-transformed S3KS waveform (**Fig.2.6b**).

Finally we compute the cross-correlation between the SKKS waveform and the Hilbert-transformed S3KS waveform

$$(u_{\text{SKKS}} \otimes H u_{\text{S3KS}})(t) = \int_{-\infty}^{\infty} u_{\text{SKKS}}(\tau) H u_{\text{S3KS}}(t + \tau) d\tau, \quad (2.3)$$

and the differential time $T_{\text{S3KS}} - T_{\text{SKKS}}$ is the lag time when the cross correlation reaches the maximum (**Fig.2.6c**). In this study, time series operations, such as deconvolution of instrument responses, filtering, Hilbert transform, and cross correlation are done in the software package SAC (Seismic Analysis Code, Helffrich *et al*, 2013).

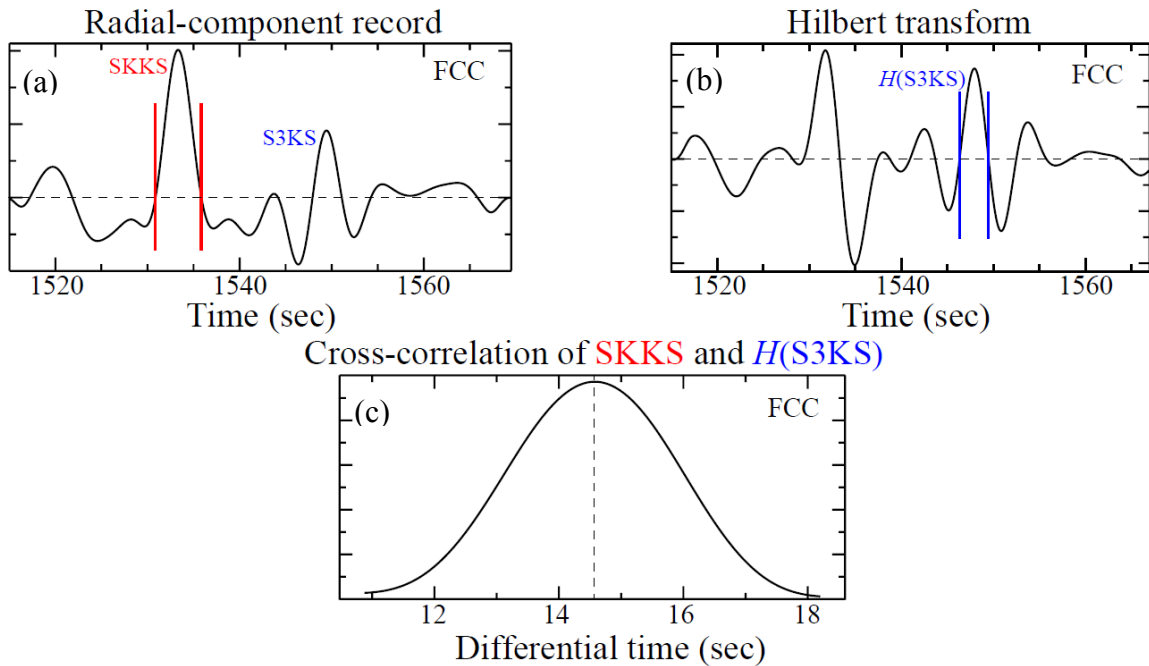


Fig. 2.7 (a) Radial-component record of the 2004 Sumatra event to station FCC (yellow triangle in **Fig. 2.3**) showing the SKKS and S3KS. Red bars indicate the time window for SKKS used in making cross-correlation measurement; (b) Hilbert transform of the record in (a). Blue bars indicate the time window for Hilbert-transformed S3KS; and (c) Cross-correlation of the windowed portions of the waveforms in (a) and (b). The dashed line shows the differential traveltime measurement. All waveforms have been band-pass filtered between 0.005 Hz and 0.2 Hz.

This results in the observed differential traveltimes between the SKKS and S3KS waves obtained from records:

$$\Delta T = T_{S3KS} - T_{SKKS}. \quad (2.4)$$

Following this process, we analyzed the waveforms of a total of 78 earthquakes and obtained high-quality measurements of differential traveltimes $T_{S3KS}-T_{SKKS}$ at 374 stations.

2.5 Differential traveltimes measurements from synthetics

The radial-component DSM synthetics in **Fig.2.5** in the two models (PREM and PREM-OC1) from the Sumatra earthquake at 54 stations in North America in the distance range 120°-140°. We use the same station FCC to illustrate the measurements of differential traveltimes $T_{S3KS}-T_{SKKS}$ from synthetics, as shown in **Fig.2.7**. The process is exactly the same as for the records: A time window is chosen for the SKKS wave (**Fig.2.7a**). Then a Hilbert transform is applied to the waveform and a time window is chosen for the transformed S3KS waveform (**Fig.2.7b**). Finally the waveforms in the two windows are cross correlated, and the differential traveltimes is determined from the maximum of the cross correlation (**Fig.2.7c**).

This results in the model-predicted differential traveltimes between the SKKS and S3KS waves obtained from synthetic seismograms:

$$\Delta \tilde{T}^{\text{MODEL}} = \tilde{T}_{S3KS}^{\text{MODEL}} - \tilde{T}_{SKKS}^{\text{MODEL}}. \quad (2.5)$$

Note that we use the same symbol in eq.(2.5) as in eq.(2.4), but with a "~" overhead to indicate model-predicted quantities. For every observed differential traveltimes, we calculate the corresponding DSM synthetics for PREM and for several PREM-like models (**Fig. 2.4**), and measure SKKS and S3KS differential times in the same way.

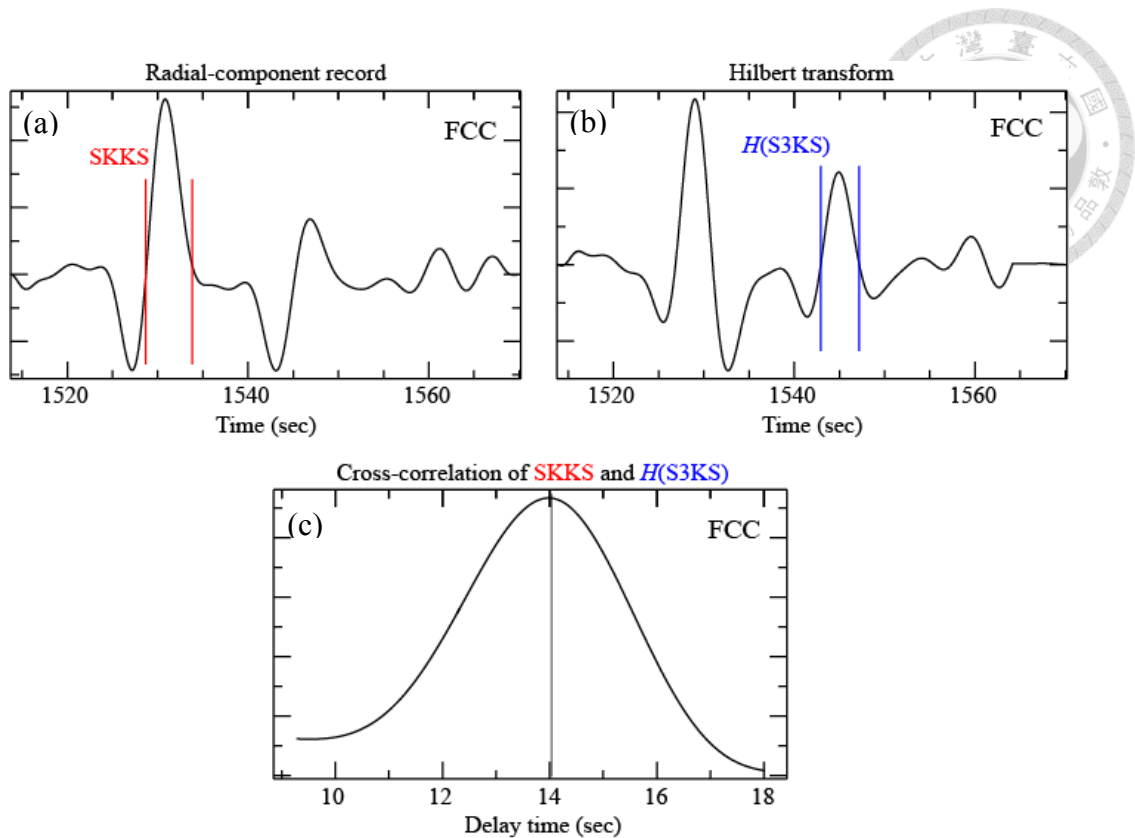


Fig. 2.8 (a) Radial-component synthetic of the Sumatra event at station FCC showing on the SKKS and S3KS waves. Red bars indicate the time window for SKKS used in making cross-correlation measurement; (b) Hilbert transform of the synthetic in (a); and (c) Cross-correlation of the windowed portions of the waveforms.

2.6 Quality control of differential traveltimes measurements

The examples in **Figs.2.6** and **2.7** demonstrated very robust measurements of differential traveltimes between SKKS and S3KS waves, as indicated by the similarity in the waveforms of SKKS and the Hilbert-transformed S3KS. However, as the epicentral distance increases, the S3KS wave becomes weaker, and the SNR decreases. In addition, radiation pattern can also reduce the strength of SKKS and S3KS waves. The effect of lateral heterogeneity introduces further complexities in the recorded waveforms. Therefore, the quality of the SKKS and S3KS waveforms are not always perfect, and there is a need to impose a quality control on both the observed and

model-predicted differential traveltime measurements. In this study, we follow these steps and criteria:

1. For each data, we determine its measurement quality based on both the recorded and synthetic seismograms. In other words, we require the waveform of the Hilbert-transformed S3KS to be similar to SKKS to be true for both record and its corresponding synthetic in PREM. The requirement for synthetic ensures that the effect of lateral heterogeneity is small. Based on the visual inspection of the recorded waveforms of SKKS and S3KS waves, a quality score of 1 to 10 is assigned, with 10 being the highest quality. Similarly, a quality score is assigned to the synthetic. As a result, the highest quality differential traveltime has a score of 20, as in the case of FCC shown in **Figs.2.6** and **2.7**.

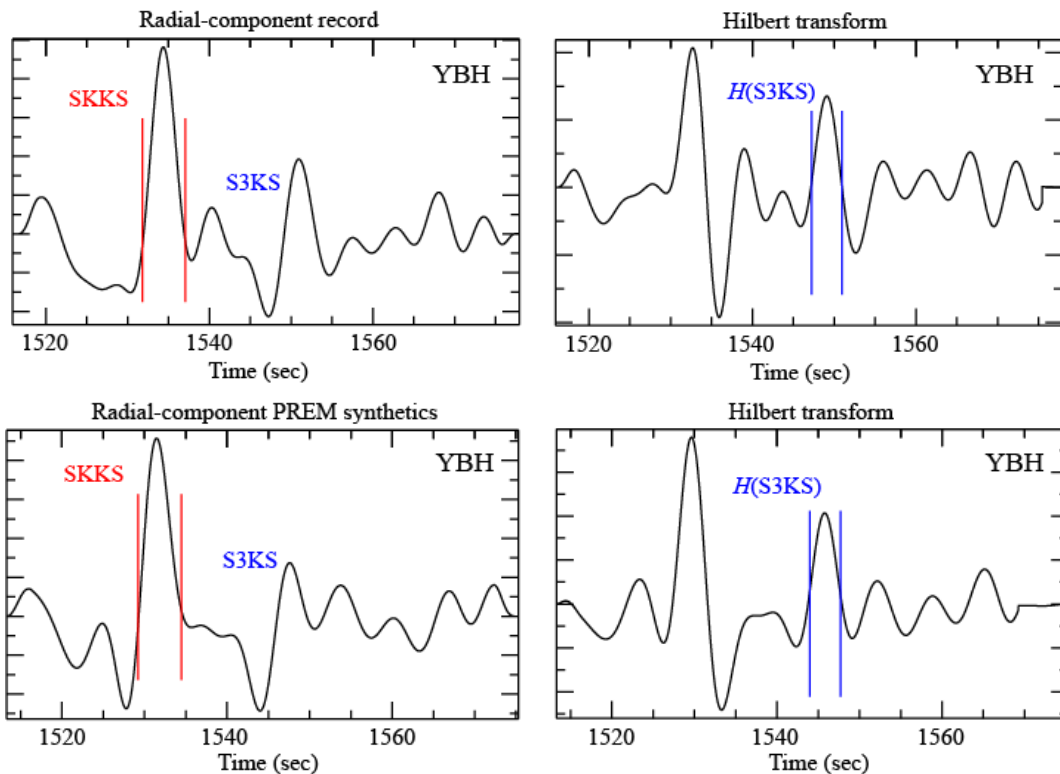


Fig. 2.9 (Top panels) Record (left) at station YBH from the Sumatra event and its Hilbert transform (right). A quality score of 10 is given to this record. (Bottom panels) Synthetic (left) and its Hilbert transform (right) for the same source-station pair. A quality score of 9 is given due to slight distortions of S3KS waveform.

- In many cases, the SKKS waveforms are very clear, but the waveforms of S3KS are affected by other phases arriving slightly earlier or later, thus distorting the beginning and/or ending parts of the S3KS waveforms. This can also happen in records and/or synthetics. We assign quality scores of 19 and 18 based on the level of distortion of the S3KS waveforms. As shown in **Figs.2.8** and **2.9**.

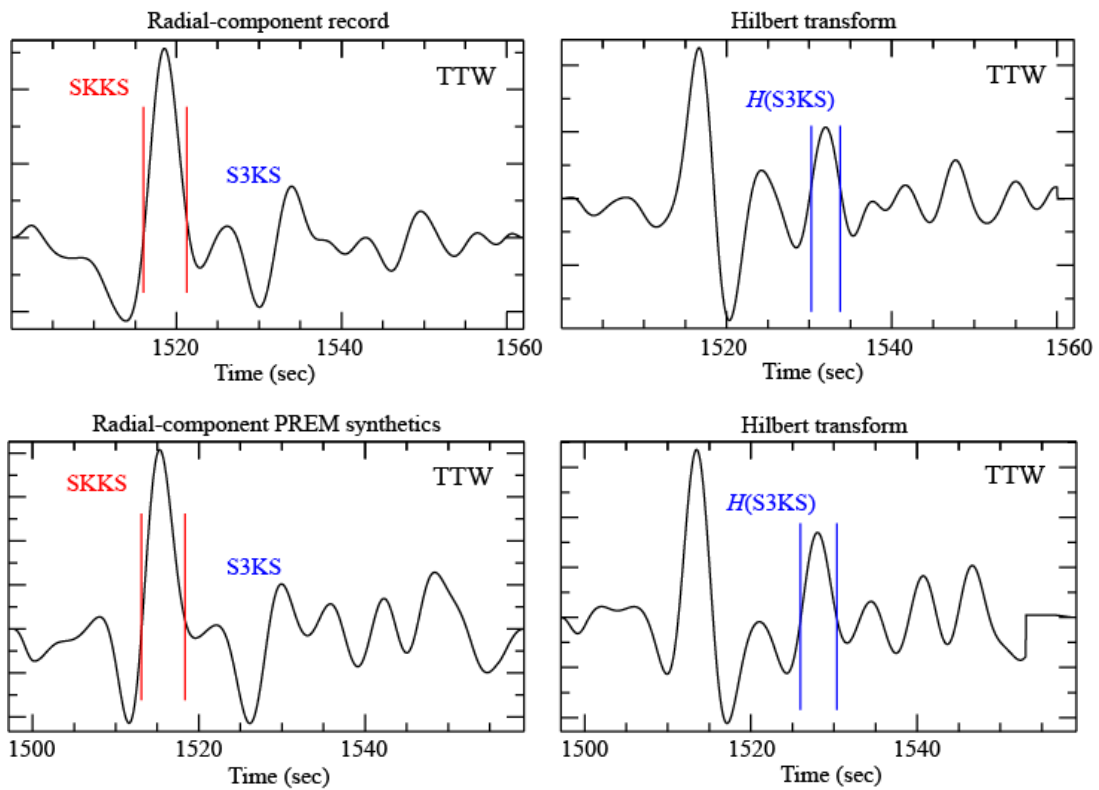


Fig. 2.10 (Top panels) Record (left) at station TTW from the Sumatra event and its Hilbert transform (right). (Bottom panels) Synthetic (left) and its Hilbert transform (right) for the same source-station pair. Both record and synthetic are given a quality score of 9 due to slight distortions in the S3KS waveforms.

- Sometimes there appears to be some anomaly in the relative amplitudes between the SKKS and S3KS waves, such as the record at station PNT from the Sumatra earthquake shown in **Fig.2.10**. This will also affect the quality score given to the measurement.

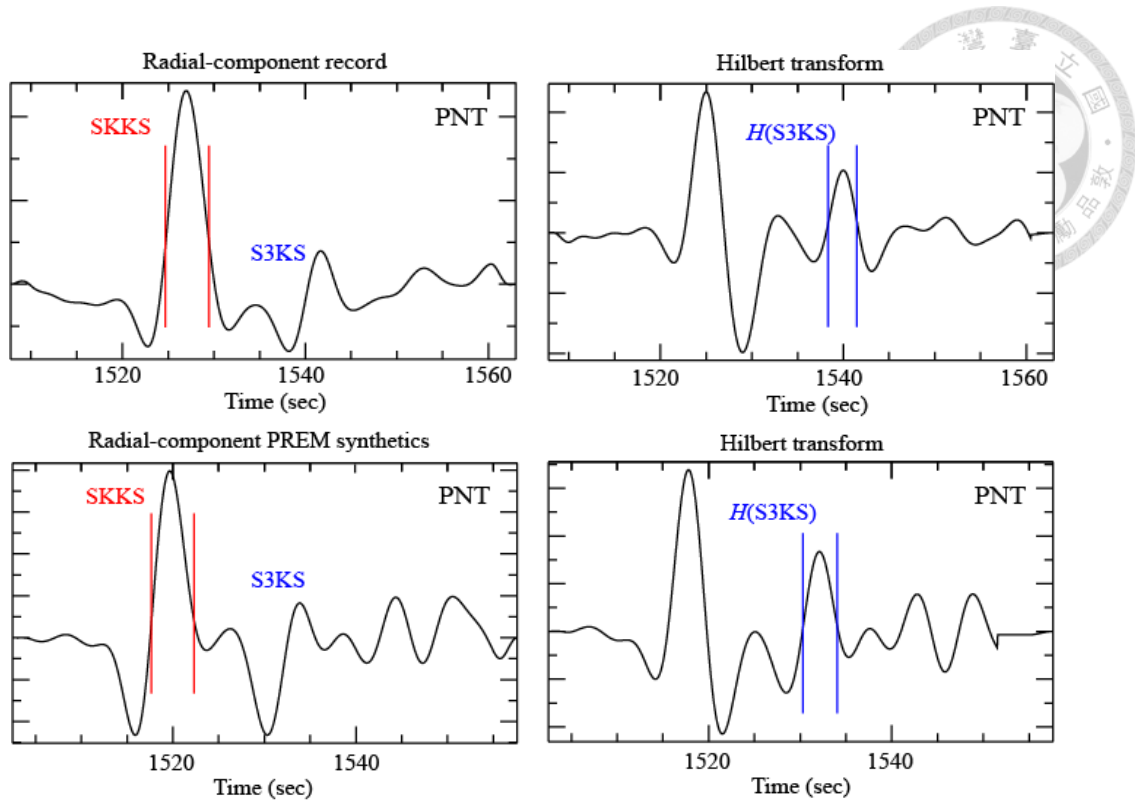


Fig. 2.11 Quality scoring for station PNT from the Sumatra event. The record is given a quality score of 9 due to anomalously large amplitude ratio between SKKS and S3KS, whereas the synthetic is given a score of 8.

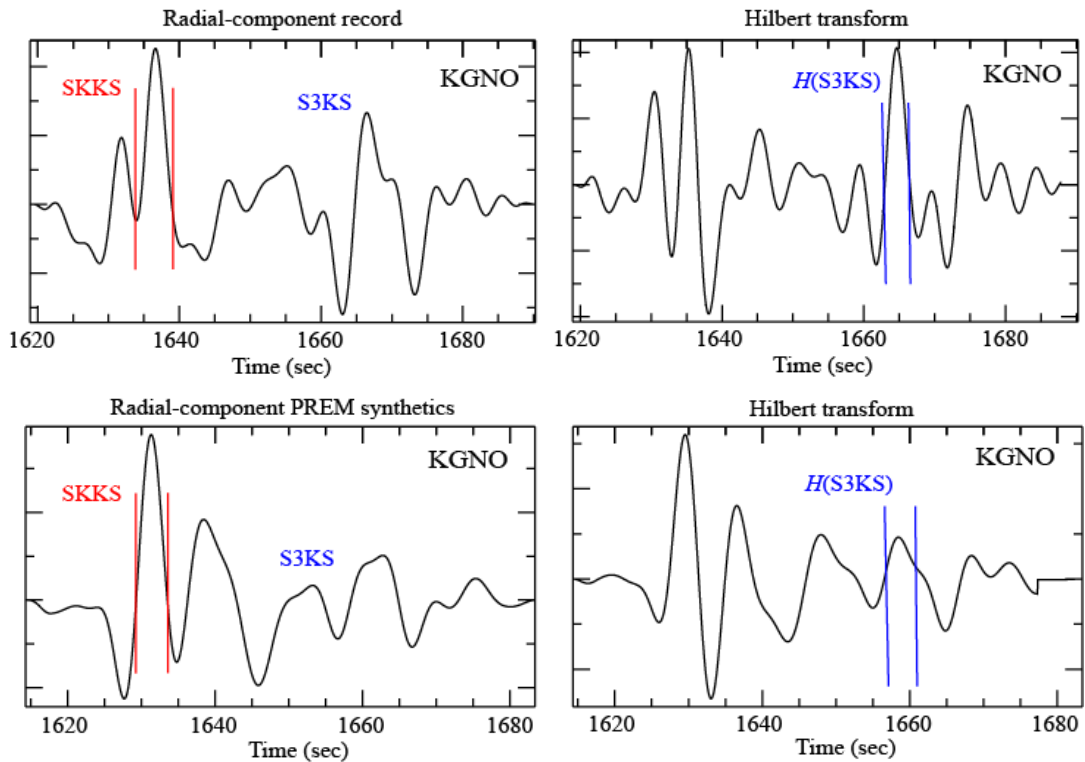


Fig. 2.12 Quality scoring for station KGNO from the Sumatra event. Both record and synthetic are given a score of 8.

4. As the epicentral distance increases, especially beyond 135° , the relative strength of S3KS in the *SmKS* group decreases, and the S3KS waveforms have increasingly larger interference with the neighboring phases. As a result, the S3KS waveforms become less clear and the differential traveltimes obtained by waveform cross correlation are less robust, as shown in **Figs.2.11** and **2.12**. In this study, only measurements with quality scores of 17 and above are used for further analysis.

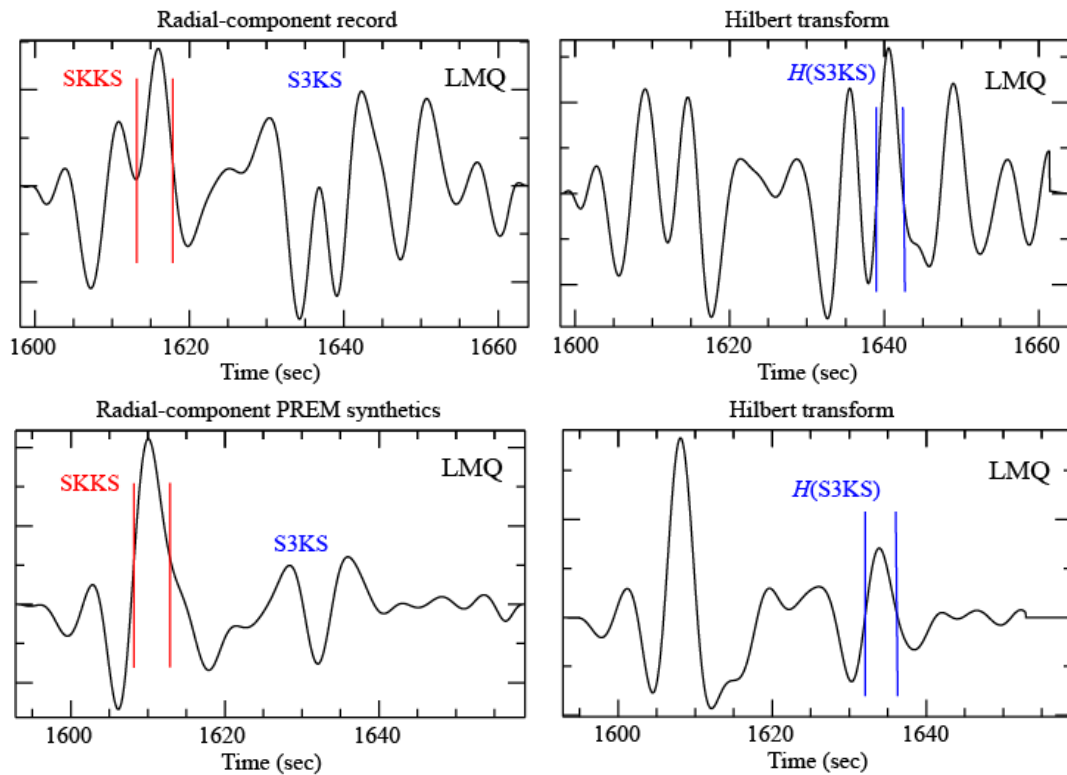


Fig. 2.13 Quality scoring for station LMQ from the Sumatra event. The record is given a quality score of 7, whereas the synthetic is given a score of 8.

Chapter 3 Modeling *SmKS* Differential Traveltimes



Follow processes described in Chapter 2, we measured the differential traveltimes between SKKS and S3KS from both recorded seismograms and the DSM synthetics in PREM as well as several PREM-like 1D models. We also assigned quality score to each observed differential traveltime measurement based on visual inspection of the record and its corresponding synthetic in PREM. In the end, a total of 606 measurements of quality score 17 and above are retained for further analysis. In this chapter, we compare the observed differential traveltimes with their corresponding predictions by PREM and PREM-like models to examine their discrepancies and their possible reasons.

3.1 Ray theory features of SKKS and S3KS waves

In order to identify the region of the Earth whose structure has the most influence on the S3KS-SKKS differential traveltimes, we first look at some ray theory features of these waves such as their ray parameters and depths of turning points in the outer core.

Fig.3.1 displays the values of the ray parameters and the turning depths of SKKS and S3KS waves in the distance range 120° - 140° , calculated for Models PREM and PREM-OC1 by the TauP Toolkit. The ray parameters of the SKKS and S3KS waves in this distance range vary in 5.8~6.5 s/deg and 6.8~7.1 s/deg, respectively. For both waves, the ray parameters monotonically decrease with epicentral distance. The S3KS waves all turn in the top 200 km of the outer core, where the SKKS waves can reach down to ~500 km below the CMB. The S3KS-SKKS differential traveltimes for these two models displayed in **Fig.3.2** clearly indicate that the model with a slower top outer core (PREM-OC1) has larger differential traveltimes at all distances.

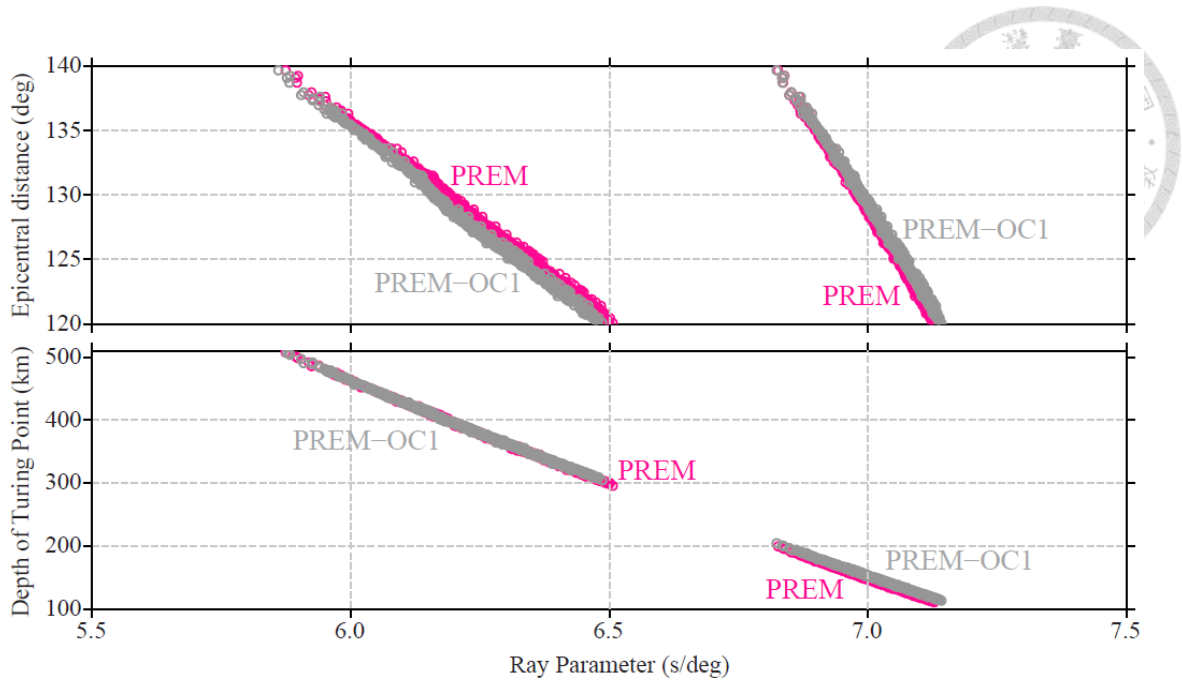


Fig. 3.1 (Top) Ray parameter distributions for the SKKS and S3KS waves in epicentral distance 120° - 140° , calculated for Models PREM (pink) and PREM-OC1 (gray) by the TauP Toolkit. Ray parameters of SKKS and S3KS decrease monotonically with distance almost linearly. (Bottom) Depths of the turning points of SKKS and S3KS measured from the CMB in the epicentral distance range 120° - 140° , calculated for Models PREM (pink) and PREM-OC1 (gray) by the TauP Toolkit. For both waves, their turning depths decrease monotonically with ray parameter (or increase with distance). SKKS turns in the depth range 300-500 km; S3KS turns in the range 100-200 km below the CMB.

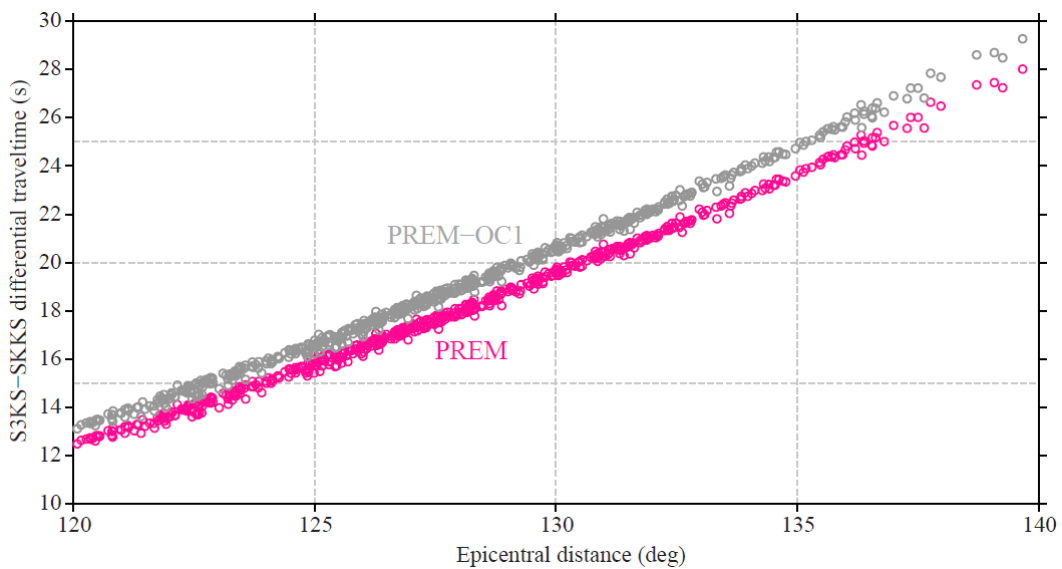


Fig. 3.2 S3KS-SKKS differential traveltimes in the epicentral distance range 120° - 140° , calculated for Models PREM (pink) and PREM-OC1 (gray) by the TauP Toolkit.

3.2 Observed and model-predicted differential traveltimes

Here we discuss the observed differential traveltimes $\Delta T = T_{S3KS} - T_{SKKS}$ obtained from recorded seismograms. After a rigorous inspection of all the recorded and synthetic waveforms of SKKS and S3KS waves, we selected 606 high-quality (quality score of 17 and above) differential traveltime measurements for further analysis. These measurements come from 78 events ($5.8 \leq M_w \leq 7.7$) and they are plotted against the epicentral distance in **Fig. 3.3**.

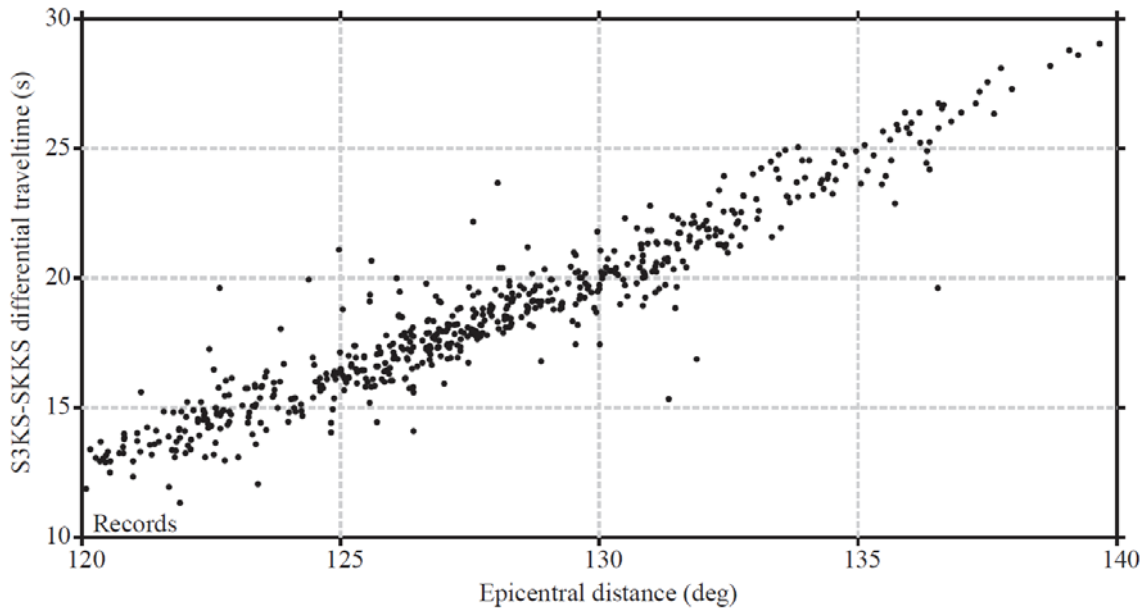


Fig. 3.3 606 observed S3KS-SKKS differential traveltimes $\Delta T = T_{S3KS} - T_{SKKS}$ with quality scores of at least 17 plotted against the epicentral distance.

All the data in **Fig.3.3** have been selected for their relatively high quality scores, and most of them are indeed clustered around a linear trend showing a clear increase in the differential traveltimes with the epicentral distance. However, the scattering of the measurements suggests a significant uncertainty in the data, and a number of them are quite far from the main cluster. Therefore, instead of using these raw measurements for analysis, we average them in 1° bins so that the main features in the data can be seen more clearly, and the comparisons with model-predicted results can also be done, as shown in **Figs.3.4-3.8**.

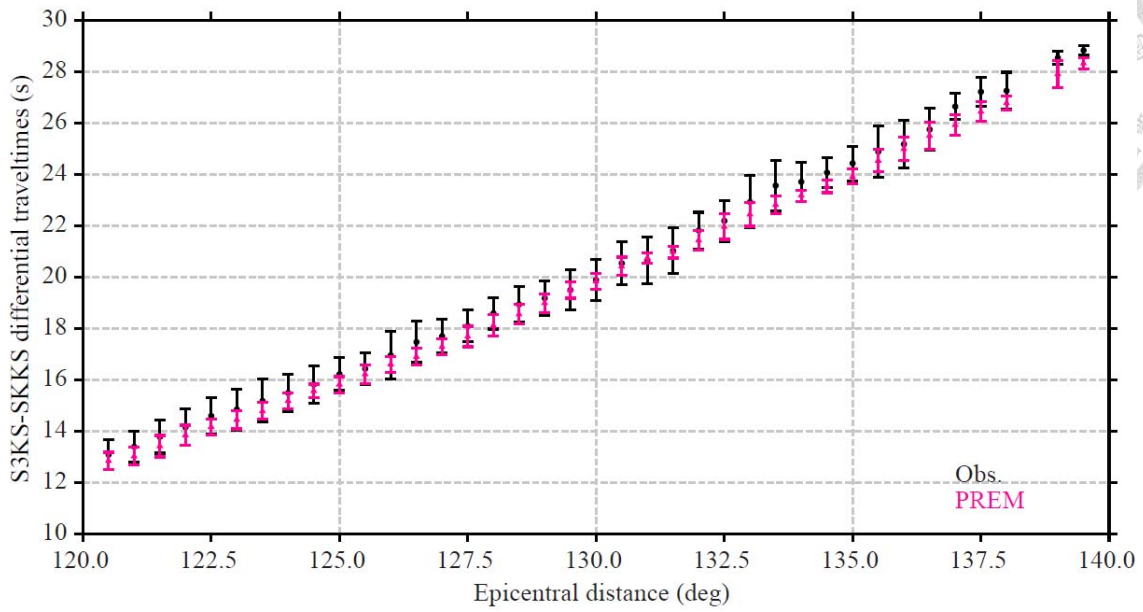


Fig. 3.4 Comparison between observed S3KS-SKKS differential traveltimes and predictions by Model PREM. The 606 measurements in **Fig.3.3** have been averaged every 0.5° over 1° bins, and plotted in black dots with bars showing the standard deviation. Purple triangles are predictions obtained from DSM synthetics for PREM and averaged in the same way. Model predictions are clearly smaller than observations, suggesting that PREM is too fast beneath the CMB.

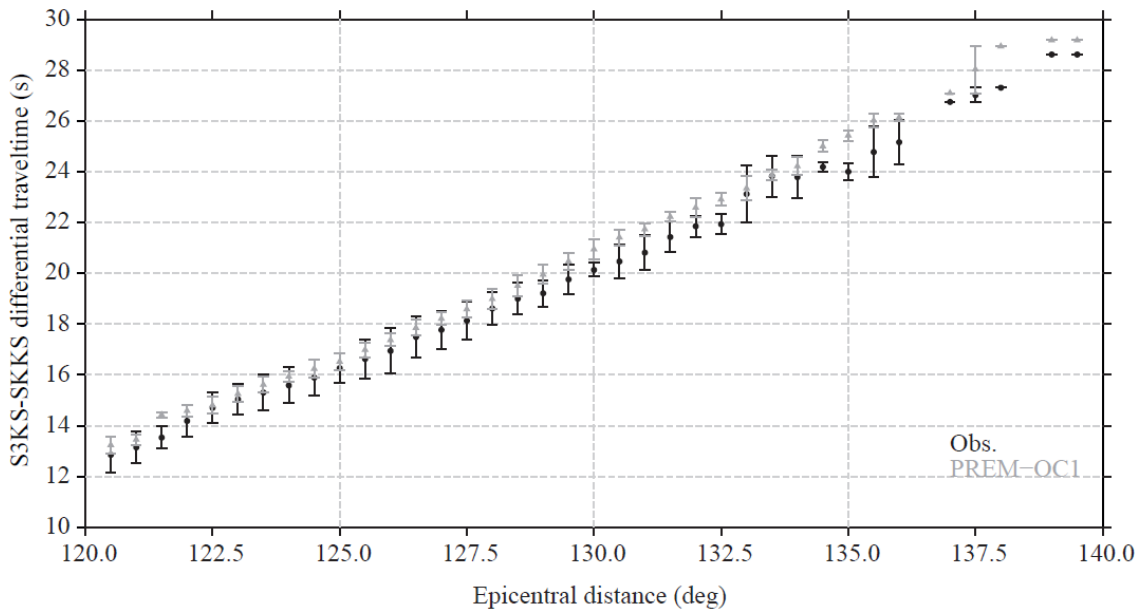


Fig. 3.5 Same as **Fig.3.4** but the predictions (gray symbols) are for Model PREM-OC1. With an average perturbation of about -0.23% below the CMB, Model PREM-OC1 is clearly too slow in the top of the outer core and will not be shown in later discussion.

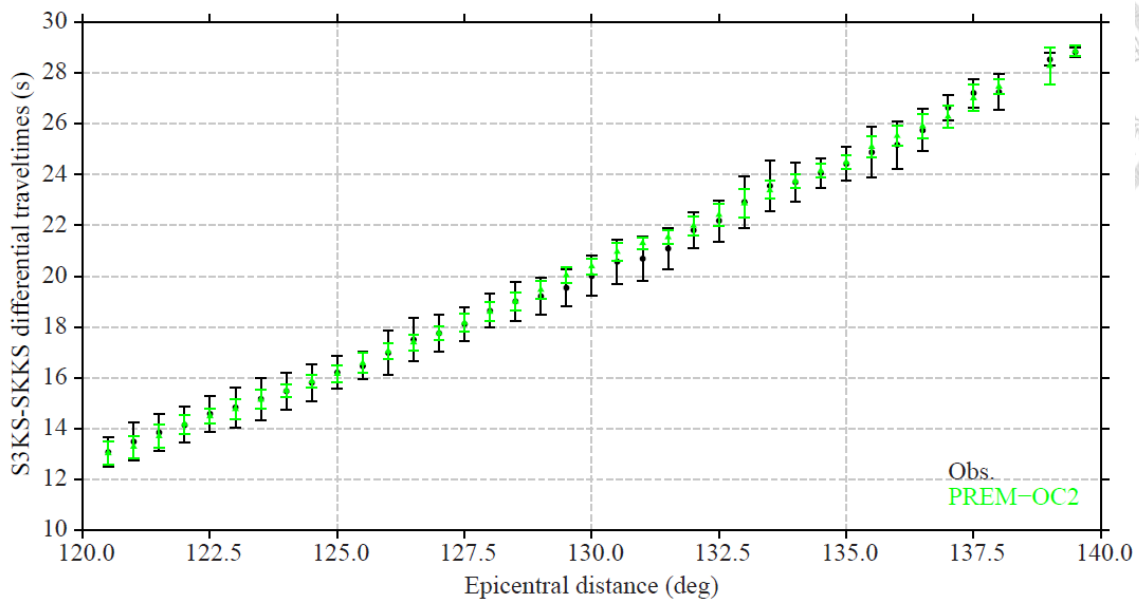


Fig. 3.6 Same as Fig.3.4 but the predictions (green symbols) are for Model PREM-OC2. With an average perturbation of about -0.11% below the CMB, Model PREM-OC2 performs better than PREM and PREM-OC1. Some of the model predictions are a bit larger than observations indicating that PREM-OC2 may be slightly too slow.

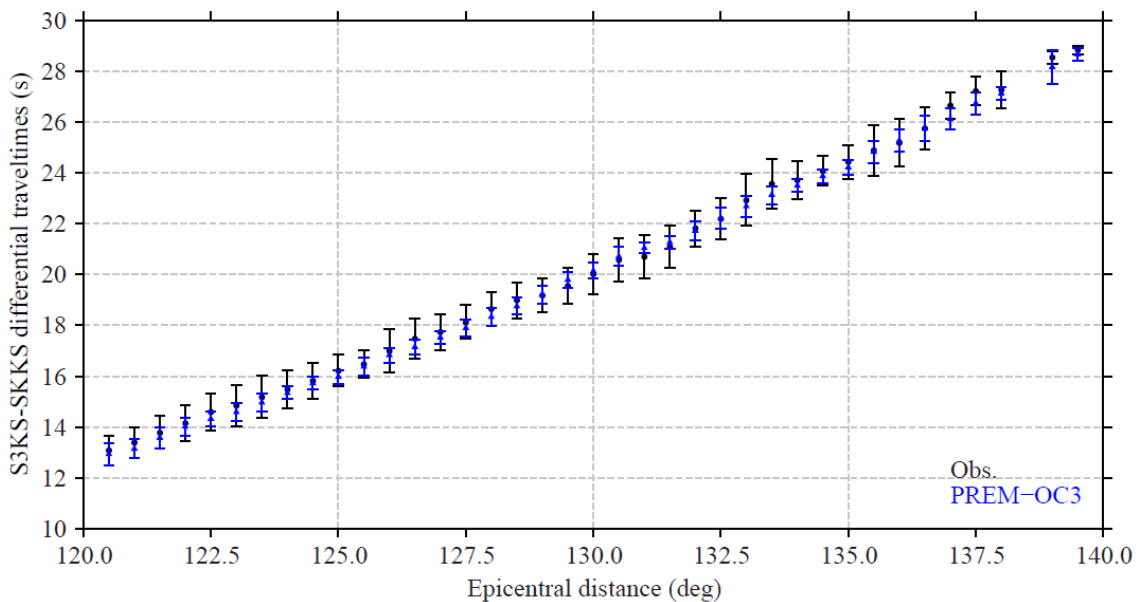


Fig. 3.7 Same as Fig.3.4 but the predictions (blue symbols) are for Model PREM-OC3. With an average perturbation of about -0.06% below the CMB, Model PREM-OC3 seems to be similar to PREM. Many model predictions are still smaller than observations.

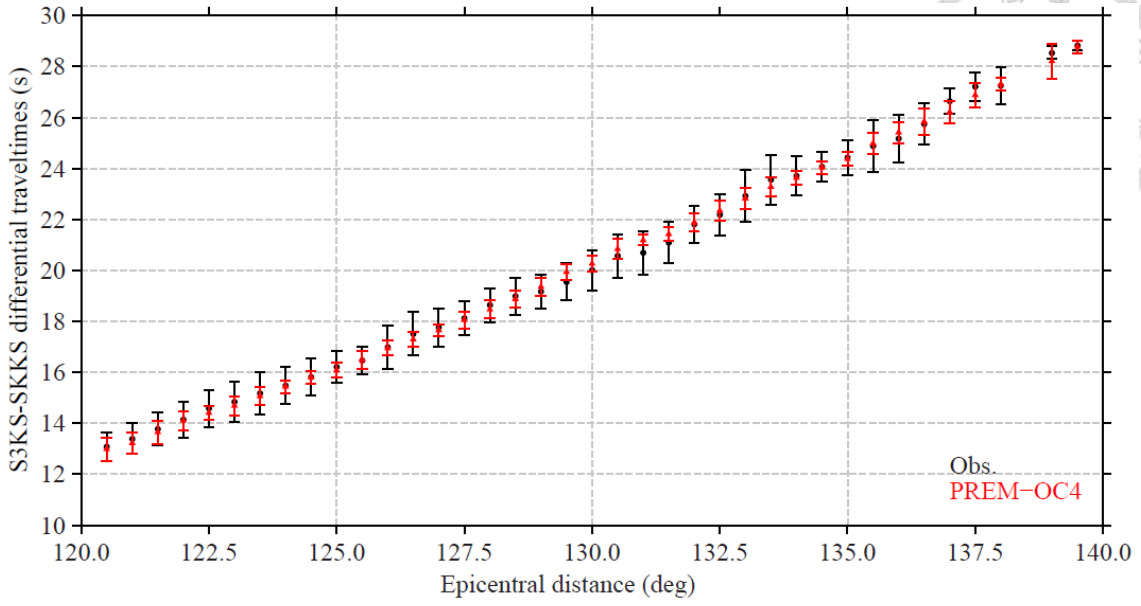


Fig. 3.8 Same as **Fig.3.4** but the predictions (red symbols) are for Model PREM-OC4. With an average perturbation of about -0.09% below the CMB, predictions by Model PREM-OC4 more closely follow the observations.

3.3 Double-differential travel times

The comparisons in **Figs.3.4-3.8** between the observed S3KS-SKKS differential traveltimes with the predictions by several PREM-like models suggest that Model PREM is indeed too fast in the top of the outer core. The tested models PREM-OC1 is too slow below the CMB, while PREM-OC3 may still be too fast. Models PREM-OC2 and PREM-OC4 seem to perform better, with predictions by PREM-OC4 showing closest agreement with the observed differential traveltimes.

Another way to make a more quantitative assessment of the performance of different models is by examining the double-differential traveltimes

$$\Delta^2 T^{\text{MODEL}} = \Delta T - \Delta \tilde{T}^{\text{MODEL}}, \quad (3.1)$$

where ΔT and $\Delta \tilde{T}^{\text{MODEL}}$ are the observed and model-predicted differential traveltimes defined in eqs.(2.4) and (2.5), respectively. An ideal model would make perfect

differential traveltime predictions so that $\Delta^2 T^{\text{MODEL}} \approx 0$. In **Figs.3.9-3.12** we plot the values of the double-differential traveltimes for the tested models. They are plotted both as against the epicentral distances as in **Figs.3.4-3.8** and in mapview.

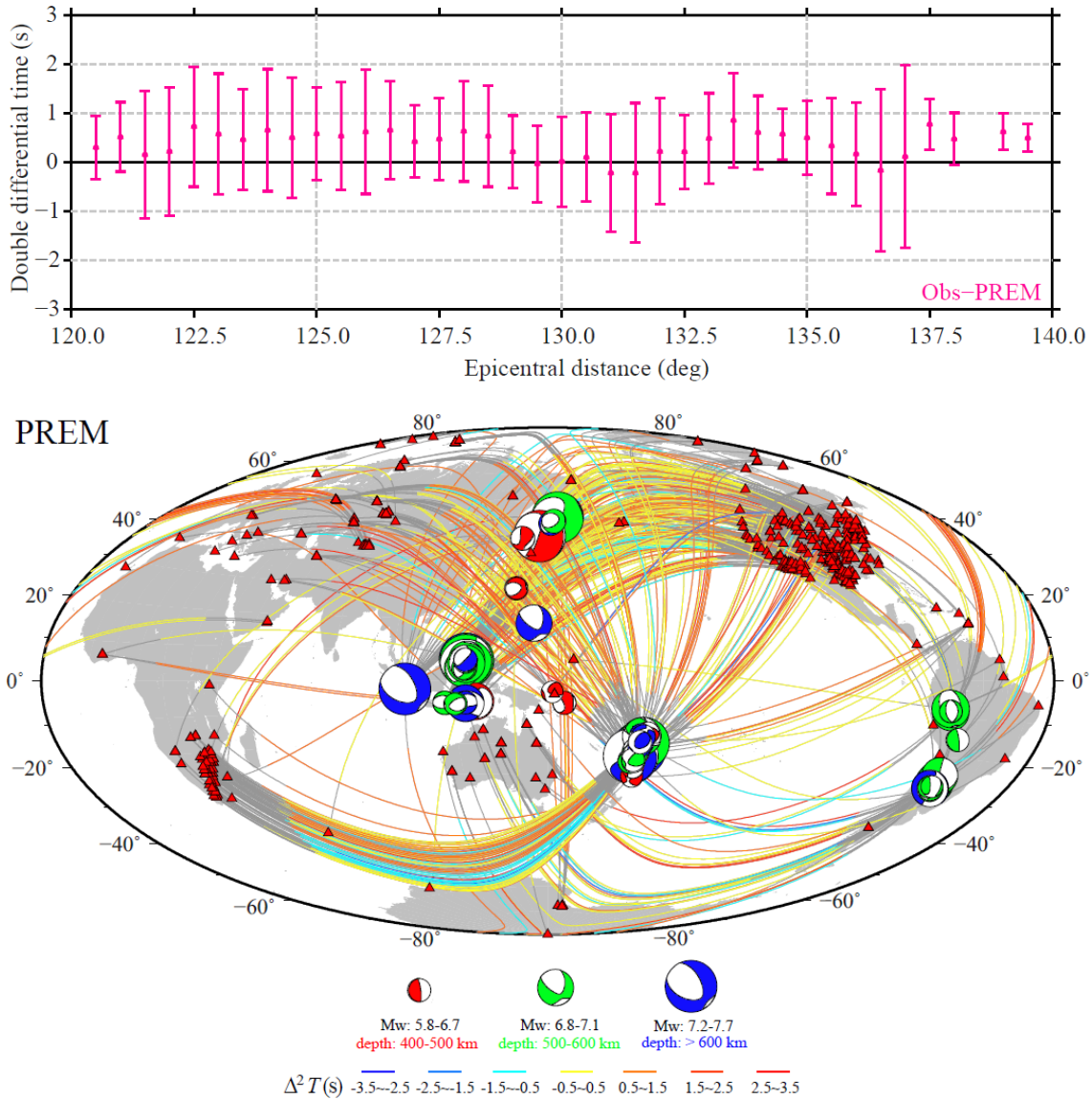
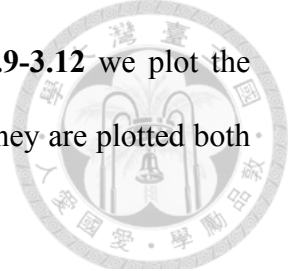


Fig. 3.9 (Top) Plot of double differential traveltimes $\Delta^2 T^{\text{PREM}}$ against epicentral distance. The data have been plotted by the values averaged every 0.5° over 1° -bins with the bars showing the standard deviation. (Bottom) 606 source-receiver great-circle paths for which we obtained the observed differential traveltime data. The paths are plotted such that portions outside the core are in gray while portions inside the core are in color. The color of a path indicates the value of $\Delta^2 T^{\text{PREM}}$. Positive values (warm colors) mean PREM is too fast in the outer core.

In the mapview plots in **Figs.3.9-3.12**, each value is plotted along the great-circle path from which the observed differential traveltime ΔT is obtained. For each great-circle, the portion of the path outside the core is plotted in gray while the portion inside the outer core is in color according to the value of $\Delta^2 T^{\text{MODEL}}$. Positive values are plotted with warm colors, indicating that the model is too fast in the outer core along those paths; negative values are plotted with cool colors, indicating that the model is too slow below the CMB along those paths. Therefore, the colors and their strengths can tell us how well a model performs in predicting the S3KS-SKKS differential traveltimes.

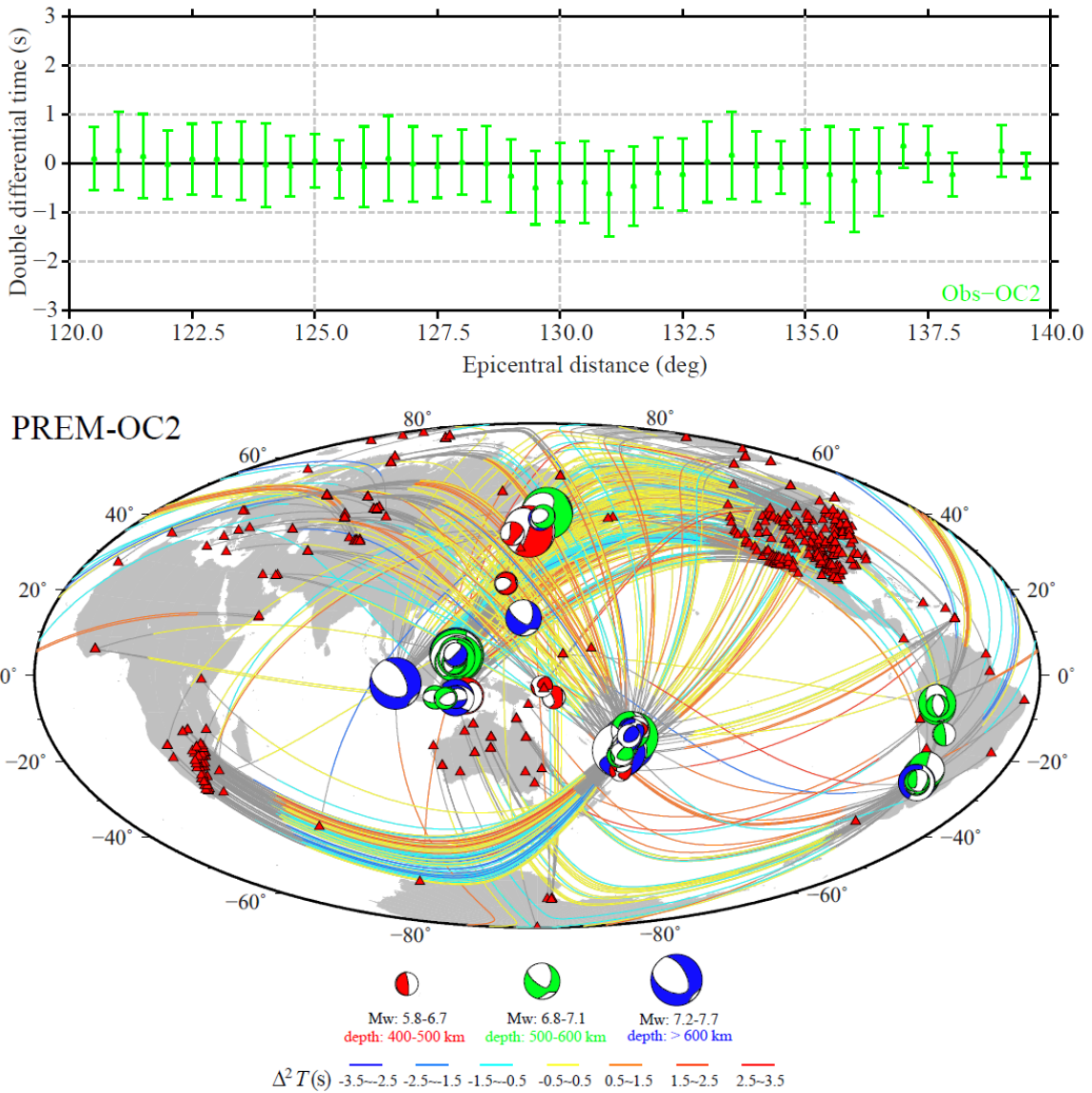


Fig. 3.10 Same as **Fig.3.9** but for Model PREM-OC2 $\Delta^2 T^{\text{PREM-OC2}}$.

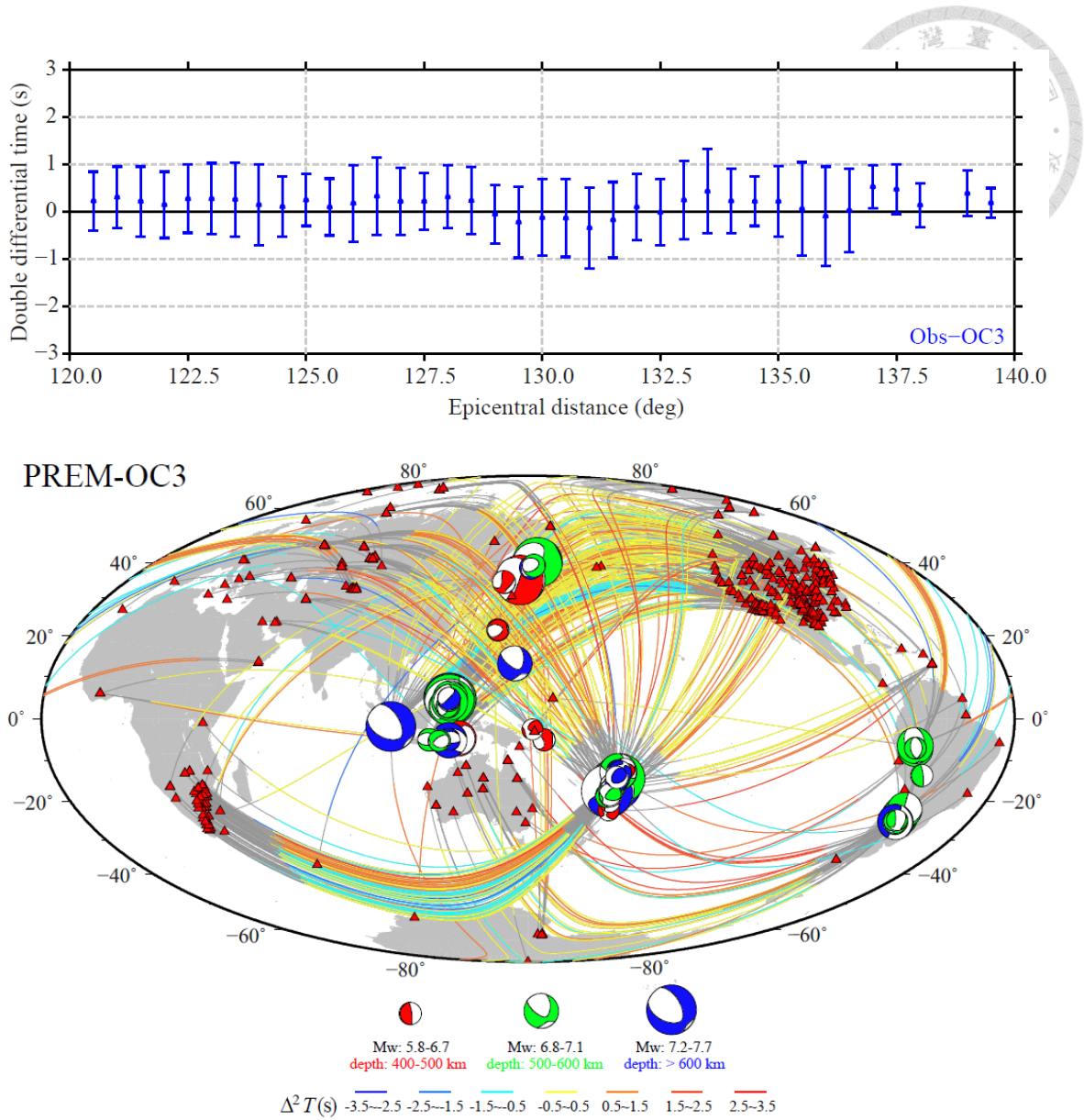


Fig. 3.11 Same as **Fig.3.9** but for Model PREM-OC3 $\Delta^2 T^{\text{PREM-OC3}}$.

Due to the location of deep earthquakes in subduction zones and the distribution of seismic stations on continents, the S3KS-SKKS paths are mostly concentrated in the Pacific Ocean, Northern Atlantic and Southern Indian Oceans, and under Eurasia. However, the dominating warm-colored paths in **Fig.3.9** strongly suggest that Model PREM is on average too fast in the top of the outer core. The same is true in the paths in **Fig.3.11** for Model PREM-OC3. The paths for Models PREM-OC2 (**Fig.3.10**) and PREM-OC4 (**Fig.3.12**) are less dominated by warm colors, and the paths also have

weaker colors, suggesting a relatively better performance by PREM-OC2 and PREM-OC4 in predicting the S3KS-SKKS differential traveltimes.

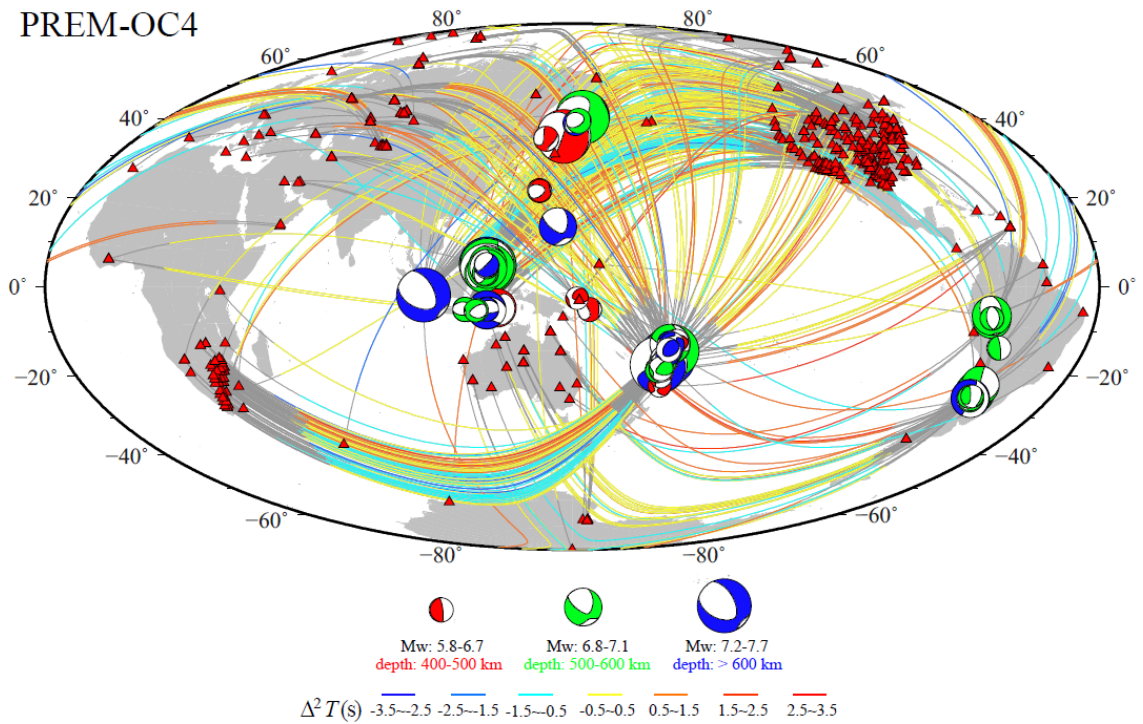
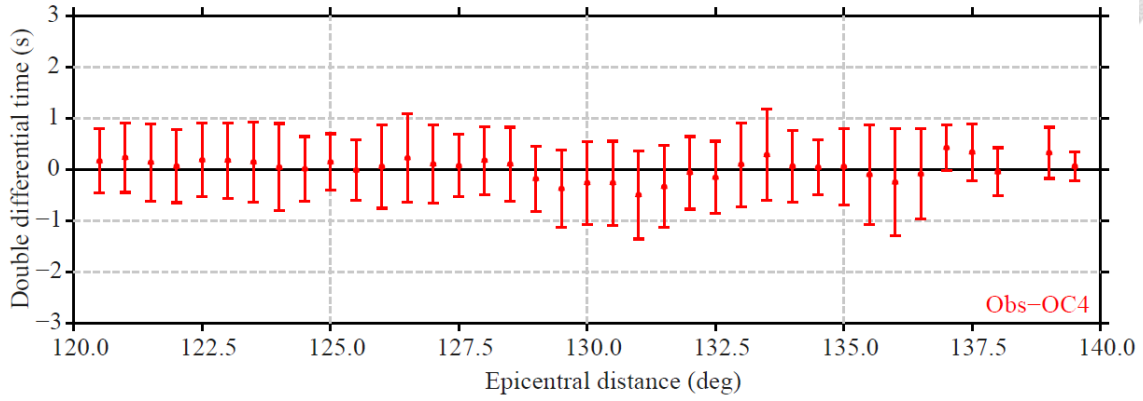
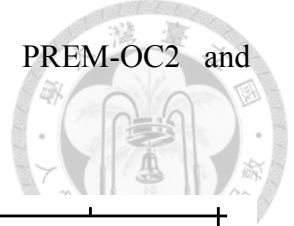


Fig. 3.12 Same as **Fig.3.9** but for Model PREM-OC4 $\Delta^2 T^{\text{PREM-OC4}}$.

3.4 Quantitative assessment of tested models

The double-differential traveltimes $\Delta^2 T^{\text{MODEL}}$ displayed in **Fig. 3.9-3.12** suggest that Models PREM-OC2 (**Fig.3.10**) and PREM-OC4 (**Fig.3.12**) provide predictions of the S3KS-SKKS differential traveltimes closer to the observed values than PREM and

PREM-OC3. Here we use the histograms in **Fig.3.13** to further quantify these observations. Values of the mean and standard deviation are given in each histogram. A positive mean value indicates the model is on average too fast relative to observation, and vice versa.

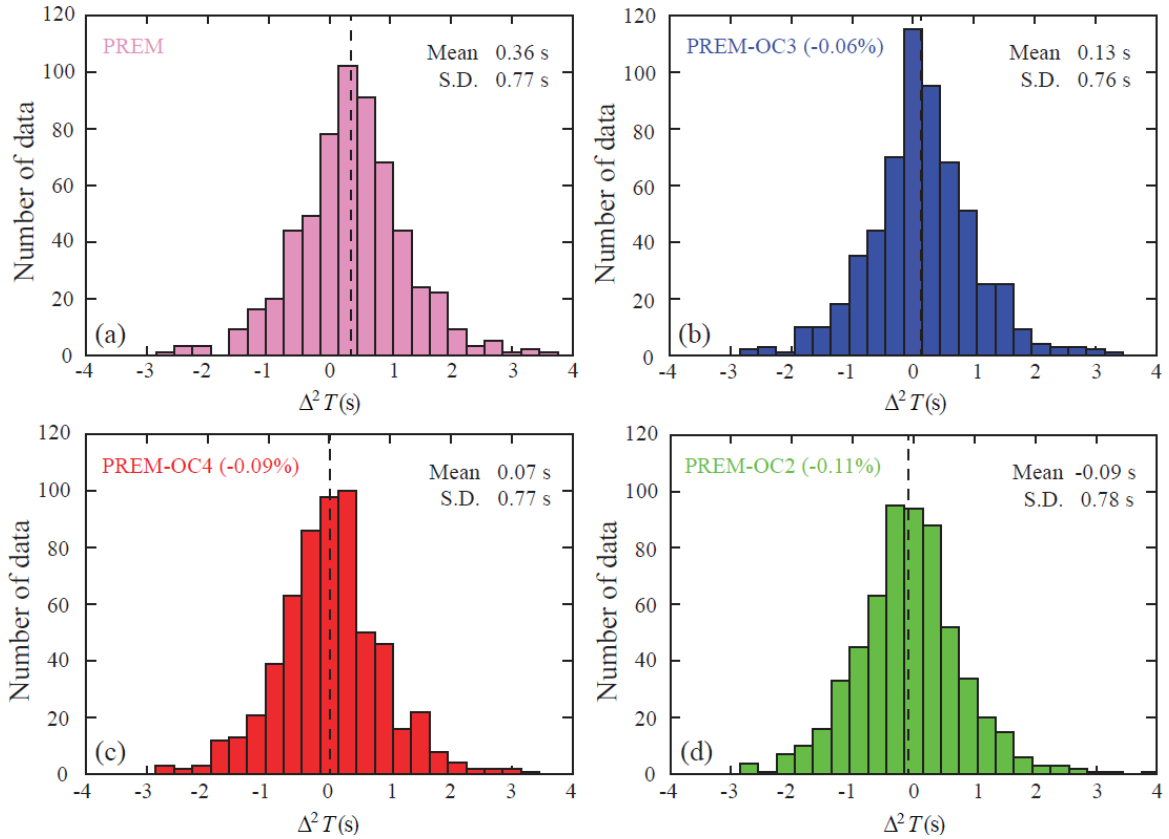
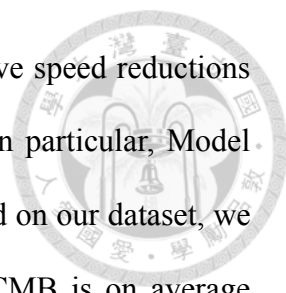


Fig. 3.13 Histograms of the double-differential traveltimes $\Delta^2 T^{\text{MODEL}}$ for the four models. (a) PREM, (b) PREM-OC3, (c) PREM-OC4, and (d) PREM-OC2. The dashed line in each plot shows the mean value. The values of the means and standard deviations are given in each plot. Also given in Panels (b), (c) and (d) are the average perturbations of the wave speed in the top of the outer core of the different models relative to PREM.

The histograms in **Fig.3.13** quantitatively confirm our observations: Model PREM is too fast. It has the largest positive mean value of 0.36 s. For Model PREM-OC3 (**Fig.3.13b**), the reduction of 0.06% from PREM in the speed in the top of the outer core is too small, resulting in a still relatively large positive mean value of 0.13 s. On the



other hand, Models PREM-OC3 and PREM-OC4, with average wave speed reductions of 0.09% and 0.11%, respectively, both have small mean values. In particular, Model PREM-OC4 has the smallest mean value of -0.07 s. Therefore, based on our dataset, we conclude that the wave speed in the ~ 400 km zone beneath the CMB is on average about 0.1% lower than that in PREM. Although the average velocity decrease relatively to PREM seems to be small, it is clearly significant in the comparison of the observed S3KS-SKKS differential traveltimes with predictions by the models we have tested. In the next chapter, we will try to quantify the optimal wave speed variation in the top of the outer core by a Bayesian inversion of the observed S3KS-SKKS differential traveltimes.

Chapter 4 Inversion of $SmKS$ Differential Traveltimes



4.1 Bayesian inversion

In the modeling results of the observed S3KS-SKKS differential traveltimes in Chapter 3, we have seen that the structure at the top region of the outer core is on average slower than PREM by about 0.1%. This suggests the possibility chemical stratification below the CMB. Our next goal is to conduct an inversion of the 606 observed S3KS-SKKS differential traveltimes between SKKS and S3KS to obtain the details of the 1D profile of the wave speed at the top of the outer core.

In our inversion problem, the data are the 606 differential traveltimes, and the unknowns are the wave speed in the uppermost layer of the outer core parameterized as wave speeds at a number of depth samples below the CMB. We can express this inverse problem as

$$\mathbf{g}(\mathbf{m}) = \mathbf{d}, \quad (4.1)$$

where \mathbf{d} is the data vector of length N ($N=606$ here), and \mathbf{m} is the unknown model parameter vector of length M . The functions g_i ($i=1, 2, \dots, N$) that relate the data \mathbf{d} to the model \mathbf{m} is almost always non-linear (such as in the case of this study), and the inverse problem (4.1) is commonly solved either using a non-linear optimization scheme or by iteratively solving its linearized version. Here we adopt the former choice and solve (4.1) by a non-linear grid search method.

Theoretically speaking, a grid search can be easy to implement. There is no need to calculate the partial derivatives of the data with respect to model parameters, nor is there a need to compute inverse matrices. We only need to be able to carry out the forward modeling given in eq.(4.1) for any given model \mathbf{m} , and drive the grid search

according to a pre-defined objective function such as

$$\varepsilon = \|\mathbf{d} - \mathbf{g}(\mathbf{m})\|, \quad (4.2)$$

where $\|\bullet\|$ represents a specific measure of the misfit between the data \mathbf{d} and its model prediction $\mathbf{g}(\mathbf{m})$, such as the L2 norm:

$$\varepsilon_{L2} = \sum_{i=1}^N [d_i - g_i(\mathbf{m})]^2. \quad (4.3)$$

Under this definition, the inverse problem would be solved once the grid search has found the model \mathbf{m} which yields the minimum value of the misfit ε_{L2} . However, in practice the model space has a high dimension (M is large), the functions $g_i(\mathbf{m})$ is non-linear, and the data d_i have uncertainty. Due to these complications, there is no basis to regard the model \mathbf{m} with the minimum misfit as the true solution to the inverse problem. We have to replace the deterministic view of the inverse problem with a probabilistic one, and here we adopt the Bayesian approach to the inversion of the S3KS-SKKS differential traveltimes data.

The basic concept of the Bayesian inversion is to make inferences about the properties of the model parameters based on the *a posteriori* probability distribution (e.g. Tarantola, 1987),

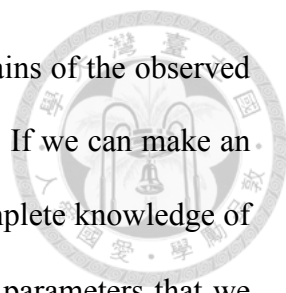
$$\sigma(\mathbf{m} | \mathbf{d}) \propto \rho(\mathbf{m})L(\mathbf{d} | \mathbf{m}), \quad (4.4)$$

where $\rho(\mathbf{m})$ is the *a priori* probability distribution of the model \mathbf{m} , $L(\mathbf{d} | \mathbf{m})$ is the likelihood function indicating the probability of predicting data \mathbf{d} by the model \mathbf{m} , and is defined as

$$L(\mathbf{d} | \mathbf{m}) = \exp\left[-\sum_{i=1}^N [d_i - g_i(\mathbf{m})]^2 / 2\tau_i^2\right]. \quad (4.5)$$

The *a posteriori* probability distribution $\sigma(\mathbf{m} | \mathbf{d})$ represents the probability of the

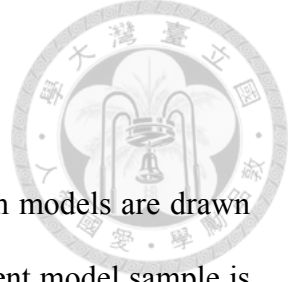




solution of the inverse problem being the model \mathbf{m} under the constraints of the observed data \mathbf{d} with standard deviation $\boldsymbol{\tau}$ and the specified prior information. If we can make an exhaustive sampling of the entire model space, we will have the complete knowledge of $\sigma(\mathbf{m} | \mathbf{d})$, which can be used to quantify the features of the model parameters that we are interested in, such as the model expectation and standard deviation. However, a complete sampling of the model space is an impossible task because of the extremely heavy computational cost.

4.2 Metropolis-Hastings Monte Carlo algorithm

As discussed in the previous section, the Bayesian inversion depends on making model inferences based on sufficient knowledge of the *a posteriori* probability distribution $\sigma(\mathbf{m} | \mathbf{d})$ which is too costly if the entire model space must be sampled. Therefore, we need an efficient way to sample the models so that we can acquire necessary knowledge of $\sigma(\mathbf{m} | \mathbf{d})$ without the need for an exhaustive search in the entire model space. This is achieved by the so-called Metropolis-Hastings Monte Carlo (MHMC) algorithm (*e.g.* Metropolis *et al.*, 1953; Hastings, 1970; Mosegaard & Tarantola, 1995). The MHMC is based on a random (i.e. Monte Carlo) sampling of the model space. The Metropolis algorithm (Metropolis *et al.*, 1953), later modified by Hastings (Hastings, 1970), provides a mechanism of rejection and acceptance of the sampling models. When the number of sampled models is large enough, the density distribution of the accepted models resembles $\sigma(\mathbf{m} | \mathbf{d})$, i.e. the MHMC samples the of the model space *a posteriori* probability distribution of the model space (Mosegaard & Tarantola, 1995). Therefore, the MHMC has a natural connection with the Bayesian inversion and its efficiency in model sampling has made it a popular choice in solving



non-linear inverse problems.

The MHMC algorithm involves the following steps:

- [1] Start with a so-called burn-in stage in which a series of random models are drawn from the model space. At the end of the burn-in stage, the current model sample is denoted as \mathbf{m}_i .
- [2] Calculate $L(\mathbf{d} | \mathbf{m}_i)$, the likelihood function of model \mathbf{m}_i as defined in eq.(4.5).
- [3] Draw a new random model \mathbf{m}_j from the model space.
- [4] Calculate $L(\mathbf{d} | \mathbf{m}_j)$.
- [5] Calculate the ratio between the values of the likelihood function of the two consecutive model samples

$$r = \frac{L(\mathbf{d} | \mathbf{m}_j)}{L(\mathbf{d} | \mathbf{m}_i)}. \quad (4.6)$$

This ratio is used as the probability by which the new model \mathbf{m}_j is accepted or rejected, i.e., if $r \geq 1$, then model \mathbf{m}_j is accepted with $\mathbf{m}_{i+1}=\mathbf{m}_j$; if $r < 1$, then a random number s between 0 and 1 is generated, and if $s \leq r$, \mathbf{m}_j is accepted with $\mathbf{m}_{i+1}=\mathbf{m}_j$, otherwise \mathbf{m}_j is rejected and $\mathbf{m}_{i+1}=\mathbf{m}_i$.

As Steps [2] to [5] are repeated and the number of accepted models increases, model expectations can be calculated frequently. Once the model expectation becomes stable, the sampling can be stopped.

4.3 Bayesian inversion of *SmKS* differential traveltimes

Although the MHMC algorithm provides an efficient scheme to conduct the Bayesian inversion, the number of model samples is still large. Since predicted data are needed to calculate the likelihood function, therefore for each sampled model we have to run the DSM simulations for all earthquakes and measure the S3KS-SKKS

differential traveltimes, which is still impractical for hundreds or thousands of models. Therefore, we use the much more efficient TauP Toolkit (Crotwell *et al.*, 1999) to predict the differential traveltimes. For a given model, there is a slight difference between the differential traveltimes calculated by the TauP Toolkit and those measured from DSM-calculated waveforms. The TauP result assumes high frequency and only SKKS and S3KS waves, whereas the DSM result is from full waveform which includes the finite-frequency effect as well as possible interference with neighboring phases near SKKS and S3KS. However, this most frequency-induced difference does not depend on the particular model. Therefore, for the sampled models in the inversion process, we calculate their predicted S3KS-SKKS differential traveltimes by TauP toolkit and then adjust them to the DSM results using the difference observed between the TauP and DSM results for model PREM, i.e.

$$g_i(\mathbf{m}) = (\Delta T_{\text{DSM}}^{\mathbf{m}})_i = (\Delta T_{\text{TauP}}^{\mathbf{m}})_i - \delta T_i^{\text{PREM}}, \quad (4.7)$$

where $(\Delta T_{\text{TauP}}^{\mathbf{m}})_i$ are the TauP-calculated differential traveltimes for model \mathbf{m} , and δT_i^{PREM} is the difference between TauP and DSM differential traveltimes for PREM

$$\delta T_i^{\text{PREM}} = (\Delta T_{\text{TauP}}^{\text{PREM}} - \Delta T_{\text{DSM}}^{\text{PREM}})_i. \quad (4.8)$$

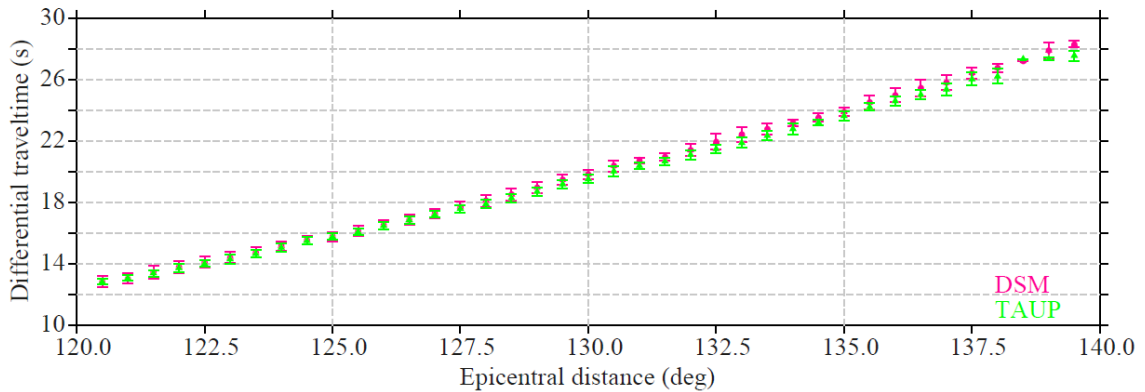


Fig. 4.1 Difference in predicted S3KS-SKKS differential traveltimes obtained by TauP (green) and DSM (purple) for PREM in the distance range 120°-140°. The values are obtained by averaging every 0.5° over 1° bins.

The values of δT_i^{PREM} shown in **Fig.4.1** are estimated every 0.5° over 1° bins in the distance range $120^\circ \sim 140^\circ$. The differential traveltime data used in the final Bayesian inversion are selected from the 606 measurements displayed in **Fig.3.3** after removing the outliers and the single data within a 1° bin ($\tau_i=0$). In the end a total of 489 S3KS-SKKS differential traveltimes are used, as shown by the black dots in **Fig.4.2a**, and the standard deviation in **Fig.4.2b** are used for τ_i in eq.(4.5). Based on the modeling results for PREM and several PREM-like models in Chapter 3, we set the *a priori* probability distribution $\rho(\mathbf{m})$ to be the uniform distribution with a wave speed perturbation of $-0.6\% \leq \delta\alpha/\alpha \leq +0.2\%$ with respect to α in PREM in the top 550 km layer of the outer core. We also impose a cosine taper so that the perturbation $\delta\alpha/\alpha$ decreases smoothly to 0 at the depth of 550 km below the CMB. The model is parameterized by α at 20 depth grids over the 550-km layer (i.e. $M=20$).

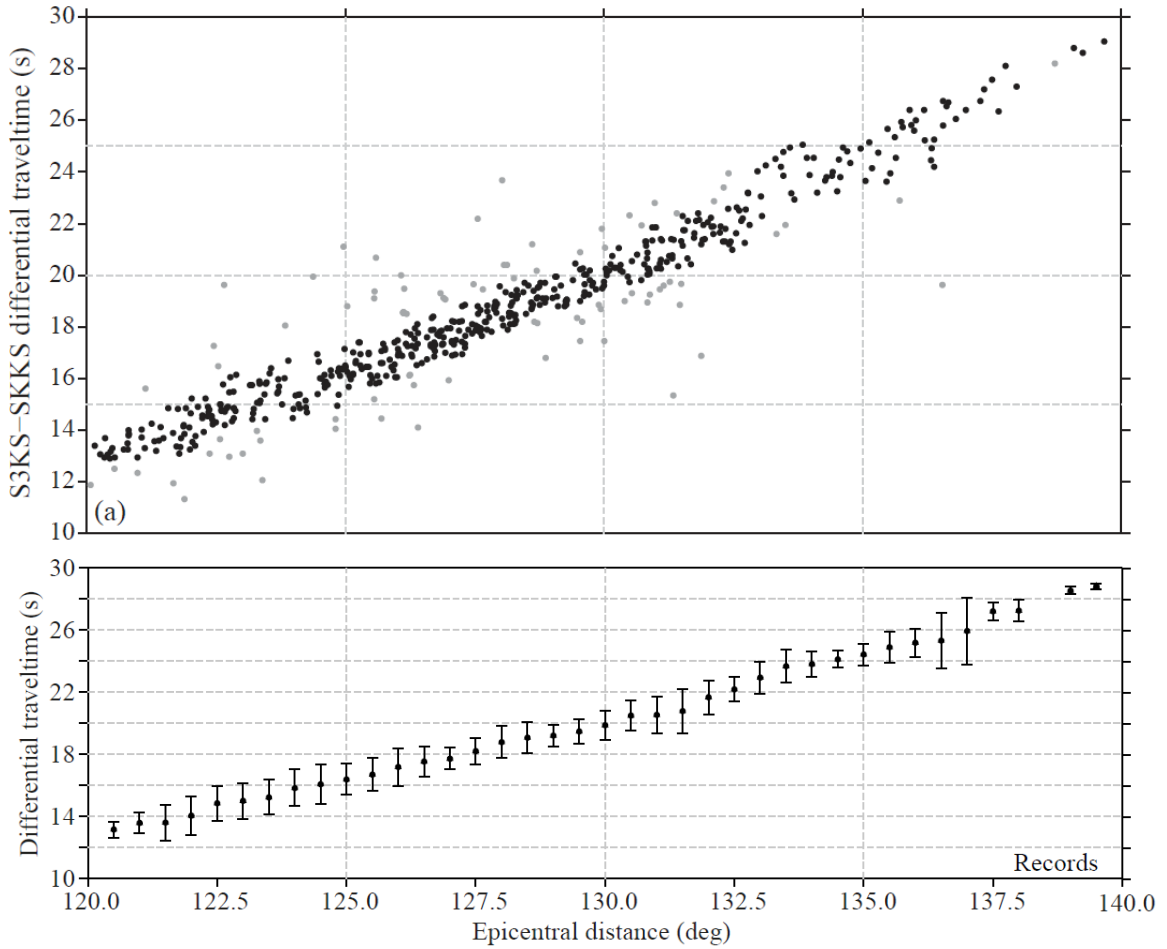


Fig. 4.2 (a) 489 differential traveltimes measurement (block dots) used in the final inversion. (b) The measurements in (a) averaged every 0.5° over 1° bins. The bars show the standard deviations used for τ_i in eq.(4.5) to evaluate the likelihood.

4.4 A slower outer core model from Bayesian inversion

We carried out the Bayesian inversion of the 489 observed S3KS-SKKS differential traveltimes on an average PC. The sampling is still very time consuming even with the efficient MHMC algorithm, taking about 2 minutes for each model on average. After continuously running for about 7 days, 5092 models were sampled, with 109 accepted models. Repeated estimation of the model expectation shows little change after sampling more than 3600 models with 50 accepted models, suggesting that the MHMC sampling has stabilized. **Fig.4.3** shows the result of Bayesian inversion from the 5092 model samples. The model expectation (red solid line) is computed by the assemble average of the 109 accepted models weighted by their respective *a posteriori* probability values.

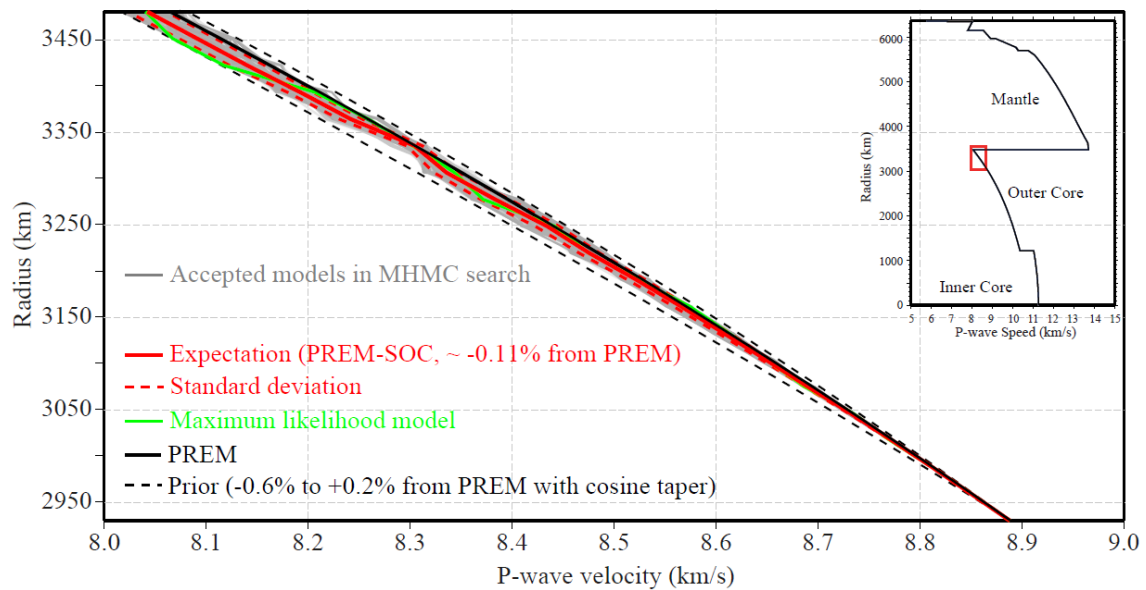


Fig. 4.3 109 accepted models (gray) by the MHMC algorithm in Bayesian inversion. The black, green and red solid lines are PREM, the maximum likelihood, and the expectation models. The red dash lines show the standard deviation of accepted models. The black dashed lines show the boundaries of the prior model: the *a priori* probability distribution, i.e. $\rho(\mathbf{m})$ in eq.(4.4), has a uniform value of 1 between the black dashed lines and 0 otherwise.

This expectation model in **Fig.4.3**, named as PREM-SOC, has an average velocity perturbation of about -0.11% from PREM in the top 550 km of the outer core, and the perturbation is variable with depth. The maximum perturbation is about -0.31% at 60 km below the CMB, while there is a narrow depth range around 150 km below the CMB where the velocity is close to PREM.

The histogram in **Fig.4.4** shows the comparison between the observed S3KS-SKKS differential traveltimes and predictions by model PREM-SOC. The values of the mean and standard deviation are not as small as those for Models PREM-OC2 and PREM-OC3 (**Fig.3.13**), although their average perturbations of the wave speed are all about -0.1%. As discussed earlier, due to the inherent uncertainty in the data and the uneven and incomplete coverage, fitness to the data is not the only criteria in determining the outcome of the Bayesian inversion, and the model expectation and its standard deviation are more meaningful results from the inversion.

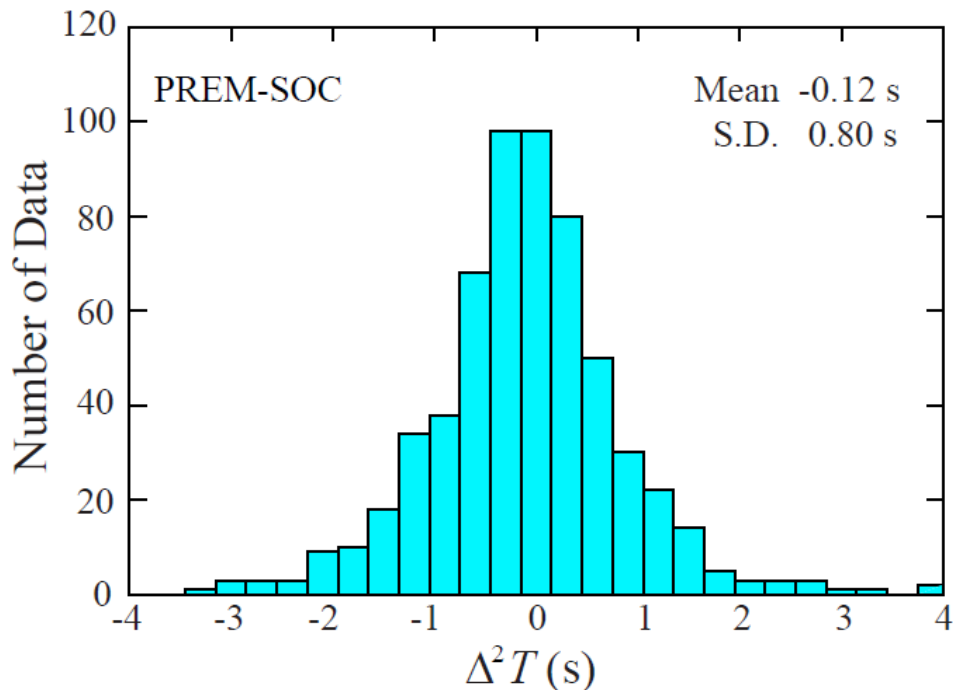


Fig. 4.4 Histogram of the double-differential times for the PREM-SOC $\Delta^2 T^{\text{PREM-SOC}}$. In this comparison the predicted differential traveltimes are obtained from DSM-calculated waveforms. The values of the means and standard deviations are given in the plot.

In Fig.4.5 we compare the expectation model from our Bayesian inversion with the Model KHOCQ of Helffrich & Kaneshima (2010). In the top 300 km of the outer core, our expectation model PREM-SOC has a good agreement with Model KHOCQ at long wavelength. The low-velocity zone in our model extends to a greater depth, and our model has a high-velocity layer ~150 km below the CMB. Our inversion result has a larger standard deviation than the error bounds of KHOCQ, perhaps due to different definitions between our standard deviation and error bounds in Helffrich & Kaneshima (2010). However, both results clearly indicate a lowered wave speed at the top of the outer core than that in PREM.

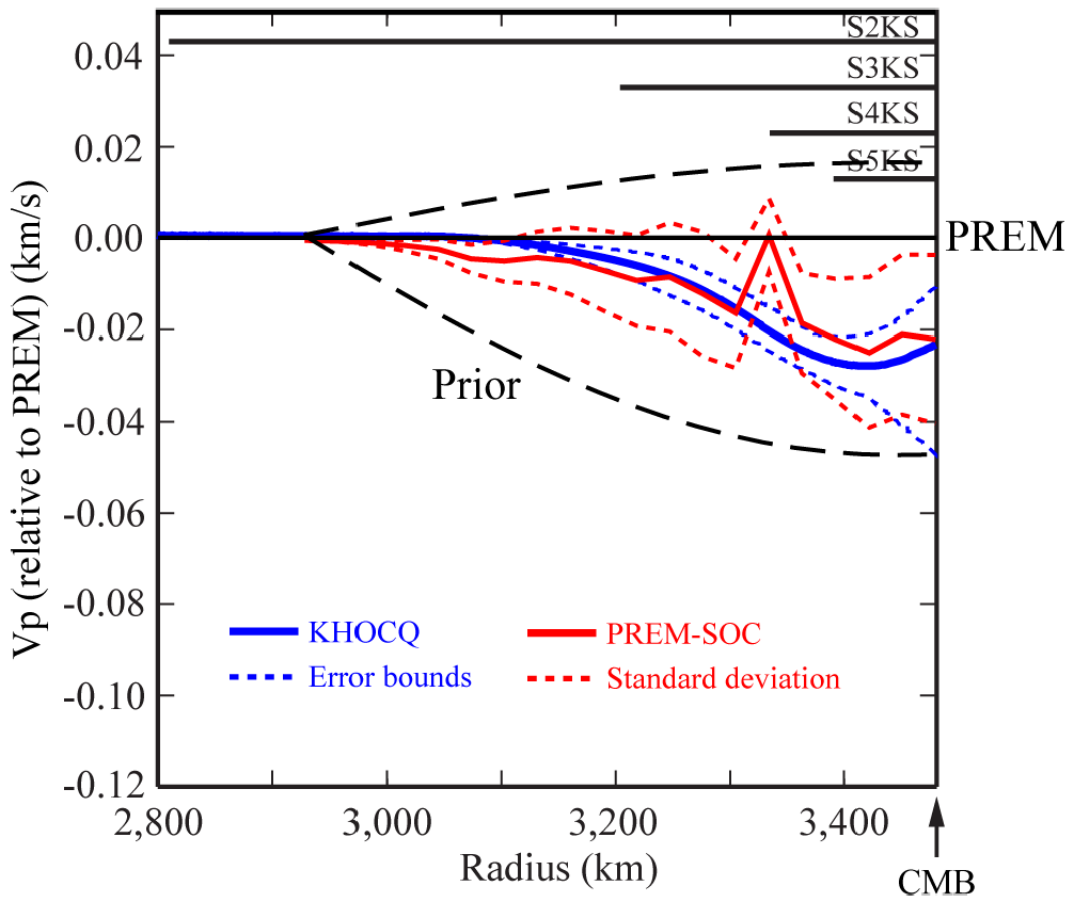


Fig. 4.5 Comparison of our inversion result with Helffrich & Kaneshima (2010). Solid red line is our expectation model PREM-SOC and red dash lines show the standard deviation. Solid blue line is Model KHOCQ in Helffrich & Kaneshima (2010), and the blue dashed lines are its error bounds. Black dashed lines show the prior in this study.

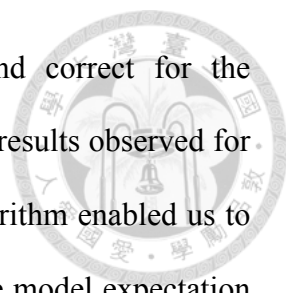
Chapter 5 Discussions and Conclusions



The Earth's outer core has been considered to be chemically well mixed, and seismological models for the outer core have been obtained by assuming a homogeneous shell composed of liquid iron. However, dynamical analyses have proposed the existence of light materials at the top of the outer core, and seismic studies have been inconclusive with evidence both for and against the existence of chemical stratification below them CMB.

The current study is an attempt at resolving this issue with seismological observations. We obtained 606 high-quality measurements of S3KS-SKKS differential traveltimes measurements using broadband records at globally distributed stations from 78 deep earthquakes in the distance range 120° - 140° . The long propagation distance and interference with neighboring phases require us to make the measurements of the differential traveltimes by waveform cross correlation. Therefore, for comparison with the observations, we use DSM-calculated waveforms to derive model-predicted differential traveltimes. Modeling experiments using PREM and several PREM-like models suggest that the actual wave speed at the top of the outer core is likely to be about 0.1% slower than PREM.

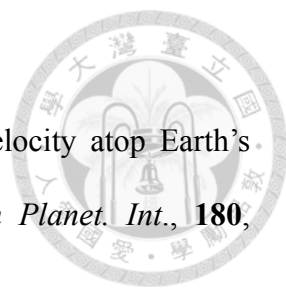
Taking the modeling results of PREM-like models as guides for determining the *a priori* probability distribution function, we carried out a Bayesian inversion using the observed S3KS-SKKS differential traveltime measurements for the velocity structure at the top of the outer core. The Metropolis-Hastings Monte Carlo algorithm was adopted to enable an efficient sampling of the model space. In addition, to further reduce the time needed for computing model-predicted data, we used Taup Toolkit to calculate the

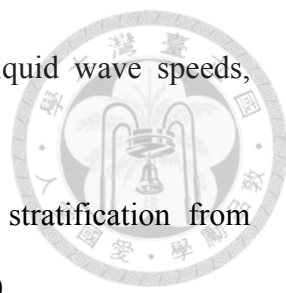



S3KS-SKKS differential traveltimes in the sampling models and correct for the finite-frequency effect using the difference between TauP and DSM results observed for PREM. The resulting Bayesian inversion based on the MHMC algorithm enabled us to achieve a successful sampling of the model space and reach a stable model expectation after 5092 model samples with 109 accepted models.

The final expected model PREM-SOC is on average slower than PREM by about 0.11% in the 550-km layer below the CMB 550 km. The expected model has a maximum perturbation of -0.31% from PREM at about 60 km below the CMB, and shows a clear variation of velocity perturbation with depth. The amount of reduction in wave speed in our expected model in the top 300 km region at the top of the outer core is similar to that proposed by some previous studies (*e.g.* Helffrich & Kaneshima, 2010). In conclusion, our result strongly supports the argument for the existence of chemical stratification of light materials at the top of the Earth's outer core.

REFERENCES

- 
- [1] Alexandrakis, C. and Eaton, D. W. Precise seismic-wave velocity atop Earth's core: No evidence for outer-core stratification, *Phys. Earth Planet. Int.*, **180**, 59-65, 2010.
- [2] Buffett, B. A. and Seagle, C. T. Stratification of the top of the core due to chemical interaction with the mantle, *J. Geophys. Res.*, **115**, B04407, 2010.
- [3] Crotwell, H. P., Owens, T. J., and Ritsema, J. The TauP Toolkit: Flexible seismic travel-time and ray-path utilities, *Seism. Res. Lett.*, **70**, 154-160, 1999.
- [4] Cummins, P. R., Geller, R. J., Hatori, T., and Takeuchi, N. DSM complete synthetic seismograms: SH, spherically symmetric, case, *Geophys. Res. Lett.*, **21**, 533-536, 1994.
- [5] Dziewonski, A. M. and Anderson, D. L. Preliminary reference Earth model, *Phys. Earth Planet. Int.*, **25**, 297-356, 1981.
- [6] Eaton, D. and Kendall, M. Improving seismic resolution of outermost core structure by multichannel analysis and deconvolution of broadband *SmKS* phases, *Phys. Earth Planet. Inter.*, **155**, 104-119, 2006.
- [7] Frost, D. J., Asahara, Y., Rubie, D. C., Miyajima, N., Dubrovinsky, L. S., Holzapfel, C., Ohtani, E., Miyahara, M., and Sakai, T. Partitioning of oxygen between the Earth's mantle and core, *J. Geophys. Res.*, **115**, B02202, 2010.
- [8] Geller, R. J. & Ohminato, T. Computation of synthetic seismograms and their partial derivatives for heterogeneous media with arbitrary natural boundary conditions using the Direct Solution Method, *Geophys. J. Int.*, **116**, 421-446, 1994.
- [9] Hastings, W. Monte Carlo simulation methods using Markov chains and their applications, *Biometrika*, **57**, 97-109, 1970.











































- 
- [10] Helffrich, G. How light element addition can lower core liquid wave speeds, *Geophys. J. Int.*, **188**, 1065-1070, 2012.
- [11] Helffrich, G. and Kaneshima, S. Outer-core compositional stratification from observed core wave speed profiles, *Nature*, **468**, 807-810, 2010.
- [12] Helffrich, G., Wookey, J., and Bastow, I. *The Seismic Analysis Code: A Primer and User's Guide*, Cambridge University Press, Cambridge, UK, 2013.
- [13] Jephcoat, A., and Olson, P. Is the inner core of the Earth pure iron? *Nature*, **325**, 332-335, 1987.
- [14] Kaneshima, S. and Helffrich, G. Vp structure of the outermost core derived from analysing large-scale array data of SmKS waves, *Geophys. J. Int.*, **93**, 1537-1555, 2013.
- [15] Kawai, K., Takeuchi, N., and Geller, R. J. Complete synthetic seismograms up to 2 Hz for transversely isotropic spherically symmetric media, *Geophys. J. Int.*, **164**, 411-424, 2006.
- [16] Lay, T., Hernlund, J., and Buffett, B. A. Core–mantle boundary heat flow, *Nat. Geosci.*, **1**, 25-32, 2008.
- [17] Lister, J. R. and Buffett, B. A. Stratification of the outer core at the core-mantle boundary, *Phys. Earth Planet. Inter.*, **105**, 5-19, 1998.
- [18] Masters, G. Observational constraints on the chemical and thermal structure of the Earth's deep interior, *Geophys. J. R. astr. Soc.*, **57**, 507-534, 1979.
- [19] Metropolis, N., Rosenbluth, A. W., Rosenbluth, M. N., Teller, A. H., and Teller, E. Equation of state calculations by fast computing machines, *J. Chem. Phys.*, **21**, 1087-1092, 1953.
- [20] Mosegaard, K. and Tarantola, A. Monte Carlo sampling of solutions to inverse problems, *J. Geophys. Res.*, **100**, 12,431-12,447, 1995.

- 
- [21] Stixrude, L., Wasserman, E., and Cohen, R. E. Composition and temperature of Earth's inner core, *J. Geophys. Res.*, **102**, 24,729-24,739, 1997.
- [22] Tanaka, S. Seismic detectability of anomalous structure at the top of the Earth's outer core with broadband array analysis of SmKS phases, *Phys. Earth Planet. Inter.*, **141**, 141-152, 2004.
- [23] Tanaka, S. Possibility of a low P-wave velocity layer in the outermost core from global SmKS waveforms, *Earth Planet. Sci. Lett.*, **259**, 486-499, 2007.
- [24] Tarantola, A. *Inverse Problem Theory: Methods for Data Fitting and Model Parameters Estimation*, Elsevier, New York, 1987.
- [25] Zhao, L., and Chevrot, S. An efficient and flexible approach to the calculation of three-dimensional full-wave Fréchet kernels for seismic tomography: II—Numerical results, *Geophys. J. Int.*, **185**, 939-954, 2011.





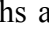
Appendix A. Earthquake Information

Table A.1. List of deep earthquakes used in this study.

No.	Event ID	Lon. (°)	Lat. (°)	Depth (km)	Mw	Geographic Location	Focal Mech.	# of Data
1	200910072141A	122.51	4.11	579.5	6.8	Celebes Sea		13
2	201003201400A	152.33	-3.32	413.5	6.6	New Ireland		0
3	201007232208A	123.59	6.54	596.8	7.3	Philippines		5
4	201007232251A	123.90	6.62	576.9	7.6	Philippines		19
5	201007232315A	123.48	6.83	641.4	7.4	Philippines		10
6	201007240535A	123.56	6.23	556.4	6.6	Philippines		14
7	201007290731A	123.41	6.69	614.0	6.6	Philippines		16
8	201011300324A	139.26	28.69	460.6	6.8	Japan		0
9	201101010956A	-63.21	-27.02	586.0	7.0	Santiago Argentina		9
10	201102101441A	123.28	4.22	517.6	6.5	Celebes Sea		20
11	201103101708A	116.71	-6.95	517.0	6.6	Bali Sea		22
12	201107290742A	179.92	-23.78	539.0	6.7	Fiji		18
13	201102211057A	178.47	-25.95	567.5	6.5	Fiji		3
14	201005241618A	-71.64	-8.08	591.4	6.4	NW Brazil		3
15	201109021347A	-63.08	-28.56	597.3	6.7	Santiago Argentina		6
16	201111221848A	-65.18	-15.40	553.8	6.6	Bolivia		3
17	201205280507A	-63.07	-28.25	591.6	6.7	Santiago Argentina		9
18	201108300657A	126.68	-6.47	468.7	6.9	Banda Sea		5
19	072504B	104.38	-2.68	600.5	7.3	Sumatra		54
20	200910041058A	123.56	6.77	625.8	6.6	Philippines		11
21	200911091044A	178.53	-17.11	603.9	7.3	Fiji		0
22	201002180113A	130.66	42.48	579.0	6.9	NE China		0
23	201302221201A	-63.00	-27.89	585.7	6.1	Santiago Argentina		2
24	201302261957A	-179.31	-21.48	626.1	5.8	Fiji		1
25	201102101439A	122.91	4.14	520.9	6.5	Celebes Sea		8
26	200908280151A	123.46	-7.09	634.4	6.9	Banda Sea		1
27	201304051300A	131.02	42.77	571.9	6.3	NE China		0
28	201304210322A	138.88	30.02	429.8	6.1	Japan		1
29	201305140032A	145.35	18.67	604.7	6.8	Mariana		2
30	201305241456A	151.48	52.36	642.4	6.7	Okhotsk		3
31	201306071254A	179.07	-23.83	557.1	5.9	Fiji		1
32	200811240902A	154.71	54.27	502.3	7.3	Okhotsk		3
33	200807050212A	153.37	54.12	610.8	7.7	Okhotsk		1
34	200801151752A	-179.34	-22.05	603.3	6.5	Fiji		1
35	201308280254A	179.84	-27.73	492.0	6.2	Kermadec		9

36	201308291352A	-178.94	-19.35	684.6	5.8	Fiji		0
37	201309040018A	138.79	30.02	412.0	6.5	Japan		3
38	201309210139A	119.92	-7.32	550.7	6.1	Flores Sea		9
39	201310010338A	152.89	53.13	592.0	6.7	Okhotsk		4
40	200710162105A	179.72	-25.70	512.4	6.6	Fiji		10
41	200710050717A	179.50	-25.27	540.8	6.5	Fiji		9
42	200705062111A	-179.04	-19.44	690.8	6.5	Fiji		4
43	200611130126A	-63.47	-26.10	573.4	6.8	Santiago Argentina		8
44	200602021248A	-178.13	-17.77	611.6	6.7	Fiji		3
45	200601022213A	-177.72	-19.80	589.5	7.2	Fiji		2
46	200503211223A	-63.54	-24.88	572.3	6.8	Santiago Argentina		4
47	200502051223A	123.67	5.47	530.6	7.1	Philippines		26
48	111704G	-178.40	-19.87	629.4	6.5	Fiji		4
49	071504C	-178.52	-17.68	577.2	7.1	Fiji		5
50	072703C	139.23	46.99	477.2	6.7	Sea of Japan		4
51	062003D	-71.89	-7.37	556.2	7.0	NW Brazil		4
52	052603E	123.85	6.90	579.7	6.8	Philippines		23
53	111702C	146.45	47.81	479.8	7.3	Kuril Is.		5
54	101202H	-71.66	-8.30	539.4	6.9	Brazil		13
55	081902A	-179.08	-21.74	630.9	7.6	Fiji		1
56	081902C	178.49	-24.16	699.3	7.7	Fiji		3
57	063002F	179.43	-22.13	631.6	6.4	Fiji		8
58	080700E	123.53	-6.95	648.3	6.5	Banda Sea		2
59	021601C	117.62	-7.11	537.9	6.0	Bali Sea		12
60	061400C	178.38	-25.45	615.4	6.4	Fiji		6
61	200609090413A	120.27	-7.23	583.2	6.3	Flores Sea		11
62	200704210712A	151.46	-3.46	405.0	6.1	New Ireland		10
63	200709250515A	-179.85	-30.69	420.6	6.2	Kermadec		9
64	200804182039A	-178.98	-17.26	577.8	6.3	Fiji		4
65	200910250753A	-178.97	-23.00	419.3	6.0	Fiji		2
66	201006300430A	179.26	-23.19	581.6	6.4	Fiji		8
67	201008161935A	-178.67	-20.74	604.0	6.2	Fiji		3
68	201012280834A	-179.73	-23.49	571.4	6.3	Fiji		4
69	201102071953A	155.34	-7.04	425.5	6.5	Solomon Is.		1
70	042300B	-63.04	-28.41	607.9	6.9	Santiago Argentina		6
71	121800A	-178.98	-21.11	655.7	6.5	Fiji		5
72	091201A	-178.90	-20.84	634.1	6.4	Fiji		4
73	201201240052A	178.72	-25.00	581.8	6.3	Fiji		14
74	201108190354A	-176.73	-16.52	415.0	6.2	Fiji		7
75	201110270015A	-179.40	-17.98	608.7	6.0	Fiji		4
76	201104031407A	-178.45	-17.65	562.3	6.4	Fiji		4
77	032998D	-178.85	-17.57	553.7	7.1	Fiji		41

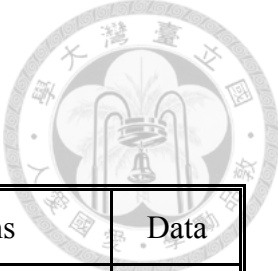
78	012798E	179.29	-22.39	629.4	6.4	Fiji		24
79	051698B	-179.35	-22.27	608.8	6.8	Fiji		0
80	082098B	139.47	28.99	425.5	7.0	Bonin		0
81	050400K	-178.31	-17.72	539.8	6.4	Fiji		0
82	050800C	150.14	-4.38	496.3	6.1	New Britain		0
83	062802B	130.45	43.74	581.5	7.3	NE China		0
84	200606270259A	-178.04	-19.77	596.7	6.3	Fiji		0
85	200701082052A	-177.68	-18.46	423.7	6.3	Fiji		0
86	200705062201A	-179.05	-19.31	691.6	6.0	Fiji		0
87	200911220748A	-178.36	-17.72	546.4	6.3	Fiji		0
88	201004112208A	-3.69	37.10	616.5	6.3	Gibraltar		0
89	201208140259A	145.70	49.97	598.2	7.7	Okhotsk		0
90	201305240544A	153.77	54.61	611.0	8.3	Okhotsk		0
91	201309020251A	133.65	42.19	454.7	5.7	Vladivostok Russia		0
92	201311031103A	123.28	4.76	543.1	6.0	Celebes Sea		0
93	201311191700A	145.18	18.54	515.2	6.0	Mariana		0
94	201205262148A	140.17	26.87	472.1	6.0	Japan		0
95	201203050746A	-63.27	-28.19	565.1	6.1	Santiago Argentina		0
96	201108190354A	-176.73	-16.52	415.0	6.2	Fiji		0
97	201101122132A	139.94	26.94	511.5	6.5	Japan		0
98	201003080947A	144.67	19.26	432.2	6.1	Mariana		0
99	200912100230A	152.77	53.44	655.7	6.3	Okhotsk		0
100	200911222247A	179.66	-31.47	437.1	6.2	Kermadec		0
101	200809031125A	-63.30	-26.85	571.3	6.3	Santiago Argentina		0
102	200807030302A	-179.69	-23.41	589.9	6.2	Fiji		0
103	200804182039A	-178.98	-17.26	577.8	6.3	Fiji		0
104	200802011210A	-179.27	-21.53	629.5	6.0	Fiji		0
105	200711190052A	-178.63	-21.05	562.5	6.3	Fiji		0
106	200707211327A	-71.30	-8.08	637.5	6.0	NW Brazil		0
107	200703090322A	133.65	43.22	451.1	6.0	Vladivostok Russia		0
108	200609220232A	-63.05	-26.85	602.4	6.0	Santiago Argentina		0
109	200606090558A	-178.62	-17.36	585.9	6.1	Fiji		0
110	200606020731A	-178.54	-20.77	584.6	6.0	Fiji		0
111	200602260308A	-179.82	-23.59	553.9	6.4	Fiji		0
112	200602241415A	-179.42	-17.94	640.9	6.1	Fiji		0
113	200509042358A	123.32	3.05	454.4	6.0	Celebes Sea		0
114	200503301741A	-179.64	-22.31	585.1	6.1	Fiji		0
115	200503211243A	-63.56	-24.71	572.2	6.4	Santiago Argentina		0
116	200503191734A	-179.27	-21.88	609.2	6.3	Fiji		0

117	120604B	-178.27	-18.84	465.6	6.1	Fiji		0
118	111204H	-63.18	-26.85	583.1	6.0	Santiago Argentina		0
119	110704A	144.52	47.93	493.0	6.1	Okhotsk		0
120	011104C	-179.20	-20.21	682.5	6.0	Fiji		0
121	083103C	132.37	43.38	493.0	6.1	Vladivostok Russia		0
122	070103B	122.67	4.69	604.6	6.0	Celebes Sea		0
123	121002C	179.28	-24.02	538.8	6.0	Fiji		0
124	102202C	-178.30	-20.50	560.5	6.1	Fiji		0
125	101702C	-178.23	-19.80	621.9	6.1	Fiji		0
126	100402E	-178.74	-20.86	650.8	6.3	Fiji		0
127	091502B	130.04	44.77	589.4	6.4	NE China		0
128	080202D	139.25	29.35	441.5	6.2	Japan		0
129	010202E	178.84	-17.63	680.8	6.1	Fiji		0
130	110501D	-178.96	-17.12	579.7	6.2	Fiji		0
131	060900Q	137.79	30.47	492.1	6.2	Japan		0
132	021300B	131.64	42.77	524.3	6.0	NE China		0
133	011500C	-179.10	-21.11	650.7	6.0	Fiji		0
134	011300B	-178.63	-17.38	564.6	6.2	Fiji		0
135	040999B	178.28	-26.37	635.6	6.1	Fiji		0
136	040899B	130.47	43.66	575.4	7.1	NE China		0
137	041498B	-179.81	-23.73	509.6	6.1	Fiji		0
138	020798B	141.87	24.92	533.6	6.4	Northern Mariana		0
139	012798D	179.29	-22.53	616.9	6.3	Fiji		0

Note: We assign a number to each earthquake (first column). The second column is the event ID used in the GCMT catalog. The event longitudes, latitudes, depths and focal mechanisms are all from the GCMT catalog. and their information for location, depth, magnitude and focal mechanism. The last column shows the number of S3KS-SKKS differential travel time data obtained from the records of each earthquake. Out of the 139 deep earthquakes, 61 have not been processed (gray background). Out of the 78 processed events, 6 of them didn't yield any data (yellow background).

Appendix B. Station Information

Table B.1. List of 374 stations yielding data.



Station Name	Lon. (°)	Lat. (°)	Geographic Locations	Data
A27A	-101.24	48.95	Central North USA	1
AAK	74.49	42.63	Kyrgyzstan	1
AAM	-83.66	42.30	NE USA	1
ABKAR	59.94	49.26	Kazakhstan	9
ABKT	58.12	37.93	Turkmenistan	5
ACSO	-82.98	40.23	NE USA	3
ADK	-176.68	51.88	Adak Is.	1
ADO	-117.43	34.55	SW USA	1
AGU01	-73.51	-45.15	Argentina	1
AKTK	58.02	50.43	Kazakhstan	2
ALLY	-80.14	41.65	NE USA	1
AML	73.69	42.13	Kyrgyzstan	1
ANDY	-79.57	33.46	SE USA	1
ANGG	-37.64	65.62	Greenland	1
ANWB	-61.79	17.67	North Atlantic Ocean	1
ARMA	151.63	-30.42	SE Australia	1
ARU	58.56	56.43	SW Russia	16
AS31	133.90	-23.67	Central Australia	4
ATKA	-174.20	52.20	Aleutian Is.	1
B1	52.58	29.84	Iran	1
B28A	-100.36	48.45	Central North USA	1
B3	53.06	30.13	Iran	1
BB23	-69.43	-25.37	Chile	1
BBGH	-59.56	13.14	Barbados	1
BEL	-116.00	34.00	SW USA	1
BGNE	-98.15	41.41	Central USA	1
BILL	166.45	68.07	Russia	3
BLA	-80.42	37.21	Central East USA	2
BLO	-86.52	39.17	Central East USA	2
BLWY	28.61	-20.14	Zimbabwe	2
BOSA	25.26	-28.61	South Africa	2
BOZ	-111.63	45.60	NW USA	3
BRAL	-87.05	31.17	SE USA	2
BRNJ	-74.57	40.68	Central East USA	1
BRVK	70.28	53.06	Kazakhstan	5
BRYW	-71.54	41.92	Central East USA	1
BSFB	-40.85	-18.83	Central East Brazil	1
BTRCK	-80.75	32.43	SE USA	1
C28A	-100.39	47.72	Central North USA	1
C36A	-92.84	47.76	NE USA	1
CAN	149.00	-35.32	SE Australia	1
CASY	110.53	-66.28	Antarctica	1
CBN	-77.37	38.20	Central East USA	2

CCM	-91.24	38.06	Central USA	2
CHKZ	70.62	53.68	Kazakhstan	4
CMSA	145.69	-31.54	New South Wales	1
COEN	143.18	-13.96	North Queensland	4
CONY	-74.47	42.67	NE USA	1
CPNY	-73.96	40.79	Central East USA	2
CRY	-116.74	33.57	SW USA	2
CRZF	51.86	-46.43	Indian Ocean	1
CTA	146.25	-20.09	NE Queensland	3
D30A	-98.76	47.11	Central North USA	1
D34A	-95.20	47.09	Central North USA	1
D47A	-83.10	47.06	SE Canada	1
D59A	-71.84	47.01	SE Canada	1
DAC	-117.59	36.28	SW USA	2
DAN	-115.38	34.64	SW USA	1
DBG	-20.22	74.31	Greenland	1
DBIC	-4.86	6.67	West Africa	3
DGMT	-104.20	48.47	Central North USA	1
DRLN	-57.50	49.26	SE Canada	5
DWDAN	-82.83	34.74	SE USA	1
E30A	-98.91	46.50	Central North USA	1
E32A	-97.07	46.59	Central North USA	1
E47A	-83.28	46.45	SE Canada	1
E58A	-73.28	46.37	SE Canada	1
EDM	-113.35	53.22	Central South Canada	1
EDW	-117.99	34.88	SW USA	1
EDW2	-117.99	34.88	SW USA	1
EKS2	73.78	42.66	Kyrgyzstan	1
EMMW	-67.46	44.71	SE Canada	3
ERM	143.16	42.02	Japan	1
EYMN	-91.50	47.95	NE USA	1
F31A	-98.25	45.86	Central North USA	1
F45A	-85.52	45.68	NE USA	1
F59A	-72.78	45.85	SE Canada	1
FCC	-94.09	58.76	Central Canada	1
FDF	-61.14	14.73	North Atlantic Ocean	10
FITZ	125.64	-18.10	Australia	1
FMP	-118.29	33.71	SW USA	1
FRB	-68.55	63.75	NE Canada	2
FUORN	10.26	46.62	Switzerland	1
FUR	-116.86	36.47	SW USA	1
FVM	-90.43	37.98	Central USA	1
G60A	-72.33	45.10	NE USA	1
GENY	-77.82	42.77	NE USA	1
GIRL	114.23	-22.64	Western Australia	1
GLA	-114.83	33.05	ES USA	1
GLMI	-84.62	44.82	NE USA	1
GO01	-69.19	-19.67	Chile	1
GREEN	-82.17	34.23	SE USA	1

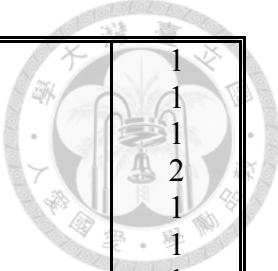
GRM	26.51	-33.31	South Africa	1
GSC	-116.81	35.30	SW USA	1
H29A	-100.21	44.63	Central North USA	1
H37A	-92.92	44.58	NE USA	1
HAST	-121.55	36.39	SW USA	1
HCNY	-74.40	42.70	NE USA	1
HDC	-84.11	10.00	Costa Rica	1
HDIL	-89.29	40.56	Central USA	1
HEBO	-123.75	45.21	NW USA	1
HEC	-116.33	34.83	SW USA	2
HKT	-95.84	29.96	SE USA	1
HLID	-114.41	43.56	NW USA	2
HNH	-72.29	43.71	NE USA	1
HNR	159.95	-9.44	Solomon Is.	2
HRV	-71.56	42.51	NE USA	4
HWUT	-111.56	41.61	Central USA	1
ICE	167.28	-77.55	Antarctica	2
ICQ	-67.27	49.52	SE Canada	1
IDI	24.89	35.29	Mediterranean	1
IRM	-115.14	34.16	SW USA	1
ISCO	-105.61	39.80	Central USA	1
J30A	-99.49	43.32	Central USA	1
JCC	-124.03	40.82	Central West USA	1
JCT	-99.80	30.48	Central South USA	1
JFWS	-90.25	42.91	NE USA	1
K33A	-97.00	42.61	Central USA	1
KAPO	-82.51	49.45	SE USA	2
KBS	11.94	78.93	Arctic Ocean	3
KEV	27.00	69.76	Finland	1
KIV	42.69	43.96	SW Russia	3
KKAR	70.51	43.10	Kazakhstan	1
KMBL	121.88	-31.37	Western Australia	1
KMBO	37.25	-1.13	Kenya	1
KNRA	128.76	-15.68	North Australia	2
KNS	-49.68	64.29	Greenland	2
KNTH	-110.80	34.33	SW USA	1
KNW	-116.71	33.71	SW USA	2
KOG	-52.73	5.21	French Guiana	1
KSU1	-96.61	39.10	Central USA	1
KURK	78.62	50.72	Kazakhstan	1
KWAJ	167.61	8.80	Marshall Is.	1
KZA	75.25	42.08	Kyrgyzstan	1
L35A	-95.54	42.11	Central USA	1
LAO	-106.22	46.69	Central North USA	1
LBNH	-71.93	44.24	NE USA	1
LBTB	25.60	-25.02	South Africa	8
LGU	-119.07	34.11	SW USA	1
LOHW	-110.60	43.61	NW USA	1
LONY	-74.58	44.62	NE USA	1

LRAL	-87.00	33.03	SE USA	2
LRW	-1.18	60.14	North Sea	1
LSZ	28.19	-15.28	Zambia	3
LTL	-90.77	30.54	SE USA	1
LVZ	34.65	67.90	Russia	10
M65A	-70.65	41.56	NE USA	1
MACI	-16.51	28.25	North Atlantic Ocean	1
MAW	62.87	-67.60	Antarctica	1
MCWV	-79.85	39.66	NE USA	1
MDND	-99.60	47.85	North USA	1
MHV	37.77	54.96	SW Russia	2
MIAR	-93.58	34.55	Central USA	1
MIB	47.34	29.80	Iraq	1
MLAC	-118.84	37.63	SW USA	1
MORW	116.04	-29.07	Western Australia	3
MPH	-89.93	35.12	Central USA	2
N23A	-105.94	40.89	Central USA	1
N39A	-92.50	40.88	Central USA	2
NATX	-94.66	31.76	SE USA	1
NCB	-74.22	43.97	NE USA	2
NE80	-112.32	30.50	NW Mexico	1
NEE2	-114.62	34.77	SW USA	1
NNA	-76.84	-11.99	Peru	1
NPNY	-74.14	41.75	NW USA	1
NRS	-45.42	61.16	Greenland	3
NUUK	-51.67	64.18	Greenland	2
O39A	-92.54	40.25	Central USA	1
OBN	36.57	55.11	Moscow	10
OLIL	-88.10	38.73	Central USA	1
ORV	-121.50	39.55	West USA	1
P32A	-98.60	39.62	Central USA	2
P39A	-92.75	39.49	Central USA	1
P40A	-92.05	39.53	Central USA	1
PAGS	-76.72	40.23	NE USA	1
PAL	-73.91	41.01	NE USA	2
PATS	158.31	6.84	North Pacific Ocean	1
PBMO	-90.43	36.78	Central USA	1
PDM	-114.14	34.30	SW USA	1
PIN	-120.87	43.81	NW USA	1
PKME	-69.29	45.26	NE USA	1
PLAL	-88.08	34.98	Central USA	1
PLCA	-70.55	-40.73	Argentina	2
PLM	-116.86	33.35	SW USA	1
PMG	147.15	-9.41	Papua New Guinea	1
PNT	-119.62	49.32	SW Canada	1
POGA	31.71	-27.35	South Africa	1
POTR	-121.94	38.20	Central West USA	1
PQI	-68.02	46.67	NE USA	1
PRNY	-76.54	42.47	NE USA	1

PSUB	-75.45	39.93	NE USA	1
PVAQ	-7.72	37.40	Spain	1
PVMO	-89.70	36.41	Central USA	2
Q24A	-105.15	38.96	Central USA	1
Q35A	-96.04	38.86	Central USA	1
R35A	-96.20	38.32	Central USA	2
R37A	-94.83	38.31	Central USA	1
RABL	152.16	-4.19	New Britain Is.	4
RCBR	-35.90	-5.83	NE Brazil	1
RDM	-116.85	33.63	SW USA	2
RPV	-118.40	33.74	SW USA	1
RRX	-117.00	34.88	SW USA	1
S02	54.00	17.13	Saudi Arabia	1
S06	54.05	17.62	Saudi Arabia	1
S32A	-98.94	37.70	Central USA	1
S36A	-95.59	37.72	Central USA	1
SA07	20.23	-31.98	South Africa	1
SA08	22.07	-31.91	South Africa	1
SA12	22.25	-29.85	South Africa	2
SA13	23.14	-29.98	South Africa	1
SA139	26.27	-25.85	South Africa	1
SA16	22.20	-28.95	South Africa	1
SA169	29.21	-22.26	NE South Africa	2
SA23	23.40	-27.93	South Africa	1
SA24	24.24	-27.88	South Africa	1
SA31	25.02	-27.00	South Africa	1
SA32	26.28	-26.87	South Africa	1
SA37	23.72	-25.97	South Africa	2
SA38	25.08	-25.93	South Africa	2
SA40	27.15	-25.90	South Africa	1
SA45	26.16	-24.88	South Africa	1
SA46	27.11	-24.84	South Africa	2
SA47	28.16	-24.85	NE South Africa	1
SA50	27.17	-23.87	NE South Africa	1
SA51	28.16	-23.86	NE South Africa	1
SA55	28.30	-22.98	NE South Africa	2
SA56	29.07	-23.01	NE South Africa	2
SA57	30.02	-22.98	NE South Africa	2
SA59	24.46	-24.84	Botswana	1
SA60	24.96	-23.85	Botswana	2
SA62	25.14	-24.85	Botswana	1
SA63	26.08	-23.66	Botswana	2
SA65	27.22	-22.82	Botswana	2
SA66	26.37	-21.90	Botswana	1
SA70	26.34	-21.09	Botswana	1
SA72	28.61	-20.14	Zimbabwe	2
SA73	30.28	-21.85	Zimbabwe	1
SA74	30.94	-21.92	Zimbabwe	2
SA75	29.00	-20.86	Zimbabwe	1

SA76	29.85	-20.64	Zimbabwe	1
SA77	30.92	-20.76	Zimbabwe	2
SA78	30.77	-19.47	Zimbabwe	2
SA79	30.52	-20.02	Zimbabwe	1
SA80	31.32	-19.96	Zimbabwe	1
SA81	21.27	-30.93	South Africa	1
SA82	22.25	-30.98	South Africa	2
SADO	-79.14	44.77	SE Canada	1
SBA	166.76	-77.85	Antarctica	4
SBC	-119.72	34.44	SW USA	1
SC01	-70.73	19.43	Caribbean Sea	1
SCHQ	-66.83	54.83	SE USA	6
SCIA	-93.22	41.91	Central USA	1
SCO	-21.95	70.49	Greenland	2
SDCO	-105.50	37.75	Central USA	1
SDMD	-76.84	39.41	NE USA	3
SDP	-120.50	34.57	NW USA	1
SEUS	-62.98	17.49	Caribbean Sea	1
SHO	-116.28	35.90	SW USA	2
SIUC	-89.22	37.71	Central USA	3
SLA	-117.28	35.89	SW USA	2
SLM	-90.24	38.64	Central USA	4
SMCO	-106.97	39.18	Central USA	1
SND	-116.61	33.55	SW USA	1
SNVB	-51.88	0.91	North Brazil	1
SPA	0.00	-90.00	Antarctica	1
SPA0	16.37	78.18	Arctic Ocean	4
SPB2	16.38	78.17	Arctic Ocean	5
SPB4	16.35	78.18	Arctic Ocean	3
SPMN	-92.80	45.22	NE USA	1
SSPA	-77.89	40.64	NE USA	3
SUMG	-38.45	72.58	Greenland	3
SUR	20.81	-32.38	South Africa	5
SUSD	-98.96	44.44	Central USA	1
T37A	-94.92	37.12	Central USA	1
TAKO	-124.08	43.74	NW USA	1
TEZI	26.02	-15.75	Zambia	2
TIN	-118.23	37.05	SW USA	1
TIP	16.76	39.18	Italy	1
TIR	19.86	41.35	Italy	1
TKM2	75.60	42.92	Kazakhstan	1
TOLO	-123.92	44.62	NW USA	1
TOV	-118.82	34.16	SW USA	2
TPH	-117.22	38.08	SW USA	2
TRIS	-12.32	-37.07	South Atlantic Ocean	2
TRO	-116.43	33.52	SW USA	1
TSUM	17.58	-19.20	Namibia	3
TTW	-121.69	47.69	NW USA	1
TUE	9.35	46.47	Italy	1

TX31	-103.67	29.33	SE USA	1
U37A	-95.12	36.41	Central USA	1
UALR	-92.34	34.78	Central USA	2
UCH	74.51	42.23	Kyrgyzstan	1
ULHL	76.24	42.25	Kyrgyzstan	4
UPAO	-80.02	40.48	NE USA	1
USIN	-87.67	37.97	Central USA	3
UTMT	-88.86	36.35	Central USA	1
V11A	-115.43	35.84	SW USA	1
V12A	-114.85	35.73	SW USA	1
V28A	-102.22	35.75	Central USA	1
V33A	-98.29	35.82	Central USA	1
V34A	-97.52	35.83	Central USA	1
VBMS	-90.52	32.22	SE USA	1
VNDA	161.85	-77.52	Antarctica	1
VOS	70.98	52.72	Kazakhstan	2
VTS	23.23	42.62	Romania	1
VTV	-117.33	34.56	SW USA	1
W13A	-113.89	35.10	SW USA	2
W30A	-100.58	35.18	Central USA	1
W32A	-99.25	35.12	Central USA	1
WB2	134.35	-19.94	Northern Territory	3
WCI	-86.29	38.23	Central USA	2
WDC	-122.54	40.58	Central West USA	1
WDD	14.52	35.84	Mediterranean Sea	1
WES	-71.32	42.38	NE USA	1
WHTX	-97.46	31.99	SE USA	3
WIN	17.10	-22.57	Namibia	1
WMC	-116.67	33.57	SW USA	1
WMOK	-98.78	34.74	Central USA	1
WRAB	134.36	-19.93	Northern Territory	1
WRKA	128.30	-25.04	Western Australia	2
WRPS	-77.87	40.79	NE USA	1
WUAZ	-111.37	35.52	Central USA	1
WVT	-87.83	36.13	Central USA	4
X30A	-100.87	34.45	Central USA	1
X32A	-99.29	34.42	Central USA	1
X36A	-96.35	34.57	Central USA	1
X38A	-94.83	34.67	Central USA	1
Y14A	-113.00	33.94	SW USA	1
Y34A	-97.76	33.96	Central USA	2
Y35A	-97.04	33.91	Central USA	1
YAK	129.68	62.03	Central Russia	2
YBH	-122.71	41.73	Central West USA	1
Z31A	-100.14	33.32	Central USA	1
Z32A	-99.48	33.31	Central USA	2
Z33A	-98.76	33.29	Central USA	1
ZOMB	35.35	-15.38	Malawi	1
ZRNK	69.00	52.95	Kazakhstan	5



115A	-112.23	32.70	SW USA	1
130A	-100.97	32.60	Central USA	1
133A	-98.92	32.61	Central USA	1
134A	-98.08	32.57	Central USA	2
136A	-96.53	32.47	Central USA	1
214A	-112.81	31.96	SW USA	1
234A	-98.14	32.00	Central USA	1
236A	-96.53	32.00	Central USA	1
332A	-99.74	31.38	Central USA	1
335A	-97.43	31.28	Central USA	2
336A	-96.84	31.39	Central South USA	1
337A	-95.89	31.32	Central South USA	1
340A	-93.89	31.42	Central South USA	1
348A	-87.90	31.41	SE USA	1
430A	-101.24	30.79	Central South USA	1
431A	-100.61	30.68	Central South USA	1
432A	-99.79	30.88	Central South USA	1
433A	-99.09	30.75	Central South USA	2
436A	-96.80	30.77	Central South USA	1
437A	-96.14	30.83	Central South USA	1
533A	-99.04	30.07	Central South USA	1
534A	-98.48	30.03	Central South USA	1
536A	-97.07	30.08	Central South USA	1
538A	-95.49	30.22	Central South USA	2
539A	-94.72	30.11	Central South USA	1
540A	-93.98	30.21	Central South USA	1
634A	-98.35	29.38	Central South USA	4
635A	-97.77	29.39	Central South USA	1
636A	-97.06	29.48	Central South USA	3
637A	-96.33	29.44	Central South USA	2
732A	-99.97	28.73	Central South USA	1
733A	-99.29	28.72	Central South USA	1
735A	-97.81	28.86	Central South USA	1
737A	-96.44	28.76	Central South USA	1
832A	-99.97	28.28	Central South USA	2
834A	-98.55	28.13	Central South USA	1
934A	-98.52	27.60	Central South USA	1

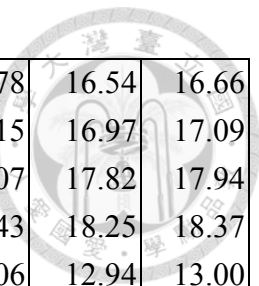
Note: List of 374 stations locations and number of data for using in this study. In our searching range, we get 1519 data from 744 stations, but we need to ensure the measurement is precision, we set criteria and finally get 606 differential travelttime measurements from 374 stations. The last column is the number data used in the station.



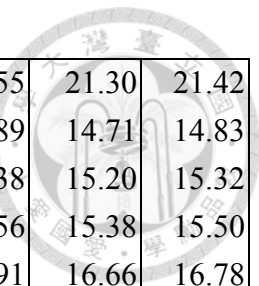
Appendix C. S3KS-SKKS Differential Traveltime Measurements

Table C.1 List of 606 observed S3KS-SKKS differential traveltimes and predictions of PREM and PREM-like models.

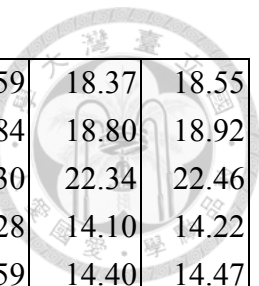
Event No.	Station Name	Distance (°)	Azimuth (°)	Quality Score	SKKS p (s/deg)	S3KS p (s/deg)	SKKS h_T (km)	S3KS h_T (km)	S3KS-SKKS Differential Times						
									TauP PREM	OBS	PREM-SOC	PREM	PREM-OC2	PREM-OC3	PREM-OC4
1	P32A	122.36	36.96	18	6.435	7.095	318.5	119.9	13.96	14.70	14.53	14.04	14.47	14.22	14.34
1	X30A	123.99	43.21	18	6.382	7.072	335.7	126.5	15.10	14.47	15.56	15.14	15.50	15.32	15.44
1	Z31A	125.12	43.92	19	6.344	7.056	347.9	131.2	15.93	16.15	16.42	15.93	16.36	16.17	16.30
1	Z32A	125.59	43.54	20	6.329	7.049	352.8	133.1	16.25	15.82	16.78	16.30	16.72	16.54	16.66
1	430A	125.72	47.14	19	6.324	7.047	354.4	133.7	16.34	16.60	16.85	16.42	16.85	16.66	16.78
1	431A	126.24	46.89	18	6.307	7.039	360.0	136.0	16.71	16.12	17.27	16.78	17.21	17.03	17.15
1	432A	126.72	46.22	17	6.291	7.031	365.3	138.2	17.04	16.85	17.64	17.09	17.58	17.33	17.52
1	JCT	126.93	46.64	17	6.283	7.028	367.6	139.1	17.19	17.00	17.76	17.27	17.76	17.52	17.64
1	WHTX	127.74	43.64	19	6.256	7.016	376.5	142.7	17.80	17.90	18.49	17.94	18.49	18.19	18.37
1	MIAR	128.70	38.53	17	6.226	7.001	386.1	146.8	18.56	19.10	19.35	18.68	19.29	18.98	19.16
1	SIUC	129.01	32.46	17	6.217	6.996	389.0	148.2	18.80	19.12	19.53	18.92	19.47	19.23	19.35
1	HKT	130.05	44.70	18	6.187	6.980	399.7	153.0	19.64	20.00	20.45	19.96	20.45	20.20	20.32
1	LRAL	133.68	34.89	18	6.069	6.921	438.8	170.1	22.59	22.93	23.50	23.01	23.50	23.25	23.38
3	R35A	122.05	36.43	17	6.443	7.098	315.8	118.8	13.79	13.55	14.28	13.92	14.22	14.10	14.16



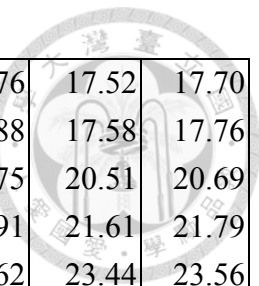
3	832A	125.56	48.35	18	6.327	7.048	353.4	133.4	16.27	19.10	16.78	16.30	16.78	16.54	16.66
3	634A	126.14	46.25	17	6.308	7.039	359.6	135.9	16.69	19.48	17.21	16.66	17.15	16.97	17.09
3	NATX	127.26	41.50	17	6.270	7.022	371.6	140.8	17.49	18.80	18.13	17.58	18.07	17.82	17.94
3	538A	127.66	43.57	17	6.256	7.016	376.1	142.6	17.79	19.45	18.43	17.94	18.43	18.25	18.37
4	S32A	120.54	38.77	17	6.492	7.121	300.5	112.4	12.80	12.50	13.12	12.82	13.06	12.94	13.00
4	W30A	120.99	42.03	17	6.478	7.114	304.7	114.3	13.07	12.95	13.55	13.12	13.43	13.31	13.37
4	U37A	123.71	37.63	18	6.391	7.076	332.2	125.2	14.88	15.50	15.38	14.95	15.32	15.14	15.26
4	X36A	124.12	40.10	19	6.378	7.070	336.8	126.9	15.19	15.38	15.62	15.26	15.56	15.44	15.50
4	SLM	124.94	32.42	20	6.350	7.059	345.2	130.1	15.79	16.35	16.24	15.81	16.24	16.05	16.11
4	732A	125.04	48.03	19	6.347	7.057	347.0	130.8	15.87	16.25	16.36	15.93	16.30	16.11	16.24
4	534A	125.41	45.82	18	6.335	7.052	350.7	132.2	16.13	16.45	16.66	16.17	16.60	16.42	16.54
4	634A	125.86	46.40	20	6.320	7.045	355.7	134.3	16.43	16.73	17.03	16.54	16.97	16.72	16.85
4	635A	126.28	46.04	18	6.306	7.038	360.2	136.1	16.73	16.93	17.27	16.78	17.27	17.03	17.15
4	636A	126.73	45.49	19	6.291	7.031	365.1	138.1	17.04	17.07	17.58	17.15	17.58	17.39	17.52
4	ACSO	127.20	25.76	20	6.274	7.024	369.6	139.9	17.39	18.20	18.01	17.52	18.01	17.76	17.88
4	PRNY	127.72	19.06	19	6.257	7.016	375.1	142.1	17.78	18.18	18.49	17.94	18.43	18.19	18.37
4	UPAO	128.21	23.18	19	6.241	7.009	380.7	144.4	18.15	19.24	18.92	18.31	18.92	18.62	18.80
4	WRPS	128.75	21.16	18	6.225	7.000	385.9	146.8	18.59	19.56	19.41	18.74	19.35	19.10	19.23
4	NPNY	129.11	17.38	17	6.215	6.995	389.3	148.3	18.88	18.80	19.65	19.04	19.65	19.35	19.53
4	PAGS	129.66	20.50	18	6.198	6.986	394.7	150.8	19.32	20.02	20.08	19.53	20.08	19.84	19.96
4	PSUB	130.36	19.54	17	6.178	6.975	401.6	153.9	19.88	20.14	20.75	20.20	20.69	20.51	20.63
4	BLA	130.83	25.75	19	6.163	6.968	406.5	156.1	20.26	20.65	21.24	20.69	21.18	21.00	21.12



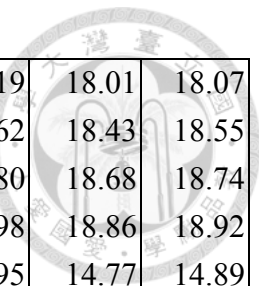
4	CBN	131.21	22.33	19	6.151	6.962	410.6	157.9	20.57	20.52	21.61	21.06	21.55	21.30	21.42
5	S36A	122.64	36.41	17	6.419	7.087	323.6	122.0	14.31	15.78	15.01	14.47	14.89	14.71	14.83
5	T37A	123.44	36.51	17	6.392	7.076	331.9	125.2	14.87	15.38	15.50	15.01	15.38	15.20	15.32
5	Y34A	123.71	41.20	17	6.383	7.072	334.9	126.4	15.08	15.97	15.62	15.20	15.56	15.38	15.50
5	OLIL	126.02	30.42	17	6.306	7.038	359.3	135.9	16.72	17.15	16.97	16.48	16.91	16.66	16.78
5	437A	126.71	43.17	17	6.283	7.028	367.3	139.2	17.22	17.18	17.64	17.21	17.64	17.46	17.58
5	735A	126.71	46.22	18	6.283	7.028	367.5	139.2	17.22	17.90	17.70	17.27	17.70	17.46	17.58
5	USIN	126.82	30.71	18	6.279	7.026	368.1	139.4	17.30	17.65	17.70	17.33	17.70	17.52	17.64
5	934A	126.90	47.95	17	6.277	7.025	369.7	140.1	17.36	19.12	17.88	17.39	17.88	17.64	17.76
5	ACSO	127.20	25.36	18	6.266	7.020	372.1	141.1	17.58	17.85	18.13	17.76	18.13	17.94	18.07
5	538A	127.52	43.34	20	6.255	7.015	376.4	142.8	17.82	17.87	18.43	17.94	18.43	18.19	18.37
6	V28A	120.08	42.36	17	6.507	7.128	295.9	110.3	12.49	11.88	12.82	13.00	12.63	12.45	12.51
6	W32A	122.42	41.29	18	6.436	7.095	318.3	119.7	13.94	14.55	14.28	14.53	14.40	14.10	14.16
6	X32A	122.81	41.98	17	6.423	7.090	322.3	121.3	14.20	14.35	14.65	14.83	14.94	14.47	14.53
6	GLMI	123.22	23.68	20	6.410	7.084	326.0	122.8	14.48	14.65	15.01	15.26	15.44	14.83	14.89
6	Y34A	124.10	41.51	19	6.381	7.072	335.8	126.5	15.11	15.00	15.81	16.05	15.50	15.56	15.69
6	HDIL	124.51	30.11	19	6.367	7.066	339.7	128.0	15.41	16.02	15.99	16.36	15.62	15.69	15.81
6	SLM	125.45	32.33	17	6.336	7.053	349.9	131.9	16.10	16.95	16.42	16.91	16.91	16.17	16.30
6	335A	125.93	43.91	19	6.320	7.045	355.6	134.2	16.43	16.32	16.78	17.21	17.15	16.60	16.72
6	634A	126.38	46.39	20	6.305	7.038	360.6	136.2	16.75	16.52	17.21	17.58	17.76	17.03	17.15
6	636A	127.25	45.48	17	6.275	7.025	370.0	140.0	17.37	17.43	18.13	18.49	18.68	17.76	17.94
6	637A	127.78	45.06	20	6.257	7.017	376.0	142.4	17.76	18.38	18.49	19.04	19.16	18.13	18.31



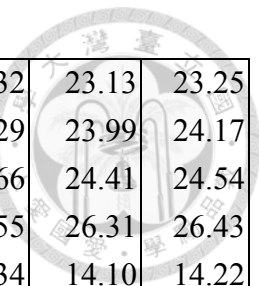
6	737A	128.10	45.82	19	6.247	7.012	379.6	143.9	18.01	19.35	18.74	19.35	19.59	18.37	18.55
6	WVT	128.59	32.65	17	6.232	7.004	384.0	145.8	18.41	18.95	19.10	19.78	19.84	18.80	18.92
6	BRAL	132.68	36.42	17	6.105	6.939	426.7	164.8	21.68	22.20	22.58	23.19	21.30	22.34	22.46
7	R35A	122.03	36.27	18	6.441	7.098	316.3	119.1	13.83	15.22	14.40	13.86	14.28	14.10	14.22
7	130A	122.50	44.42	20	6.426	7.091	321.3	121.0	14.15	14.30	14.71	14.16	14.59	14.40	14.47
7	R37A	122.84	35.41	20	6.415	7.086	324.5	122.3	14.37	15.50	14.83	14.34	14.77	14.59	14.65
7	332A	124.04	44.90	19	6.376	7.069	337.6	127.3	15.23	15.35	15.75	15.32	15.69	15.50	15.62
7	134A	124.49	42.74	20	6.361	7.063	342.2	129.1	15.57	16.65	15.99	15.56	15.93	15.75	15.87
7	433A	124.86	45.14	20	6.349	7.058	346.3	130.6	15.84	16.27	16.24	15.81	16.24	16.05	16.11
7	WHTX	125.26	42.91	19	6.335	7.052	350.5	132.2	16.12	17.40	16.54	16.05	16.48	16.30	16.42
7	335A	125.70	43.59	18	6.321	7.045	355.3	134.2	16.41	17.07	16.91	16.42	16.85	16.66	16.78
7	634A	126.17	46.06	17	6.305	7.038	360.5	136.3	16.75	17.80	17.27	16.78	17.21	17.03	17.15
7	536A	126.67	44.55	17	6.288	7.030	365.9	138.5	17.11	18.35	17.70	17.21	17.64	17.46	17.58
7	636A	127.03	45.14	17	6.276	7.024	369.9	140.1	17.37	17.95	17.94	17.46	17.94	17.70	17.88
7	637A	127.56	44.71	19	6.258	7.016	375.8	142.5	17.77	18.80	18.43	17.88	18.43	18.13	18.31
7	340A	127.99	41.10	20	6.244	7.010	380.3	144.3	18.09	19.57	18.86	18.31	18.80	18.55	18.74
7	539A	128.26	42.96	18	6.236	7.005	383.1	145.6	18.31	19.88	19.04	18.49	18.98	18.74	18.92
7	540A	128.70	42.34	18	6.223	6.999	387.4	147.5	18.66	20.17	19.35	18.80	19.35	19.10	19.23
7	BRAL	132.40	36.05	20	6.107	6.939	425.7	164.6	21.62	22.57	22.77	22.16	22.77	22.52	22.64
9	KMBL	121.74	185.12	17	6.454	7.103	310.6	116.7	13.57	13.37	14.10	13.55	13.98	13.79	13.92
9	MORW	124.23	179.21	18	6.373	7.068	336.4	126.8	15.30	15.15	15.81	15.38	15.75	15.56	15.62
9	CTA	125.15	214.43	17	6.342	7.055	347.2	130.9	15.97	17.02	16.48	15.99	16.42	16.24	16.30



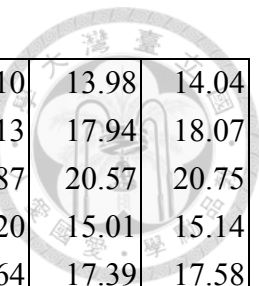
9	AS31	126.97	199.74	17	6.281	7.027	366.4	138.6	17.24	17.95	17.82	17.27	17.76	17.52	17.70
9	WRKA	127.07	193.11	20	6.278	7.026	367.3	139.0	17.32	18.23	17.94	17.33	17.88	17.58	17.76
9	WB2	130.31	201.85	19	6.178	6.976	401.0	153.7	19.87	20.20	20.81	20.20	20.75	20.51	20.69
9	COEN	131.88	215.41	19	6.128	6.950	418.3	161.3	21.12	21.20	21.97	21.30	21.91	21.61	21.79
9	RABL	133.84	233.18	17	6.062	6.917	441.4	171.2	22.75	25.05	23.62	23.13	23.62	23.44	23.56
9	KNRA	135.99	196.72	17	5.989	6.882	464.9	181.0	24.66	25.60	25.76	25.27	25.76	25.51	25.70
10	SCIA	123.36	32.11	17	6.410	7.084	326.3	122.8	14.47	15.15	15.32	14.53	15.20	14.89	15.08
10	Q35A	123.83	36.55	18	6.394	7.078	331.4	124.8	14.81	16.02	15.38	14.71	15.26	14.95	15.14
10	N39A	124.46	32.53	20	6.373	7.069	338.0	127.3	15.27	16.95	15.56	15.14	15.50	15.32	15.38
10	V34A	124.81	40.29	17	6.362	7.064	342.1	128.8	15.53	14.43	15.81	15.44	15.75	15.62	15.69
10	O39A	124.88	33.09	17	6.359	7.063	342.6	129.0	15.59	16.40	15.87	15.50	15.81	15.69	15.75
10	Z33A	125.48	43.54	17	6.339	7.054	349.4	131.6	16.03	15.82	16.42	16.05	16.36	16.24	16.30
10	P40A	125.66	33.40	17	6.333	7.052	350.9	132.2	16.14	15.85	16.54	16.17	16.54	16.36	16.48
10	Y35A	126.29	41.88	17	6.312	7.042	358.0	135.1	16.58	17.27	16.97	16.42	16.91	16.66	16.85
10	134A	126.36	43.85	18	6.310	7.041	358.9	135.5	16.62	17.18	17.03	16.42	16.97	16.72	16.85
10	234A	126.65	44.47	18	6.300	7.036	362.1	136.7	16.84	17.32	17.21	16.60	17.15	16.91	17.03
10	433A	126.66	46.32	20	6.300	7.036	362.3	136.9	16.84	17.88	17.21	16.60	17.15	16.91	17.03
10	533A	127.07	47.01	20	6.286	7.030	366.8	138.7	17.13	16.90	17.46	16.97	17.39	17.21	17.33
10	WHTX	127.13	44.07	19	6.284	7.029	367.3	138.9	17.17	16.93	17.46	17.03	17.46	17.21	17.33
10	832A	127.31	49.45	20	6.278	7.026	369.6	139.8	17.31	17.20	17.58	17.21	17.58	17.39	17.52
10	136A	127.48	43.00	17	6.272	7.023	371.2	140.4	17.44	19.65	17.70	17.33	17.76	17.52	17.64
10	733A	127.60	48.59	17	6.268	7.022	372.8	141.1	17.53	17.80	17.88	17.52	17.82	17.64	17.76



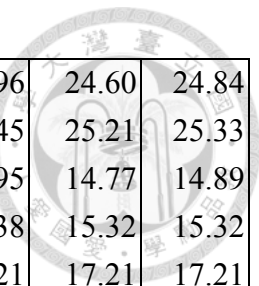
10	336A	127.90	44.30	19	6.257	7.017	376.0	142.3	17.75	18.97	18.13	17.82	18.19	18.01	18.07
10	436A	128.29	44.91	17	6.245	7.011	380.3	144.1	18.05	18.47	18.62	18.25	18.62	18.43	18.55
10	834A	128.47	48.79	17	6.240	7.008	382.1	144.9	18.19	19.70	18.80	18.49	18.80	18.68	18.74
10	337A	128.61	43.77	17	6.235	7.006	383.3	145.4	18.30	18.77	18.98	18.62	18.98	18.86	18.92
11	BOZ	123.20	38.79	18	6.415	7.087	326.5	122.9	14.36	15.75	15.08	14.53	14.95	14.77	14.89
11	SND	124.09	53.99	17	6.386	7.074	336.1	126.6	15.00	15.37	15.56	15.08	15.50	15.26	15.38
11	NEE2	125.32	51.99	18	6.345	7.057	349.2	131.5	15.91	16.37	16.36	15.93	16.30	16.11	16.24
11	W13A	125.79	51.37	19	6.329	7.050	354.2	133.5	16.23	16.10	16.78	16.30	16.72	16.54	16.60
11	A27A	127.26	30.63	17	6.280	7.027	370.0	139.9	17.27	16.95	18.13	17.46	18.07	17.76	17.94
11	214A	127.62	54.73	20	6.267	7.021	374.4	141.7	17.54	17.95	18.25	17.64	18.19	17.94	18.07
11	B28A	128.03	30.64	20	6.253	7.015	378.6	143.4	17.84	18.32	18.55	17.88	18.55	18.19	18.37
11	C28A	128.49	31.37	19	6.239	7.008	383.2	145.4	18.21	18.50	18.92	18.25	18.86	18.55	18.74
11	MDND	128.81	30.80	19	6.230	7.003	386.3	146.8	18.46	19.10	19.16	18.62	19.10	18.86	18.98
11	SMCO	129.26	43.90	19	6.216	6.996	391.0	148.9	18.82	18.98	19.53	19.04	19.53	19.29	19.41
11	D30A	129.73	31.03	20	6.202	6.989	395.3	150.9	19.20	19.82	20.02	19.59	20.02	19.84	19.90
11	E30A	130.05	31.71	20	6.193	6.984	398.5	152.4	19.46	20.12	20.45	19.96	20.39	20.20	20.32
11	H29A	130.54	34.37	19	6.179	6.976	403.4	154.6	19.85	19.30	20.87	20.39	20.87	20.63	20.81
11	E32A	130.93	30.51	20	6.167	6.970	407.4	156.3	20.16	21.35	21.30	20.63	21.24	21.00	21.12
11	SUSD	131.35	33.81	20	6.153	6.963	412.1	158.4	20.50	21.38	21.55	20.87	21.55	21.24	21.42
11	J30A	131.75	35.30	20	6.140	6.957	416.6	160.3	20.82	21.62	21.85	21.12	21.79	21.48	21.67
11	C36A	132.11	26.66	17	6.128	6.951	420.2	161.9	21.10	21.60	22.03	21.42	21.97	21.73	21.85
11	EYMN	132.55	25.56	19	6.113	6.943	425.1	164.0	21.45	21.62	22.34	21.85	22.34	22.09	22.22



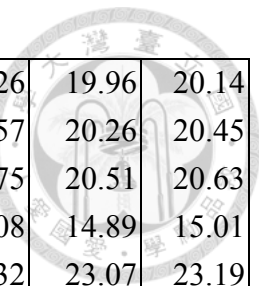
11	K33A	133.62	34.49	19	6.078	6.926	437.3	169.3	22.34	23.18	23.32	22.89	23.32	23.13	23.25
11	H37A	134.42	29.65	18	6.050	6.912	446.4	173.1	23.05	24.00	24.29	23.62	24.29	23.99	24.17
11	L35A	134.76	34.01	17	6.039	6.907	450.5	174.8	23.35	24.35	24.72	23.99	24.66	24.41	24.54
11	N39A	137.27	33.06	17	5.952	6.867	480.0	186.7	25.56	26.75	26.49	26.00	26.55	26.31	26.43
12	SCHQ	122.43	39.03	19	6.437	7.096	320.1	120.5	13.90	14.40	14.40	13.79	14.34	14.10	14.22
12	SPB5	124.99	355.92	18	6.353	7.060	347.0	130.7	15.72	16.43	16.24	15.75	16.17	15.99	16.11
12	SPB1	124.99	355.91	18	6.353	7.060	346.9	130.7	15.72	16.39	16.24	15.75	16.17	15.99	16.11
12	SPA0	125.00	355.91	18	6.353	7.060	347.0	130.7	15.73	16.43	16.24	15.75	16.17	15.99	16.11
12	SPB4	125.00	355.92	18	6.353	7.060	347.0	130.7	15.73	16.45	16.24	15.75	16.17	15.99	16.11
12	SPB2	125.00	355.91	18	6.353	7.060	347.1	130.8	15.73	16.43	16.24	15.75	16.17	15.99	16.11
12	SPB3	125.00	355.91	18	6.353	7.060	347.1	130.8	15.73	16.45	16.24	15.75	16.17	15.99	16.11
12	DAG	126.17	5.21	19	6.314	7.042	359.6	135.8	16.55	17.35	16.97	16.48	16.97	16.72	16.85
12	ARU	126.74	323.70	17	6.295	7.034	366.0	138.4	16.95	17.30	17.46	16.97	17.46	17.21	17.33
12	SUMG	126.78	13.50	17	6.293	7.033	366.2	138.5	16.97	17.70	17.46	17.03	17.46	17.21	17.33
12	NUUK	127.57	25.65	20	6.266	7.021	375.1	142.0	17.57	18.50	18.19	17.70	18.13	17.94	18.07
12	KNS	128.30	25.04	19	6.242	7.010	382.8	145.3	18.12	18.25	18.86	18.31	18.86	18.62	18.74
12	DBG	128.31	6.86	18	6.242	7.009	382.8	145.3	18.13	19.10	18.86	18.31	18.86	18.62	18.74
12	DRLN	128.76	45.08	18	6.229	7.002	387.5	147.4	18.48	18.85	19.35	18.80	19.35	19.10	19.23
12	LVZ	131.00	343.40	20	6.162	6.968	409.5	157.3	20.28	21.85	21.24	20.63	21.24	20.94	21.12
12	NRS	131.52	27.43	19	6.145	6.959	415.4	159.9	20.70	22.30	21.61	21.00	21.55	21.30	21.42
12	SCO	131.56	9.63	18	6.143	6.958	415.6	160.0	20.73	21.75	21.61	21.06	21.61	21.36	21.48
12	ANGG	131.78	19.84	18	6.136	6.955	418.1	161.1	20.91	22.10	21.79	21.24	21.79	21.48	21.67



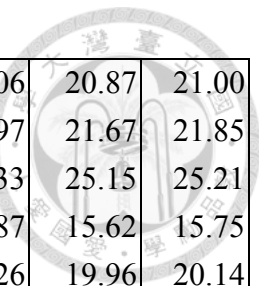
13	ZR NK	121.87	317.80	17	6.452	7.103	315.7	118.8	13.61	14.15	14.16	13.86	14.10	13.98	14.04
13	ABKAR	127.63	313.38	17	6.261	7.018	377.2	142.9	17.69	17.90	18.13	17.70	18.13	17.94	18.07
13	TEZI	130.64	215.94	17	6.171	6.972	404.1	155.0	20.08	20.80	20.87	20.32	20.87	20.57	20.75
14	ARMA	123.54	225.26	19	6.395	7.078	331.2	124.9	14.80	16.20	15.26	14.83	15.20	15.01	15.14
14	CMSA	126.84	220.32	17	6.285	7.029	366.6	138.7	17.16	19.30	17.70	17.15	17.64	17.39	17.58
14	ULHL	135.75	34.45	17	5.996	6.886	464.1	180.6	24.47	25.93	25.88	25.57	25.94	25.82	25.88
15	MORW	122.85	179.03	17	6.417	7.087	320.6	120.8	14.34	14.85	14.83	14.34	14.77	14.59	14.65
15	ATKA	124.66	315.75	18	6.357	7.061	347.1	130.9	15.64	15.76	15.99	15.56	15.93	15.75	15.81
15	AS31	125.73	199.21	18	6.322	7.046	351.4	132.5	16.40	17.35	16.85	16.42	16.85	16.60	16.72
15	WB2	129.09	201.23	19	6.213	6.994	387.8	147.7	18.92	19.17	19.59	18.98	19.59	19.29	19.47
15	COEN	130.84	214.52	20	6.160	6.966	405.6	155.8	20.33	20.88	21.24	20.69	21.18	21.00	21.12
15	RABL	133.13	231.97	18	6.085	6.928	432.2	167.4	22.16	24.25	23.07	22.52	23.07	22.77	22.95
16	ABKAR	124.26	40.42	18	6.376	7.070	339.1	127.8	15.23	14.70	15.87	15.38	15.81	15.62	15.75
16	BRVK	128.71	32.86	20	6.229	7.002	386.6	147.0	18.49	18.15	19.29	18.62	19.23	18.92	19.10
16	YAK	132.24	350.60	17	6.119	6.946	422.9	163.2	21.32	21.65	22.34	21.67	22.28	21.97	22.16
17	AS31	126.04	199.36	18	6.312	7.041	354.4	133.8	16.60	17.00	17.09	16.60	17.09	16.85	16.97
17	WRKA	126.10	192.81	17	6.310	7.040	354.7	133.9	16.64	16.88	17.15	16.66	17.09	16.91	17.03
17	WB2	129.40	201.41	17	6.205	6.989	390.4	148.9	19.15	19.82	19.96	19.41	19.90	19.71	19.84
17	GIRL	129.54	176.80	17	6.200	6.987	391.3	149.3	19.27	20.23	20.08	19.53	20.08	19.84	19.96
17	BILL	130.46	337.93	20	6.173	6.973	408.3	156.9	20.01	19.95	20.51	20.51	20.87	20.75	20.39
17	COEN	131.10	214.77	20	6.153	6.962	408.2	156.9	20.52	20.60	21.48	20.75	21.42	21.12	21.30
17	RABL	133.31	232.29	20	6.080	6.926	434.2	168.2	22.30	24.50	23.19	22.64	23.19	22.95	23.07



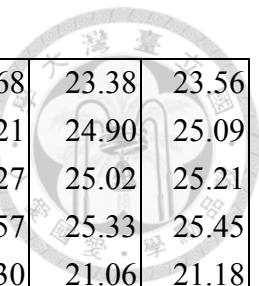
17	KNRA	135.05	196.27	17	6.020	6.897	451.8	175.6	23.84	23.65	24.96	24.23	24.96	24.60	24.84
17	PATS	135.53	249.64	17	6.004	6.889	461.7	179.7	24.28	23.95	25.45	24.84	25.45	25.21	25.33
18	Q24A	123.29	47.16	17	6.417	7.088	325.2	122.3	14.31	13.97	12.63	14.22	14.95	14.77	14.89
18	F31A	124.87	36.98	17	6.365	7.066	341.7	128.6	15.45	15.37	13.92	15.26	15.38	15.32	15.32
18	D34A	125.97	34.31	17	6.328	7.050	353.3	133.1	16.23	16.05	17.15	16.60	17.21	17.21	17.21
18	V33A	129.54	48.14	20	6.213	6.994	391.7	149.2	18.91	20.90	22.22	19.47	20.02	19.78	19.90
18	348A	139.25	48.02	19	5.898	6.839	498.5	194.9	27.24	28.62	30.76	28.50	28.99	28.87	28.93
19	PNT	120.35	31.79	17	6.494	7.122	300.1	112.3	12.74	12.95	15.93	12.39	12.70	12.51	12.57
19	EDM	120.81	25.37	18	6.481	7.116	303.6	113.8	13.01	14.00	13.00	12.82	12.94	12.88	12.88
19	FCC	122.24	11.25	20	6.436	7.095	316.3	119.0	13.93	14.57	14.34	14.04	14.28	14.16	14.22
19	SCHQ	127.52	353.60	19	6.261	7.018	371.2	140.6	17.69	18.05	20.39	17.39	17.82	17.64	17.70
19	ULM	129.59	16.76	20	6.198	6.986	394.2	150.6	19.33	20.27	20.02	19.29	19.78	19.53	19.71
19	KAPO	133.03	6.15	19	6.088	6.930	429.8	166.3	22.09	23.05	25.51	22.46	23.01	22.77	22.89
19	SADO	137.97	3.75	17	5.924	6.851	486.1	189.7	26.48	27.30	24.66	26.55	27.65	27.04	27.34
20	JFWS	121.79	28.74	17	6.448	7.100	314.0	118.2	13.70	13.10	14.28	13.79	14.16	13.98	14.10
20	PBMO	126.25	33.82	18	6.301	7.036	361.3	136.7	16.84	16.15	17.15	16.72	17.15	16.97	17.09
20	DBIC	126.83	283.50	19	6.281	7.027	369.4	139.9	17.25	17.82	17.76	17.27	17.76	17.52	17.64
20	WCI	127.31	29.53	17	6.265	7.019	372.9	141.4	17.62	17.35	18.19	17.76	18.19	17.94	18.07
20	HNH	127.75	14.50	18	6.250	7.013	377.3	143.1	17.94	18.60	18.68	18.25	18.68	18.43	18.55
20	WVT	128.14	32.42	19	6.238	7.007	382.0	145.1	18.25	17.90	19.16	18.74	19.16	18.98	19.10
20	SSPA	128.86	20.94	19	6.217	6.995	388.7	148.1	18.83	19.70	19.84	19.29	19.84	19.59	19.71
20	HRV	129.06	14.38	18	6.211	6.992	390.4	148.9	18.99	19.95	19.96	19.35	19.90	19.65	19.84



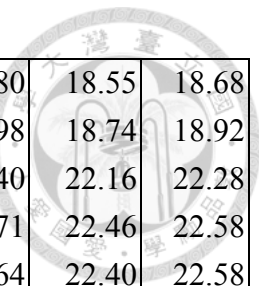
20	BRYW	129.62	14.62	18	6.195	6.984	396.0	151.5	19.44	20.03	20.32	19.65	20.26	19.96	20.14
20	CPNY	130.00	17.36	18	6.183	6.978	399.8	153.2	19.74	19.75	20.57	19.90	20.57	20.26	20.45
20	SDMD	130.32	20.74	18	6.174	6.973	403.0	154.7	20.00	20.40	20.87	20.14	20.75	20.51	20.63
23	MORW	123.36	178.99	18	6.402	7.080	327.1	123.3	14.66	13.60	15.14	14.71	15.08	14.89	15.01
23	RABL	133.47	232.32	19	6.075	6.924	437.0	169.4	22.43	24.77	23.32	22.77	23.32	23.07	23.19
24	SPB2	122.76	356.20	17	6.417	7.087	326.5	123.1	14.35	12.97	14.95	14.47	14.83	14.71	14.77
25	P38A	125.04	34.08	19	6.354	7.060	344.5	129.8	15.71	18.80	16.11	15.62	16.05	15.87	15.93
25	Z32A	125.29	43.76	18	6.345	7.057	347.4	130.9	15.90	16.95	16.30	15.81	16.24	16.05	16.17
25	P39A	125.57	33.69	19	6.336	7.053	350.1	131.9	16.09	19.37	16.48	16.05	16.48	16.24	16.36
25	133A	126.08	44.14	18	6.319	7.045	355.9	134.2	16.44	20.00	16.85	16.36	16.85	16.60	16.72
25	X38A	127.56	39.52	19	6.269	7.022	372.0	140.8	17.51	22.18	18.01	17.64	18.01	17.82	17.94
25	236A	128.07	43.29	17	6.251	7.014	378.0	143.1	17.88	20.40	18.62	18.13	18.55	18.37	18.49
25	EMMW	130.49	9.71	17	6.180	6.977	401.0	153.5	19.82	22.32	20.81	20.14	20.75	20.51	20.63
25	VBMS	131.88	38.84	17	6.135	6.954	416.6	160.4	20.93	16.88	22.03	21.42	22.03	21.79	21.91
26	PVAQ	126.48	311.81	17	6.292	7.032	365.7	138.5	17.03	16.60	17.46	16.97	17.46	17.21	17.33
28	HDC	122.61	52.88	17	6.443	7.099	351.2	132.1	13.77	14.80	14.47	14.22	14.40	14.34	14.34
29	BOSA	124.72	247.74	19	6.354	7.060	346.3	130.6	15.71	16.32	16.17	15.69	16.11	15.93	16.05
29	MACI	130.16	338.93	18	6.181	6.977	400.3	153.4	19.81	20.75	20.51	19.71	20.45	20.08	20.26
30	VNDA	129.77	177.08	19	6.188	6.980	402.9	154.7	19.61	19.60	20.08	19.84	20.32	20.08	20.20
30	ICE	130.02	175.58	20	6.181	6.976	405.3	155.8	19.81	21.07	20.32	20.14	20.57	20.39	20.51
30	SBA	130.29	175.80	19	6.173	6.972	408.2	157.0	20.03	21.05	20.63	20.39	20.81	20.63	20.75
31	NRS	131.92	27.17	19	6.130	6.951	420.5	162.2	21.07	21.95	22.03	21.30	21.97	21.67	21.85



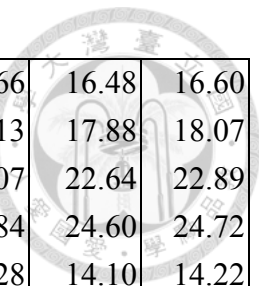
32	POGA	130.86	279.47	17	6.170	6.972	407.3	156.3	20.06	20.25	21.12	20.57	21.06	20.87	21.00
32	SBA	132.07	176.59	20	6.131	6.952	422.5	162.9	21.03	22.23	21.97	21.36	21.97	21.67	21.85
32	BB23	136.54	66.35	18	5.979	6.879	471.7	183.4	24.87	19.62	25.27	24.96	25.33	25.15	25.21
33	CASY	124.38	199.47	17	6.365	7.065	345.6	130.3	15.48	19.95	15.93	15.44	15.87	15.62	15.75
34	BLWY	129.96	215.07	19	6.187	6.980	398.7	152.6	19.64	21.80	20.26	19.65	20.26	19.96	20.14
35	E58A	120.81	50.48	17	6.492	7.122	302.8	113.3	12.77	13.80	12.15	12.15	12.09	12.09	12.09
35	F59A	121.07	51.15	17	6.485	7.118	305.2	114.4	12.93	14.03	12.63	12.70	12.57	12.63	12.57
35	G60A	121.26	52.07	17	6.479	7.115	307.1	115.1	13.04	14.25	13.06	13.06	13.00	13.00	13.00
35	M65A	121.88	56.41	17	6.460	7.107	313.1	117.6	13.44	14.20	14.22	14.04	14.16	14.10	14.16
35	D59A	121.89	49.92	17	6.460	7.106	313.3	117.6	13.44	13.85	14.22	14.04	14.16	14.10	14.16
35	ICQ	125.15	47.25	20	6.353	7.060	347.5	130.8	15.72	16.18	16.24	15.44	16.17	15.81	15.99
35	SCHQ	125.49	40.73	18	6.342	7.056	351.2	132.2	15.96	16.13	16.24	15.69	16.17	15.93	16.05
35	ABKAR	129.73	312.39	19	6.205	6.990	395.7	151.1	19.13	20.18	19.96	19.41	19.84	19.65	19.78
35	NUUK	131.12	27.06	19	6.163	6.969	409.7	157.3	20.25	21.35	21.12	20.63	21.12	20.87	21.00
37	SC01	123.21	33.76	17	6.426	7.092	320.3	120.3	14.13	14.43	14.59	14.47	14.53	14.47	14.53
37	SEUS	128.31	26.82	19	6.255	7.017	375.4	141.9	17.79	19.22	18.43	18.01	18.43	18.25	18.31
37	FDF	131.53	26.14	18	6.158	6.966	408.0	156.4	20.36	21.75	21.00	20.57	21.00	20.81	20.94
38	FRB	123.35	4.49	19	6.406	7.083	328.0	123.5	14.55	15.80	15.14	14.71	15.01	14.89	14.95
38	DBIC	125.21	273.00	17	6.345	7.056	349.1	131.6	15.92	16.68	16.48	15.81	16.42	16.11	16.30
38	N23A	127.31	43.16	18	6.274	7.024	371.5	140.6	17.40	18.85	17.94	17.33	17.88	17.64	17.76
38	BGNE	132.13	38.71	18	6.123	6.948	421.3	162.5	21.22	22.87	22.09	21.42	22.03	21.79	21.91
38	SPMN	132.79	31.37	17	6.102	6.937	428.5	165.6	21.75	23.18	22.64	22.03	22.64	22.40	22.52



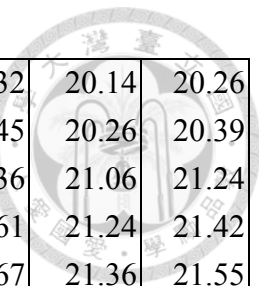
38	KAPO	133.97	20.24	19	6.062	6.918	441.5	171.2	22.75	23.88	23.68	23.07	23.68	23.38	23.56
38	D47A	135.77	22.54	17	6.000	6.888	462.5	179.9	24.35	25.73	25.15	24.60	25.21	24.90	25.09
38	F45A	135.91	25.64	17	5.995	6.886	464.2	180.6	24.47	26.40	25.27	24.72	25.27	25.02	25.21
38	E47A	136.20	23.17	18	5.985	6.881	467.6	181.9	24.72	25.23	25.51	25.09	25.57	25.33	25.45
39	ICE	130.73	175.92	20	6.165	6.969	411.0	158.1	20.22	21.93	21.36	20.75	21.30	21.06	21.18
39	SBA	131.00	176.14	19	6.156	6.964	414.0	159.4	20.44	21.85	21.55	20.94	21.55	21.30	21.42
39	GO01	133.51	60.55	17	6.073	6.923	439.2	170.3	22.48	21.95	23.38	22.83	23.38	23.13	23.25
39	MAW	137.50	214.55	17	5.938	6.859	487.2	190.2	26.01	27.57	26.67	26.18	26.73	26.49	26.61
40	WES	120.45	54.37	18	6.501	7.126	300.1	112.1	12.61	12.90	12.09	12.09	12.02	12.02	12.02
40	CHKZ	121.49	318.76	17	6.470	7.111	309.9	116.3	13.23	13.70	13.92	13.31	13.79	13.49	13.67
40	BRVK	121.67	318.02	17	6.464	7.108	311.8	117.1	13.35	13.90	13.98	13.49	13.86	13.67	13.73
40	ZRNK	122.44	317.88	20	6.440	7.098	319.5	120.2	13.84	14.22	14.65	14.34	14.59	14.53	14.59
40	ARU	128.17	322.80	20	6.249	7.013	380.9	144.3	17.94	18.55	18.74	18.25	18.74	18.49	18.62
40	ABKAR	128.27	313.58	20	6.246	7.012	382.0	144.8	18.02	18.43	18.86	18.43	18.86	18.68	18.80
40	ABKT	129.63	299.01	19	6.206	6.991	395.3	150.9	19.11	19.65	20.39	19.65	20.32	20.02	20.20
40	DRLN	130.23	46.18	17	6.188	6.981	401.1	153.6	19.59	20.30	20.02	19.53	20.02	19.78	19.90
40	TSUM	132.11	203.00	17	6.128	6.951	417.7	160.8	21.09	21.90	22.16	21.73	22.16	21.97	22.03
40	LVZ	132.78	342.83	19	6.106	6.940	428.4	165.5	21.62	23.20	22.71	22.09	22.71	22.40	22.58
41	VOS	120.79	317.83	18	6.488	7.119	304.0	113.9	12.86	13.50	13.86	13.37	13.73	13.61	13.67
41	ZRNK	121.99	318.06	19	6.451	7.102	315.9	118.8	13.62	14.10	14.47	13.86	14.34	14.10	14.22
41	LBTB	124.00	208.78	18	6.386	7.074	332.8	125.4	15.00	14.82	15.75	15.38	15.69	15.56	15.62
41	ZOMB	126.58	224.71	17	6.300	7.036	361.6	136.6	16.84	16.75	17.82	17.27	17.76	17.52	17.64



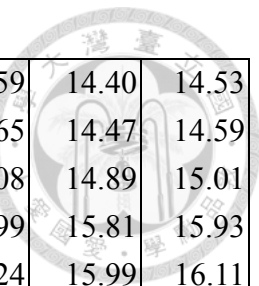
41	ARU	127.70	322.97	19	6.262	7.019	376.9	142.8	17.66	18.20	18.86	18.25	18.80	18.55	18.68
41	ABKAR	127.83	313.81	20	6.257	7.017	378.4	143.4	17.76	17.82	19.04	18.49	18.98	18.74	18.92
41	LVZ	132.31	342.87	18	6.118	6.946	424.2	163.7	21.33	23.40	22.46	21.91	22.40	22.16	22.28
41	TSUM	132.42	203.41	18	6.115	6.944	422.3	162.9	21.42	21.20	22.71	22.16	22.71	22.46	22.58
41	KEV	132.65	347.38	19	6.107	6.940	427.9	165.3	21.61	22.10	22.71	22.16	22.64	22.40	22.58
42	GRM	122.15	205.25	17	6.428	7.091	319.5	120.5	14.12	14.90	14.59	14.10	14.47	14.28	14.40
42	SUR	125.08	200.56	17	6.331	7.049	350.3	132.3	16.21	16.10	16.60	16.11	16.54	16.36	16.48
42	LVZ	127.11	344.74	17	6.263	7.018	375.7	142.6	17.66	18.20	18.07	18.01	18.07	18.07	18.07
42	LSZ	136.32	219.75	17	5.964	6.870	474.0	184.8	25.28	24.45	26.55	26.00	26.61	26.31	26.49
43	HNR	124.97	235.84	17	6.350	7.058	345.9	130.4	15.81	21.10	16.17	15.81	16.17	15.99	16.11
43	CTAO	125.77	215.06	20	6.323	7.047	353.5	133.3	16.36	17.10	16.85	16.42	16.85	16.66	16.78
43	CTA	125.77	215.05	20	6.323	7.047	353.5	133.3	16.36	17.17	16.91	16.42	16.85	16.66	16.78
43	AS31	127.75	200.26	20	6.256	7.016	374.6	141.9	17.79	18.82	18.43	17.94	18.43	18.25	18.37
43	BILL	128.54	338.44	17	6.232	7.004	386.5	147.0	18.41	19.60	19.29	18.55	19.23	18.98	19.16
43	FITZ	135.18	192.33	17	6.018	6.896	454.8	176.8	23.90	24.15	24.54	24.17	24.60	24.35	24.48
43	ZRNK	135.71	39.72	17	6.000	6.887	464.6	180.8	24.37	22.90	25.02	24.54	25.09	24.84	24.96
43	CHKZ	136.38	38.27	19	5.977	6.877	472.5	183.9	24.95	24.20	25.88	25.76	26.00	25.88	25.94
44	ARU	122.88	326.44	19	6.414	7.086	326.9	123.2	14.40	14.75	14.77	14.40	14.71	14.34	14.65
44	TRIS	123.84	166.35	17	6.383	7.072	333.6	125.8	15.08	18.05	15.56	15.08	15.56	15.32	15.44
44	OBN	134.30	332.81	17	6.044	6.908	448.8	174.4	23.25	23.80	23.80	23.19	23.80	23.50	23.68
45	BOSA	127.00	205.45	18	6.280	7.027	367.2	139.0	17.27	15.93	17.82	17.27	17.76	17.52	17.70
45	RCBR	134.62	120.23	17	6.035	6.904	450.9	175.2	23.45	24.95	24.29	23.86	24.35	24.11	24.23



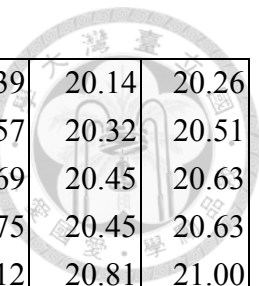
46	HNR	125.59	236.61	17	6.329	7.049	352.6	133.0	16.23	20.68	16.66	16.30	16.66	16.48	16.60
46	BILL	127.38	338.77	20	6.269	7.022	374.4	141.8	17.52	17.90	18.19	17.64	18.13	17.88	18.07
46	COEN	133.42	216.94	18	6.078	6.925	435.0	168.5	22.34	24.20	23.13	22.28	23.07	22.64	22.89
46	CHKZ	135.46	37.48	18	6.008	6.892	461.5	179.6	24.15	23.62	24.84	24.35	24.84	24.60	24.72
47	KSU1	122.11	36.43	20	6.449	7.101	314.0	118.0	13.67	13.78	14.34	13.92	14.28	14.10	14.22
47	WMOK	123.45	41.78	19	6.405	7.082	328.0	123.5	14.57	14.43	14.95	14.53	14.89	14.71	14.77
47	CCM	125.89	33.90	20	6.324	7.047	353.8	133.4	16.33	16.45	16.78	16.36	16.72	16.54	16.66
47	SLM	126.03	32.70	20	6.320	7.045	355.2	134.0	16.43	17.00	16.91	16.42	16.85	16.66	16.78
47	AAM	126.34	25.01	19	6.309	7.040	358.4	135.3	16.65	17.55	17.15	16.72	17.09	16.91	17.03
47	FVM	126.40	33.39	20	6.307	7.039	359.3	135.6	16.69	17.35	17.21	16.78	17.15	16.97	17.09
47	SIUC	127.25	32.75	20	6.278	7.026	368.6	139.4	17.30	18.23	17.88	17.39	17.88	17.64	17.76
47	UALR	127.53	37.61	18	6.269	7.022	371.9	140.7	17.51	17.90	18.13	17.58	18.13	17.88	18.01
47	BLO	127.54	29.54	20	6.268	7.022	371.8	140.7	17.51	17.90	18.19	17.58	18.13	17.88	18.01
47	USIN	127.88	31.39	19	6.257	7.017	375.6	142.2	17.77	18.80	18.43	17.82	18.43	18.13	18.31
47	PVMO	127.93	34.23	19	6.255	7.016	376.3	142.5	17.81	18.90	18.49	17.88	18.43	18.19	18.31
47	GENY	128.18	20.07	20	6.247	7.012	378.5	143.4	18.00	18.55	18.68	18.07	18.68	18.37	18.55
47	NCB	128.21	16.40	18	6.246	7.011	378.8	143.5	18.02	18.52	18.74	18.07	18.68	18.37	18.55
47	ALLY	128.31	22.68	19	6.243	7.010	380.1	144.0	18.10	19.43	18.80	18.19	18.74	18.49	18.62
47	ACSO	128.33	25.96	18	6.242	7.010	380.5	144.2	18.11	19.23	18.80	18.19	18.80	18.49	18.68
47	UTMT	128.44	33.66	20	6.239	7.008	381.7	144.8	18.20	19.35	18.92	18.31	18.86	18.62	18.74
47	MPH	128.72	35.55	20	6.231	7.004	384.5	146.0	18.43	19.15	19.10	18.62	19.10	18.86	18.98
47	WVT	129.17	33.06	20	6.218	6.997	388.8	148.0	18.79	19.60	19.47	19.04	19.47	19.23	19.35



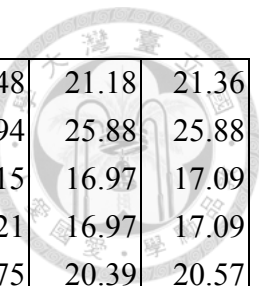
47	SSPA	130.03	21.42	18	6.192	6.983	396.9	151.7	19.48	20.25	20.32	19.84	20.32	20.14	20.26
47	MCWV	130.13	23.76	19	6.189	6.982	398.0	152.1	19.56	20.43	20.45	19.96	20.45	20.26	20.39
47	PAL	131.02	17.63	18	6.162	6.968	406.7	156.1	20.27	20.27	21.42	20.69	21.36	21.06	21.24
47	LTL	131.34	40.53	18	6.152	6.962	411.0	158.0	20.53	15.35	21.67	20.87	21.61	21.24	21.42
47	SDMD	131.49	21.24	20	6.147	6.960	412.0	158.4	20.65	21.32	21.73	21.00	21.67	21.36	21.55
47	LRAL	131.91	35.15	17	6.133	6.953	417.1	160.6	20.98	21.38	21.85	21.18	21.79	21.48	21.67
47	BLA	131.95	25.99	19	6.131	6.952	417.3	160.7	21.02	21.40	21.85	21.24	21.85	21.55	21.73
47	CBN	132.35	22.51	19	6.118	6.946	421.6	162.6	21.34	21.80	22.09	21.55	22.09	21.79	21.97
48	TRIS	121.87	166.91	17	6.445	7.099	313.8	118.1	13.76	9.53	14.47	13.98	14.34	14.16	14.28
48	ARU	124.47	325.60	17	6.360	7.062	344.7	130.0	15.60	15.40	15.93	15.50	15.87	15.69	15.75
48	ABKT	128.13	303.03	17	6.238	7.007	384.2	146.1	18.26	20.40	19.10	18.55	19.10	18.86	18.98
48	OBN	136.03	331.69	17	5.982	6.879	469.9	183.0	24.83	26.00	25.63	25.02	25.63	25.33	25.51
49	ABKAR	123.69	317.84	17	6.392	7.076	334.2	126.0	14.87	15.43	15.44	14.89	15.38	15.14	15.26
49	AKTK	124.63	319.58	18	6.361	7.063	344.1	129.7	15.57	15.88	15.93	15.69	15.93	15.81	15.87
49	SUR	126.89	200.50	18	6.285	7.029	365.4	138.2	17.16	17.35	17.70	17.21	17.70	17.46	17.58
49	LBTB	131.49	209.66	17	6.141	6.957	413.5	159.2	20.78	19.67	21.73	21.12	21.67	21.42	21.55
49	KIV	136.62	316.16	17	5.968	6.873	474.8	184.8	25.17	26.55	27.04	26.73	27.16	26.98	27.10
19	TTW	120.16	34.24	18	6.500	7.125	298.5	111.6	12.64	13.40	13.00	12.63	12.88	12.76	12.82
19	HEBO	120.27	37.55	18	6.497	7.123	299.6	112.0	12.70	13.06	13.12	12.76	12.94	12.88	12.94
19	TOLO	120.47	38.22	18	6.491	7.120	301.3	112.8	12.82	13.18	13.24	12.88	13.18	13.06	13.12
19	TAKO	120.80	39.17	17	6.482	7.116	304.3	114.2	13.01	13.26	13.55	13.06	13.43	13.31	13.37
19	JCC	122.24	42.15	18	6.436	7.095	318.7	120.0	13.93	14.47	14.40	13.98	14.34	14.16	14.22



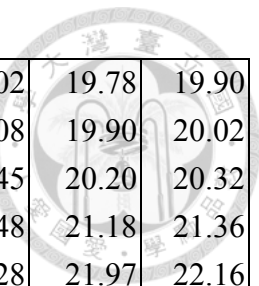
19	YBH	122.67	40.64	19	6.423	7.089	323.1	121.7	14.23	14.72	14.71	14.22	14.59	14.40	14.53
19	PIN	122.76	37.69	19	6.420	7.088	324.0	122.1	14.29	15.46	14.71	14.28	14.65	14.47	14.59
19	WDC	123.35	41.76	18	6.400	7.080	330.1	124.5	14.69	15.05	15.14	14.71	15.08	14.89	15.01
19	ORV	124.55	42.36	20	6.361	7.063	343.0	129.3	15.57	16.00	16.05	15.56	15.99	15.81	15.93
19	POTR	124.90	44.00	20	6.349	7.058	346.8	130.8	15.83	16.10	16.24	15.75	16.24	15.99	16.11
19	HAST	126.02	45.79	20	6.312	7.041	358.9	135.6	16.60	16.90	17.03	16.54	16.97	16.78	16.91
19	HLID	126.72	34.62	20	6.288	7.030	366.2	138.6	17.10	17.40	17.52	17.09	17.52	17.33	17.46
19	BOZ	126.90	31.08	17	6.282	7.027	368.0	139.3	17.24	17.60	17.70	17.21	17.70	17.46	17.58
19	MLAC	127.32	43.12	19	6.267	7.021	373.0	141.3	17.55	17.65	18.07	17.58	18.07	17.88	18.01
19	SDP	127.61	47.32	18	6.258	7.016	376.5	142.7	17.77	18.65	18.37	17.88	18.37	18.13	18.25
19	TIN	128.03	43.44	19	6.244	7.010	380.9	144.5	18.08	23.68	18.74	18.25	18.74	18.49	18.62
19	TPH	128.17	41.80	18	6.240	7.008	382.2	145.1	18.19	18.40	18.86	18.37	18.86	18.62	18.74
19	DGMT	128.20	23.90	18	6.239	7.007	382.1	145.1	18.22	18.82	18.86	18.43	18.92	18.68	18.80
19	SBC	128.25	47.08	17	6.238	7.007	383.1	145.5	18.26	18.12	18.92	18.43	18.92	18.74	18.86
19	LAO	128.72	26.69	18	6.224	6.999	387.2	147.4	18.64	19.52	19.47	19.04	19.47	19.29	19.41
19	LGU	128.88	47.13	20	6.219	6.997	389.3	148.4	18.76	19.10	19.59	19.16	19.59	19.41	19.53
19	TOV	129.04	46.96	18	6.214	6.994	390.8	149.1	18.90	19.45	19.78	19.29	19.78	19.53	19.65
19	FUR	129.27	43.35	18	6.207	6.991	393.0	150.1	19.08	18.87	20.02	19.53	19.96	19.78	19.90
19	SLA	129.28	44.21	19	6.207	6.991	393.2	150.1	19.09	19.05	20.02	19.53	20.02	19.78	19.90
19	EDW2	129.28	45.71	18	6.207	6.991	393.3	150.2	19.09	19.05	20.02	19.53	20.02	19.78	19.90
19	EDW	129.28	45.71	18	6.207	6.991	393.3	150.2	19.09	19.02	20.02	19.53	20.02	19.78	19.90
19	RPV	129.54	47.21	18	6.200	6.987	395.8	151.3	19.29	19.00	20.32	19.78	20.26	20.02	20.14



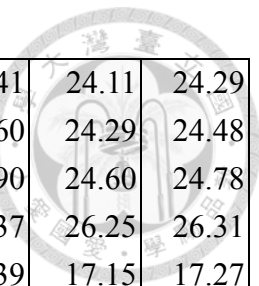
19	FMP	129.63	47.19	18	6.197	6.985	396.7	151.7	19.36	19.35	20.45	19.84	20.39	20.14	20.26
19	ADO	129.85	45.79	20	6.190	6.982	398.8	152.7	19.55	19.45	20.63	20.02	20.57	20.32	20.51
19	SHO	129.97	43.65	19	6.187	6.980	399.9	153.2	19.64	19.50	20.75	20.14	20.69	20.45	20.63
19	RRX	130.00	45.19	20	6.186	6.979	400.2	153.3	19.67	19.60	20.75	20.14	20.75	20.45	20.63
19	HEC	130.49	44.87	20	6.172	6.972	405.1	155.5	20.05	19.73	21.18	20.51	21.12	20.81	21.00
19	RDM	130.72	46.52	20	6.164	6.968	407.6	156.7	20.24	19.82	21.36	20.63	21.30	21.00	21.18
19	KNW	130.78	46.35	20	6.162	6.967	408.3	156.9	20.29	20.43	21.42	20.69	21.36	21.06	21.18
19	CRY	130.84	46.53	20	6.160	6.966	408.8	157.2	20.33	20.02	21.42	20.75	21.36	21.06	21.24
19	PLM	130.85	46.84	20	6.160	6.966	409.0	157.3	20.34	20.25	21.48	20.75	21.36	21.06	21.24
19	WMC	130.88	46.49	20	6.159	6.965	409.4	157.4	20.37	20.05	21.48	20.75	21.42	21.12	21.30
19	TRO	131.08	46.41	18	6.152	6.962	411.5	158.4	20.53	20.45	21.61	20.87	21.55	21.24	21.42
19	BEL	131.15	45.62	19	6.150	6.961	412.3	158.7	20.58	19.60	21.67	20.94	21.61	21.30	21.48
19	DAN	131.26	44.55	19	6.146	6.959	413.4	159.2	20.67	20.75	21.73	21.00	21.67	21.36	21.55
19	IRM	131.68	44.95	20	6.132	6.952	418.1	161.2	21.01	20.43	21.97	21.24	21.91	21.61	21.79
19	PDM	132.30	44.19	19	6.112	6.942	425.0	164.2	21.50	21.30	22.22	21.61	22.22	21.91	22.09
19	GLA	132.48	46.04	19	6.106	6.939	426.9	165.1	21.64	20.98	22.34	21.73	22.34	22.03	22.22
19	KNTH	134.57	42.01	19	6.036	6.904	450.7	175.1	23.45	23.80	24.41	23.86	24.48	24.17	24.35
19	NE80	135.62	47.52	19	6.000	6.887	463.2	180.3	24.38	25.35	25.33	24.66	25.33	25.02	25.21
19	SDCO	135.64	34.39	17	5.999	6.887	462.8	180.2	24.40	24.55	25.33	24.66	25.33	24.96	25.15
19	PLCA	136.55	185.60	17	5.968	6.873	472.5	184.0	25.18	26.75	26.06	25.51	26.06	25.82	26.00
50	TSUM	125.29	279.71	18	6.350	7.059	347.8	130.9	15.78	16.50	16.42	15.93	16.42	16.17	16.30
50	SNVB	131.32	14.86	20	6.158	6.966	408.2	156.6	20.37	20.77	21.12	20.63	21.12	20.87	21.00



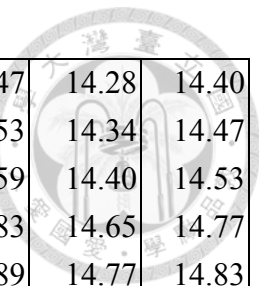
50	SUR	131.62	264.53	19	6.148	6.961	415.1	159.6	20.61	22.10	21.48	20.94	21.48	21.18	21.36
50	SPA	136.80	180.00	17	5.973	6.876	475.4	184.8	25.02	26.05	25.88	25.76	25.94	25.88	25.88
51	S02	126.39	74.22	18	6.304	7.038	362.1	136.8	16.75	18.10	17.21	16.72	17.15	16.97	17.09
51	S06	126.41	73.61	18	6.304	7.038	362.3	136.9	16.76	17.76	17.21	16.72	17.21	16.97	17.09
51	PATS	130.20	272.72	18	6.185	6.979	401.6	153.8	19.69	20.30	20.81	19.96	20.75	20.39	20.57
51	ULHL	135.30	33.87	20	6.016	6.895	457.5	177.8	23.95	24.75	24.72	24.35	24.78	24.60	24.72
52	TX31	121.83	49.28	17	6.452	7.102	313.4	117.8	13.61	13.70	13.86	13.49	13.79	13.67	13.73
52	CCM	124.61	33.47	19	6.361	7.063	341.8	128.9	15.56	15.65	15.99	15.44	15.87	15.62	15.81
52	SLM	124.73	32.28	19	6.357	7.061	343.0	129.3	15.64	16.10	15.99	15.50	15.93	15.69	15.81
52	SIUC	125.95	32.31	19	6.316	7.043	356.3	134.5	16.50	17.40	16.91	16.54	16.85	16.72	16.78
52	BLO	126.21	29.15	19	6.308	7.039	358.9	135.6	16.68	17.25	17.15	16.72	17.15	16.97	17.03
52	UALR	126.29	37.09	17	6.305	7.038	360.0	136.0	16.74	16.85	17.21	16.78	17.21	17.03	17.09
52	USIN	126.58	30.96	20	6.295	7.034	362.9	137.2	16.95	17.60	17.52	16.97	17.46	17.21	17.39
52	PVMO	126.65	33.76	18	6.293	7.033	363.9	137.6	17.00	17.25	17.52	17.03	17.52	17.27	17.39
52	WCI	127.06	29.71	18	6.279	7.026	368.2	139.4	17.29	17.45	17.88	17.21	17.88	17.58	17.76
52	MPH	127.45	35.04	18	6.266	7.020	372.8	141.2	17.59	18.10	18.19	17.52	18.13	17.82	18.01
52	WVT	127.88	32.59	20	6.251	7.014	377.4	143.0	17.90	18.70	18.37	17.82	18.37	18.07	18.25
52	CONY	127.92	17.09	18	6.249	7.013	377.4	143.0	17.93	18.55	18.43	17.82	18.37	18.13	18.25
52	PLAL	128.60	33.75	20	6.229	7.002	384.8	146.3	18.48	18.70	18.98	18.49	18.92	18.74	18.86
52	SSPA	128.64	21.15	18	6.228	7.002	384.8	146.3	18.51	19.40	18.98	18.49	18.98	18.74	18.86
52	HRV	128.86	14.61	20	6.222	6.998	386.9	147.2	18.69	18.95	19.23	18.74	19.16	18.98	19.10
52	PAL	129.61	17.44	17	6.200	6.987	394.3	150.6	19.29	19.20	19.90	19.47	19.90	19.71	19.84



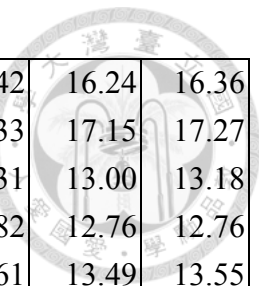
52	BRNJ	129.71	18.20	17	6.197	6.985	395.3	151.1	19.37	19.25	20.02	19.53	20.02	19.78	19.90
52	CPNY	129.79	17.59	18	6.194	6.984	396.2	151.4	19.43	19.70	20.08	19.59	20.08	19.90	20.02
52	SDMD	130.10	20.97	19	6.185	6.979	399.2	152.8	19.68	20.18	20.45	19.90	20.45	20.20	20.32
52	DWDAN	131.52	29.60	17	6.140	6.956	414.4	159.6	20.82	21.15	21.55	20.94	21.48	21.18	21.36
52	GREEN	132.25	29.41	17	6.116	6.944	422.5	163.1	21.40	21.90	22.28	21.67	22.28	21.97	22.16
52	ANDY	134.12	27.57	17	6.053	6.913	443.5	172.1	22.98	23.20	23.99	23.25	23.99	23.62	23.80
52	BTRCK	134.41	29.52	18	6.044	6.908	446.9	173.5	23.24	23.85	24.23	23.50	24.23	23.86	24.11
53	CRZF	124.81	237.10	17	6.366	7.066	344.4	129.6	15.43	14.05	15.93	15.62	15.87	15.81	15.87
53	SBA	126.01	174.78	19	6.326	7.048	358.0	135.0	16.29	17.48	16.78	16.11	16.72	16.42	16.60
53	LBTB	128.63	274.42	20	6.238	7.008	384.4	145.9	18.22	18.87	19.16	18.49	19.10	18.86	18.98
53	NNA	129.24	60.03	20	6.220	6.998	389.2	148.1	18.71	18.80	19.71	18.80	19.65	19.23	19.47
53	SUR	136.55	270.41	18	5.981	6.880	471.6	183.3	24.82	25.80	25.57	25.27	25.63	25.45	25.57
54	CAN	122.10	218.97	17	6.448	7.101	314.2	118.1	13.68	13.40	14.28	13.61	14.16	13.92	14.10
54	YAK	124.13	348.04	17	6.382	7.072	336.0	126.6	15.09	14.85	15.50	14.95	15.38	15.20	15.32
54	CHKZ	125.52	26.57	19	6.336	7.052	351.1	132.3	16.11	16.00	16.60	16.05	16.54	16.30	16.42
54	KURK	131.08	24.71	19	6.159	6.966	408.9	157.1	20.35	19.45	21.24	20.69	21.24	21.00	21.12
54	KKAR	132.08	37.24	20	6.126	6.950	420.4	162.1	21.15	21.88	22.16	21.48	22.03	21.79	21.91
54	EKS2	134.27	35.76	19	6.053	6.913	445.0	172.6	22.99	23.67	23.80	23.32	23.86	23.62	23.74
54	ERM	134.51	323.37	18	6.045	6.909	447.8	173.8	23.20	23.25	24.11	23.44	24.05	23.74	23.93
54	AML	134.54	36.40	18	6.044	6.909	448.2	173.9	23.22	24.48	24.11	23.50	24.11	23.80	23.99
54	AAK	134.70	35.32	18	6.038	6.906	449.9	174.7	23.37	24.80	24.23	23.56	24.17	23.93	24.11
54	UCH	134.96	35.76	17	6.029	6.902	453.0	175.9	23.59	24.90	24.35	23.74	24.35	24.05	24.23



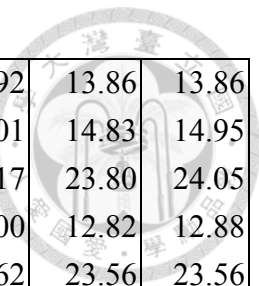
54	TKM2	135.13	34.28	18	6.023	6.899	455.0	176.8	23.75	25.15	24.41	23.80	24.41	24.11	24.29
54	KZA	135.48	35.43	19	6.011	6.893	459.1	178.5	24.06	25.67	24.60	23.99	24.60	24.29	24.48
54	ULHL	135.94	34.56	17	5.996	6.886	464.3	180.6	24.47	25.82	24.84	24.35	24.90	24.60	24.78
55	OBN	137.35	330.38	18	5.939	6.858	485.0	189.3	26.01	27.20	26.25	26.12	26.37	26.25	26.31
56	ARU	126.27	323.33	18	6.290	7.030	367.5	139.3	17.07	17.70	17.39	16.91	17.39	17.15	17.27
56	LVZ	130.98	342.80	18	6.143	6.957	415.8	160.5	20.76	22.80	21.79	21.06	21.79	21.42	21.67
56	MHV	137.76	327.11	17	5.919	6.848	491.9	192.6	26.64	28.10	27.65	27.16	27.71	27.47	27.59
57	SCHQ	121.43	38.36	18	6.458	7.105	313.4	117.9	13.49	14.12	13.92	13.49	13.86	13.67	13.79
57	FDF	122.37	86.18	19	6.428	7.092	322.5	121.5	14.11	14.80	14.65	14.16	14.59	14.40	14.47
57	KBS	122.85	357.14	18	6.413	7.085	327.6	123.6	14.43	14.85	15.01	14.89	15.08	15.01	15.08
57	ARU	125.15	324.32	18	6.337	7.052	352.2	133.0	16.09	16.15	16.30	15.93	16.30	16.11	16.24
57	SUMG	125.28	13.10	18	6.332	7.050	353.5	133.5	16.18	17.40	16.85	16.30	16.78	16.54	16.66
57	ABKT	127.61	301.48	19	6.254	7.014	379.3	143.9	17.86	17.90	18.86	18.25	18.80	18.55	18.74
57	DRLN	127.91	44.10	19	6.244	7.010	382.3	145.2	18.09	18.77	18.62	18.01	18.55	18.31	18.49
57	OBN	136.99	329.44	19	5.949	6.864	481.4	187.6	25.68	26.40	26.00	25.88	26.06	26.00	26.06
58	DBIC	128.77	272.97	19	6.217	6.995	390.8	149.1	18.83	19.70	19.53	19.10	19.53	19.29	19.41
58	PLCA	130.81	165.86	19	6.155	6.963	408.9	157.3	20.46	21.15	21.55	21.00	21.48	21.30	21.42
59	TOV	121.58	54.21	17	6.464	7.108	310.4	116.5	13.35	14.85	13.92	13.37	13.79	13.61	13.73
59	TPH	121.77	49.37	18	6.458	7.106	312.2	117.3	13.47	14.83	14.10	13.49	13.98	13.79	13.92
59	HLID	121.89	42.45	18	6.455	7.104	313.3	117.7	13.55	11.33	14.16	13.61	14.10	13.86	13.98
59	DAC	122.00	51.50	17	6.451	7.102	314.6	118.2	13.62	13.25	14.22	13.61	14.16	13.92	14.04
59	SLA	122.35	51.85	17	6.440	7.097	318.1	119.7	13.85	14.90	14.47	13.79	14.34	14.10	14.22



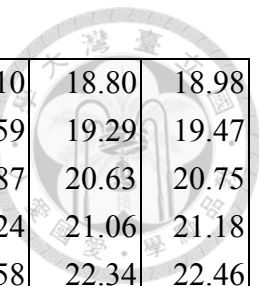
59	VTV	122.67	53.38	18	6.430	7.093	321.4	120.9	14.06	14.20	14.59	14.04	14.47	14.28	14.40
59	BOZ	122.85	39.28	17	6.424	7.090	322.9	121.5	14.19	14.47	14.65	14.16	14.53	14.34	14.47
59	GSC	122.89	52.40	18	6.423	7.090	323.6	121.8	14.21	16.15	14.71	14.16	14.59	14.40	14.53
59	RDM	123.30	54.33	17	6.410	7.084	327.9	123.5	14.49	15.07	14.89	14.47	14.83	14.65	14.77
59	CRY	123.40	54.37	17	6.406	7.083	328.9	123.9	14.55	12.07	15.01	14.53	14.89	14.77	14.83
59	HWUT	124.60	43.59	18	6.366	7.066	341.5	128.7	15.43	15.80	15.87	15.50	15.81	15.69	15.75
59	ISCO	129.45	43.11	17	6.209	6.992	393.0	149.9	19.03	20.45	19.96	19.41	19.90	19.71	19.84
60	LBNH	121.07	52.19	17	6.471	7.111	309.4	116.3	13.21	13.72	13.67	13.12	13.55	13.31	13.43
60	HRV	121.13	54.24	17	6.470	7.110	310.0	116.5	13.26	13.30	13.67	13.18	13.61	13.37	13.49
60	FRB	122.71	29.09	19	6.419	7.088	326.0	122.9	14.29	14.85	14.77	14.34	14.65	14.53	14.59
60	FDF	123.48	88.71	20	6.394	7.077	333.4	125.7	14.83	15.85	15.44	14.95	15.32	15.20	15.26
60	SCHQ	124.60	39.65	19	6.357	7.061	346.1	130.5	15.65	16.15	15.99	15.56	15.99	15.81	15.93
60	DRLN	130.93	45.88	20	6.155	6.964	412.1	158.7	20.45	21.85	21.12	20.63	21.12	20.87	21.00
61	SHO	121.14	52.32	18	6.473	7.112	307.5	115.5	13.18	15.62	13.49	13.37	13.43	13.43	13.43
61	KNW	121.31	54.89	17	6.468	7.110	309.4	116.2	13.29	13.57	13.67	13.49	13.61	13.55	13.61
61	HEC	121.35	53.54	17	6.466	7.109	309.8	116.4	13.31	13.20	13.73	13.55	13.67	13.61	13.67
61	V11A	121.81	52.18	17	6.452	7.102	314.3	118.2	13.61	13.35	14.10	13.92	14.10	14.04	14.04
61	V12A	122.30	52.16	20	6.436	7.096	319.2	120.2	13.93	15.22	14.53	14.22	14.47	14.34	14.40
61	LOHW	122.73	42.05	17	6.423	7.089	323.5	121.8	14.22	14.90	14.89	14.59	14.83	14.71	14.77
61	W13A	123.23	52.62	20	6.407	7.082	328.8	123.9	14.56	14.82	15.14	14.65	15.08	14.89	15.01
61	Y14A	124.24	53.72	17	6.373	7.068	339.7	128.1	15.29	14.88	15.69	15.32	15.62	15.50	15.56
61	WUAZ	125.07	51.41	18	6.345	7.056	348.5	131.4	15.91	15.68	16.30	15.99	16.30	16.17	16.24



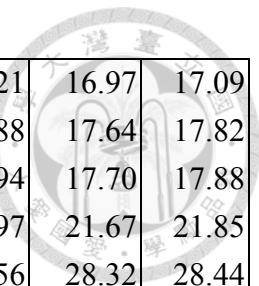
61	115A	125.20	54.95	18	6.341	7.055	350.0	131.9	16.00	16.60	16.42	16.11	16.42	16.24	16.36
61	AGU01	126.41	167.91	19	6.301	7.036	360.7	136.3	16.83	14.10	17.39	16.91	17.33	17.15	17.27
62	IDI	121.40	309.67	17	6.484	7.118	304.0	113.7	12.94	13.60	13.55	12.57	13.31	13.00	13.18
62	LONY	122.46	37.54	17	6.451	7.103	314.2	117.9	13.61	17.27	13.00	12.70	12.82	12.76	12.76
62	TIR	122.58	318.07	18	6.447	7.101	315.4	118.4	13.69	15.00	13.67	13.31	13.61	13.49	13.55
62	NCB	123.02	38.03	17	6.433	7.095	319.9	120.1	13.99	13.10	13.73	13.79	13.73	13.73	13.73
62	HCNY	123.57	39.42	18	6.415	7.087	325.5	122.4	14.35	16.40	14.77	14.77	14.77	14.77	14.77
62	FUORN	125.42	327.99	18	6.353	7.061	345.1	129.8	15.70	16.45	15.81	15.50	15.75	15.62	15.69
62	HRV	125.45	38.27	18	6.352	7.061	345.5	130.0	15.72	17.00	15.93	15.75	15.87	15.81	15.87
62	TIP	125.69	317.14	20	6.344	7.057	348.3	131.0	15.90	16.60	16.17	15.87	16.11	15.99	16.05
62	TUE	126.00	328.36	18	6.334	7.053	351.3	132.1	16.12	16.05	16.48	16.24	16.48	16.36	16.42
62	WDD	128.87	314.56	17	6.238	7.008	382.9	145.0	18.21	16.80	18.86	18.31	18.80	18.55	18.74
63	FDF	121.92	91.23	17	6.466	7.110	310.4	116.4	13.30	14.85	13.12	12.82	13.00	12.88	12.94
63	BBGH	122.55	93.73	18	6.446	7.101	316.6	118.9	13.71	16.48	13.92	13.86	13.92	13.86	13.86
63	ANWB	122.66	87.82	18	6.443	7.099	317.9	119.4	13.78	19.62	14.10	14.04	14.04	14.04	14.04
63	VOS	125.11	315.39	17	6.362	7.065	344.8	129.7	15.50	15.97	15.93	15.75	15.87	15.81	15.87
63	BRVK	125.56	315.75	17	6.347	7.058	349.7	131.6	15.84	15.20	16.54	16.17	16.48	16.36	16.48
63	ZRNK	126.33	315.54	17	6.321	7.047	357.9	134.9	16.37	15.75	17.03	16.05	16.91	16.48	16.72
63	LSZ	126.93	214.58	18	6.301	7.037	360.6	135.9	16.80	19.07	17.33	16.91	17.33	17.15	17.21
63	KBS	131.41	356.98	18	6.161	6.968	410.5	157.5	20.29	22.40	21.12	20.63	21.06	20.87	21.00
63	KMBO	132.61	235.03	17	6.121	6.948	421.7	162.4	21.25	22.50	22.40	21.73	22.40	22.09	22.28
64	FDF	120.41	82.79	18	6.495	7.123	301.1	112.7	12.73	13.05	13.18	13.00	13.12	13.06	13.06



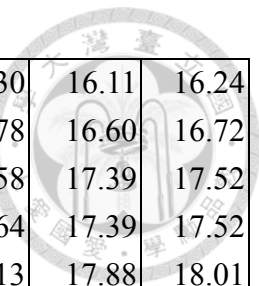
64	ARU	122.01	326.44	19	6.446	7.100	316.7	119.2	13.72	14.65	13.98	13.79	13.92	13.86	13.86
64	DRLN	123.34	41.98	20	6.404	7.081	330.5	124.6	14.61	15.90	15.08	14.65	15.01	14.83	14.95
64	OBN	133.47	332.60	19	6.076	6.924	437.9	169.7	22.40	23.85	24.29	23.32	24.17	23.80	24.05
65	BSFB	121.68	132.02	18	6.474	7.113	305.8	114.5	13.14	11.95	13.18	12.63	13.00	12.82	12.88
65	LSZ	133.59	217.46	17	6.089	6.932	431.6	166.7	22.04	24.95	23.50	23.38	23.62	23.56	23.56
66	PKME	120.99	50.06	17	6.478	7.114	307.2	115.3	13.08	12.35	13.24	13.00	13.12	13.06	13.12
66	EMMW	122.27	50.77	17	6.438	7.096	320.0	120.5	13.90	13.93	14.53	14.10	14.47	14.28	14.40
66	SCHQ	122.35	38.76	20	6.435	7.095	320.9	120.8	13.96	14.55	14.59	14.22	14.53	14.40	14.47
66	FDF	122.59	86.91	20	6.427	7.092	322.8	121.6	14.12	15.00	14.65	14.16	14.53	14.34	14.47
66	LBTB	125.70	209.71	17	6.325	7.047	352.7	133.0	16.33	14.45	16.85	16.42	16.78	16.66	16.72
66	SUMG	126.35	13.23	17	6.303	7.037	363.1	137.3	16.79	17.95	17.27	16.85	17.27	17.09	17.15
66	BLWY	128.28	215.92	18	6.239	7.007	381.4	144.7	18.23	18.13	18.86	18.37	18.80	18.55	18.68
66	WIN	131.32	202.15	18	6.147	6.959	411.4	158.3	20.66	20.65	21.55	21.00	21.48	21.24	21.42
67	FDF	120.50	84.73	17	6.490	7.120	302.8	113.5	12.84	13.30	13.92	13.43	13.86	13.67	13.79
67	NRS	128.23	26.72	17	6.238	7.007	384.1	146.0	18.26	18.95	19.65	19.23	19.65	19.47	19.53
67	TEZI	136.38	215.66	17	5.973	6.875	470.9	183.4	25.04	25.25	25.21	24.72	25.27	24.96	25.15
68	BRVK	120.36	318.90	18	6.497	7.124	301.0	112.7	12.68	13.70	12.88	12.57	12.82	12.70	12.76
68	ARU	126.70	323.88	17	6.292	7.032	366.8	138.8	17.01	18.40	17.46	17.03	17.46	17.27	17.33
68	ABKAR	127.10	314.84	18	6.279	7.026	371.2	140.6	17.30	17.32	17.76	17.39	17.76	17.58	17.70
68	LVZ	130.81	343.60	18	6.164	6.969	408.7	157.1	20.22	21.30	21.06	20.57	21.00	20.81	20.94
69	VTS	124.99	318.05	18	6.366	7.066	341.6	128.5	15.43	17.15	15.93	15.56	15.87	15.75	15.81
70	ADK	126.19	315.29	18	6.305	7.038	363.0	137.3	16.75	18.50	17.27	16.78	17.21	17.03	17.15



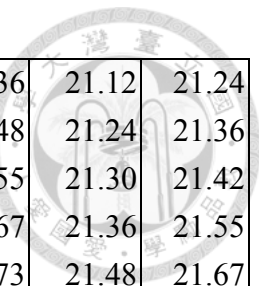
70	KWAJ	128.61	257.98	18	6.226	7.000	387.6	147.6	18.57	21.20	19.10	18.49	19.10	18.80	18.98
70	WRAB	129.08	201.25	20	6.212	6.993	389.7	148.6	18.95	19.95	19.59	18.98	19.59	19.29	19.47
70	ARU	130.54	38.51	17	6.169	6.971	407.8	156.7	20.12	20.55	20.81	20.39	20.87	20.63	20.75
70	AKTK	130.88	46.43	17	6.158	6.965	411.6	158.4	20.39	20.15	21.24	20.81	21.24	21.06	21.18
70	PMG	132.41	222.23	17	6.108	6.940	425.5	164.5	21.62	23.95	22.58	22.09	22.58	22.34	22.46
71	FDF	120.82	85.04	17	6.474	7.112	307.7	115.7	13.16	13.85	13.73	13.18	13.61	13.43	13.55
71	LBTB	128.30	208.74	18	6.230	7.002	383.9	146.0	18.48	19.10	19.04	18.49	19.04	18.74	18.92
71	B3	132.57	291.97	17	6.097	6.934	431.6	167.2	21.89	22.62	23.13	22.83	23.13	23.01	23.07
71	B1	132.97	291.56	18	6.084	6.927	436.1	169.2	22.22	24.02	23.80	23.50	23.74	23.62	23.68
71	KIV	138.71	313.31	18	5.896	6.836	500.0	196.1	27.36	28.20	27.16	27.22	27.28	27.28	27.28
72	FDF	120.72	84.86	17	6.480	7.115	305.9	114.9	13.04	13.25	13.49	13.00	13.37	13.18	13.24
72	ARU	125.00	325.13	17	6.341	7.054	350.6	132.3	16.00	16.50	16.11	15.81	16.11	15.99	16.05
72	MHV	136.19	330.17	17	5.976	6.876	472.1	183.9	24.98	26.40	25.39	25.15	25.45	25.33	25.39
72	OBN	136.65	330.95	18	5.960	6.869	477.5	186.0	25.38	26.70	25.94	25.82	26.00	25.94	26.00
73	BRVK	120.55	318.32	18	6.491	7.120	303.2	113.7	12.82	12.95	13.12	12.70	12.94	12.82	12.88
73	FDF	123.16	88.28	19	6.409	7.083	328.7	123.9	14.51	15.75	15.01	14.47	14.95	14.71	14.83
73	PQI	123.47	49.33	20	6.399	7.079	332.6	125.4	14.73	15.80	15.26	14.77	15.20	14.95	15.08
73	EMMW	123.78	51.70	17	6.388	7.075	335.9	126.6	14.95	15.00	15.44	14.95	15.38	15.14	15.26
73	SPB1	126.12	355.56	19	6.310	7.041	360.9	136.4	16.62	18.56	17.21	16.66	17.21	16.97	17.09
73	SPA0	126.12	355.56	19	6.310	7.041	360.9	136.4	16.62	18.55	17.21	16.66	17.21	16.97	17.09
73	SPB4	126.13	355.57	19	6.310	7.040	360.9	136.4	16.63	18.54	17.27	16.66	17.21	16.97	17.09
73	SPB2	126.13	355.56	19	6.310	7.040	361.0	136.4	16.63	18.56	17.21	16.66	17.21	16.97	17.09



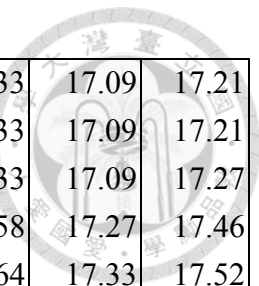
73	SPB3	126.13	355.56	19	6.310	7.040	361.0	136.4	16.63	18.57	17.21	16.66	17.21	16.97	17.09
73	ARU	127.06	322.99	17	6.279	7.026	371.4	140.6	17.30	17.40	17.94	17.33	17.88	17.64	17.82
73	ABKAR	127.14	313.92	20	6.276	7.025	372.2	141.0	17.36	17.50	18.01	17.39	17.94	17.70	17.88
73	LVZ	131.84	342.66	18	6.129	6.951	420.6	162.3	21.08	22.15	22.03	21.30	21.97	21.67	21.85
73	OBN	139.08	327.44	17	5.893	6.835	501.3	196.5	27.45	28.80	28.50	28.02	28.56	28.32	28.44
73	KIV	139.67	309.22	18	5.874	6.826	508.0	199.3	28.01	29.05	28.99	28.44	29.05	28.75	28.93
74	ARU	122.58	327.18	18	6.446	7.101	316.7	118.9	13.72	13.65	14.16	13.79	14.04	13.92	13.98
74	SCO	123.90	9.93	18	6.403	7.082	330.1	124.1	14.61	16.70	15.38	14.77	15.26	15.08	15.20
74	LVZ	124.85	346.11	20	6.371	7.069	340.3	128.0	15.31	14.95	15.62	15.26	15.56	15.38	15.50
74	ABKT	127.57	305.34	19	6.280	7.028	370.3	139.9	17.24	18.00	17.94	17.52	17.94	17.76	17.88
74	LBTB	133.33	208.28	18	6.098	6.936	428.2	165.2	21.81	21.60	22.83	22.28	22.83	22.58	22.71
74	LRW	136.33	3.22	17	5.995	6.887	464.7	180.4	24.45	24.92	25.51	24.96	25.51	25.27	25.39
74	MIB	137.63	296.23	17	5.951	6.867	481.0	186.9	25.58	26.35	27.04	26.61	27.04	26.86	26.98
75	ARU	122.38	326.11	17	6.431	7.093	321.7	121.2	14.05	13.10	14.83	14.22	14.71	14.53	14.65
75	KNS	122.78	23.52	17	6.418	7.087	325.7	122.7	14.32	16.05	14.83	14.34	14.71	14.53	14.65
75	LVZ	125.62	344.89	17	6.324	7.047	355.7	134.3	16.35	16.10	16.78	16.30	16.72	16.54	16.66
75	OBN	133.92	332.06	17	6.057	6.915	444.4	172.5	22.90	24.55	23.86	23.19	23.86	23.56	23.74
76	ARU	122.61	326.41	18	6.429	7.092	322.3	121.3	14.08	14.75	14.65	14.34	14.59	14.47	14.53
76	ABKAR	123.72	317.87	20	6.393	7.077	333.9	125.8	14.85	15.70	15.56	14.95	15.50	15.26	15.38
76	ABKT	126.86	304.43	20	6.288	7.030	367.8	139.2	17.10	17.85	17.64	17.09	17.64	17.39	17.52
76	OBN	134.05	332.70	18	6.058	6.916	444.0	172.2	22.87	24.55	23.86	23.19	23.80	23.50	23.68
77	ARU	122.34	326.36	20	6.439	7.097	319.1	120.1	13.88	14.55	14.04	13.73	13.98	13.86	13.92



77	KEV	125.45	349.26	18	6.336	7.053	351.7	132.6	16.10	16.45	16.36	15.93	16.30	16.11	16.24
77	KOG	125.95	96.39	20	6.320	7.045	357.1	134.8	16.44	16.55	16.85	16.42	16.78	16.60	16.72
77	SA08	126.87	202.31	19	6.289	7.031	364.3	137.7	17.08	17.30	17.64	17.15	17.58	17.39	17.52
77	SUR	126.88	200.85	19	6.288	7.031	364.4	137.8	17.09	17.35	17.64	17.15	17.64	17.39	17.52
77	SA07	127.45	200.48	19	6.269	7.022	370.6	140.3	17.52	17.75	18.13	17.64	18.13	17.88	18.01
77	SA82	127.64	202.98	20	6.262	7.019	372.9	141.2	17.66	17.65	18.31	17.76	18.31	18.07	18.19
77	SA81	128.05	202.04	18	6.248	7.013	377.4	143.0	17.96	18.05	18.68	18.07	18.68	18.37	18.55
77	SA13	128.19	204.42	17	6.244	7.010	379.1	143.7	18.08	18.10	18.80	18.25	18.80	18.49	18.68
77	SA12	128.65	203.61	20	6.231	7.003	383.7	145.7	18.44	18.20	19.23	18.62	19.16	18.92	19.04
77	SA16	129.48	204.06	20	6.206	6.990	391.9	149.4	19.10	18.35	19.96	19.35	19.90	19.65	19.84
77	SA32	129.54	209.47	20	6.204	6.989	392.6	149.8	19.15	17.45	20.02	19.41	20.02	19.71	19.90
77	SA24	129.58	206.77	19	6.203	6.989	393.0	149.9	19.18	18.20	20.08	19.47	20.02	19.78	19.90
77	SA23	129.90	205.90	17	6.194	6.984	396.1	151.3	19.44	18.85	20.32	19.71	20.32	20.02	20.20
77	SA40	129.94	210.99	20	6.193	6.983	396.6	151.6	19.47	18.70	20.39	19.78	20.39	20.08	20.26
77	SA31	130.01	208.13	20	6.191	6.982	397.2	151.8	19.53	17.45	20.45	19.84	20.45	20.14	20.32
77	SA139	130.40	210.15	20	6.179	6.976	401.2	153.7	19.85	19.00	20.81	20.14	20.75	20.45	20.63
77	SA57	130.80	216.00	19	6.167	6.970	405.3	155.5	20.16	21.30	21.06	20.39	21.00	20.75	20.87
77	SA46	130.84	211.71	20	6.165	6.969	405.5	155.6	20.20	18.95	21.06	20.45	21.06	20.75	20.94
77	SA38	130.89	208.90	19	6.164	6.968	406.0	155.9	20.24	19.25	21.12	20.45	21.06	20.81	20.94
77	SA74	131.10	217.74	20	6.157	6.965	408.7	157.0	20.40	21.40	21.24	20.63	21.24	20.94	21.12
77	SA51	131.10	213.48	20	6.157	6.965	408.5	156.9	20.40	20.25	21.24	20.63	21.24	20.94	21.12
77	SA45	131.27	210.73	18	6.151	6.962	410.3	157.7	20.54	19.75	21.36	20.81	21.36	21.12	21.24

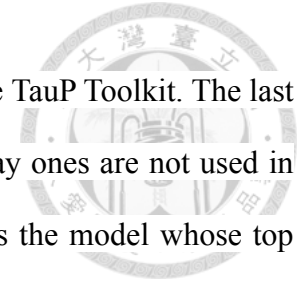


77	SA56	131.30	215.06	20	6.150	6.962	410.8	157.9	20.57	21.40	21.42	20.81	21.36	21.12	21.24
77	LBTB	131.43	210.05	19	6.146	6.959	411.9	158.4	20.67	20.35	21.55	20.94	21.48	21.24	21.36
77	SA37	131.47	207.46	20	6.145	6.959	412.4	158.6	20.70	18.85	21.55	21.00	21.55	21.30	21.42
77	SA50	131.61	212.48	20	6.140	6.957	414.1	159.4	20.81	20.65	21.67	21.12	21.67	21.36	21.55
77	SA55	131.74	214.30	19	6.136	6.954	415.6	160.0	20.92	21.45	21.79	21.24	21.73	21.48	21.67
77	SA169	131.82	215.78	19	6.133	6.953	416.6	160.4	20.98	22.40	21.85	21.30	21.79	21.55	21.73
77	SA77	132.01	218.71	17	6.127	6.950	418.8	161.4	21.13	22.05	22.03	21.48	21.97	21.73	21.85
77	SA63	132.34	211.53	20	6.116	6.944	422.1	162.8	21.40	21.30	22.28	21.79	22.28	22.03	22.16
77	SA65	132.45	213.34	19	6.112	6.943	423.4	163.4	21.48	21.30	22.40	21.85	22.40	22.16	22.28
77	SA60	132.72	210.21	20	6.104	6.938	426.4	164.7	21.70	21.25	22.64	22.09	22.64	22.40	22.52
77	SA76	132.74	217.76	19	6.103	6.938	426.8	164.9	21.71	22.55	22.64	22.09	22.64	22.40	22.52
77	SA79	132.81	218.95	17	6.101	6.937	427.8	165.3	21.77	21.95	22.77	22.16	22.71	22.46	22.64
77	SA75	133.05	216.72	19	6.093	6.933	430.3	166.4	21.96	22.30	22.95	22.40	22.95	22.71	22.83
77	SA78	133.08	219.68	19	6.092	6.932	430.8	166.6	21.99	22.60	23.01	22.40	22.95	22.71	22.89
77	SA66	133.64	213.15	20	6.073	6.923	436.8	169.2	22.47	23.15	23.50	22.83	23.44	23.19	23.32
77	OBN	133.81	332.53	20	6.067	6.920	440.8	170.9	22.63	23.70	23.80	23.07	23.80	23.50	23.68
77	SA72	133.84	216.92	20	6.066	6.920	439.2	170.2	22.65	23.15	23.62	23.01	23.62	23.32	23.50
77	SA70	134.33	213.75	19	6.049	6.911	444.8	172.5	23.08	23.45	24.05	23.38	24.05	23.74	23.93
78	SA82	122.55	203.42	19	6.423	7.089	320.9	120.9	14.22	13.20	14.53	14.22	14.53	14.34	14.47
78	KBS	123.10	357.10	20	6.405	7.082	330.2	124.5	14.59	15.10	15.20	14.77	15.14	14.95	15.08
78	SA12	123.56	204.00	19	6.390	7.075	331.5	125.0	14.93	14.15	15.75	15.38	15.69	15.56	15.62
78	SA47	125.31	212.52	17	6.332	7.050	350.6	132.3	16.19	15.95	17.03	16.48	16.97	16.72	16.85



78	SA46	125.84	211.54	19	6.314	7.042	356.2	134.6	16.56	16.40	17.39	16.78	17.33	17.09	17.21
78	SA38	125.85	208.91	20	6.314	7.042	356.3	134.6	16.57	16.00	17.39	16.85	17.33	17.09	17.21
78	SA57	125.88	215.54	20	6.313	7.041	357.0	134.9	16.59	17.80	17.46	16.85	17.33	17.09	17.27
78	SA74	126.23	217.15	20	6.301	7.036	360.8	136.5	16.83	17.90	17.64	16.97	17.58	17.27	17.46
78	SA56	126.37	214.64	20	6.296	7.034	362.2	137.0	16.94	17.80	17.70	17.03	17.64	17.33	17.52
78	LBTB	126.40	209.97	19	6.295	7.033	362.3	137.1	16.96	15.80	17.70	17.03	17.64	17.33	17.52
78	SA37	126.41	207.56	17	6.295	7.033	362.4	137.1	16.97	15.60	17.70	17.03	17.64	17.33	17.52
78	SA73	126.65	216.59	20	6.287	7.029	365.4	138.3	17.13	19.80	17.82	17.09	17.76	17.46	17.64
78	SA62	126.76	209.62	19	6.283	7.028	366.2	138.7	17.21	16.65	17.88	17.15	17.76	17.46	17.64
78	SA55	126.79	213.92	19	6.282	7.027	366.8	138.9	17.24	18.35	17.88	17.15	17.76	17.52	17.64
78	SA169	126.90	215.30	19	6.278	7.025	368.1	139.4	17.32	18.05	17.88	17.15	17.82	17.52	17.70
78	SA59	127.07	208.97	18	6.272	7.023	369.7	140.1	17.45	18.05	17.94	17.21	17.88	17.58	17.76
78	SA77	127.16	218.01	20	6.269	7.021	371.1	140.6	17.52	18.55	18.01	17.21	17.88	17.58	17.76
78	SA63	127.33	211.32	18	6.264	7.019	372.7	141.3	17.64	17.95	18.01	17.21	17.94	17.64	17.82
78	SA65	127.47	213.00	18	6.259	7.017	374.4	141.9	17.74	16.75	18.07	17.21	18.01	17.64	17.82
78	SA80	127.56	219.00	19	6.256	7.015	375.6	142.4	17.81	19.35	18.07	17.27	18.01	17.64	17.88
78	SA60	127.70	210.08	17	6.251	7.013	376.7	142.9	17.91	17.75	18.13	17.27	18.07	17.70	17.88
78	SA78	128.26	218.87	17	6.234	7.004	383.0	145.6	18.36	19.70	18.19	17.52	18.13	17.82	18.01
78	SA72	128.94	216.27	17	6.214	6.994	389.6	148.6	18.90	20.35	19.10	18.98	19.16	19.10	19.10
78	LVZ	129.51	343.51	17	6.197	6.985	397.5	152.2	19.36	21.00	20.08	19.65	20.14	19.90	20.02

Note: The first and second columns are the event ID numbers in **Table A.1** and the station names in **Table B.1**, respectively. Columns



for p and h_T are ray parameters and depths of turning points below the CMB, respectively, both calculated in PREM by the TauP Toolkit. The last 7 columns are respectively the S3KS-SKKS differential traveltimes obtained by TauP in PREM, from records (OBS, gray ones are not used in the Bayesian inversion), and from DSM-calculated synthetic seismograms for 5 different models. Model PREM-SOC is the model whose top 550 km of the outer core is obtained by the inversion of the observed differential traveltimes (Column OBS).